

Department of Precision and Microsystems Engineering

Analysis and Performance of a lightweight over-actuated 450mm wafer chuck

Name: Rein Boshuisen

Report no: ME10.021 Coach: dr. ir. D. Laro

prof. dr. ir. J. van Eijk

Professor: prof. ir. R.H. Munnig Schmidt

Specialisation: Mechatronics
Type of report: Masters Thesis
Date: Delft, May 24, 2010

Preface

Bijna acht jaar geleden begon ik mijn studie Technische Natuurkunde in Delft. Al na korte tijd besloot ik te stoppen met deze studie. Mijn belangrijkste beweegreden: "Ik hou niet van dat nano-gebeuren. Geef mij maar iets wat je kan zien zonder hulpmiddelen." Nu schrijf ik hier de laatste noot van mijn rapport, en geloof het of niet, het gaat over "nano-gebeuren". Blijkbaar had ik acht jaar geleden al in de gaten dat het eigenlijk toch wel interessant was. Natuurlijk is het onderzoek dat ik nu heb gedaan in geen opzicht te vergelijken met nano-onderzoek in de Natuurkunde.

Negen maanden stage en onderzoek bij MI-Partners heeft mij oprecht geinteresseerd voor de mechanica en dynamica. Voorheen vond ik voornamelijk de studie interessant, ik heb nu het idee dat ik ook echt iets kan bijdragen in de techniek. De mogelijkheden voor zelfstandig onderzoek en het onderzoeksonderwerp sprak me zeer aan. Ik ben erg blij dat ik destijds de keuze heb gemaakt om bij MI-Partners in Eindhoven de laatste loodjes van mijn studie te volbrengen. Ik ben MI-Partners dan ook dankbaar voor de mogelijkheden die jullie geboden hebben.

De begeleiding bij MI is heel divers geweest. Zo kom je er na een tijdje achter dat je voor een praktische, elektrische vraag het best bij Lucas aan kan kloppen. Voor de regeltechniek en de "matlab uitvindsels" wordt Jamie altijd enthousiast. Het maken van tekeningen van nieuwe onderdelen kon 'even tussendoor' geregeld worden met Dennis. Dick, mijn begeleider, hielp goed met nieuwe concepten, of andere dingen die weleens mis konden zijn. Tips over metingen en verbeteringen die gedaan konden worden kon ik goed met Dick bespreken. De hulp van Dick is door mij zeer gewaardeerd. Als we het allebei even niet meer wisten, dan was er altijd nog Jan, die van buitenaf het onderzoek volgde. Jan kan met een snelle beoordeling van het probleem vaak een goede tip geven. Natuurlijk zijn er ook nog de andere werknemers en studenten bij MI-Partners die voor de nodige afleiding zorgden. Ik wil jullie allemaal bedanken voor de hulp en samenwerking die ik de afgelopen maanden van jullie heb mogen ontvangen.

Er rest nog een grote groep mensen die mij, direct of indirect, hebben geholpen de afgelopen maanden. Mijn (oud)-huisgenoten die, net als ik, soms in de weekends aan het werk waren, waardoor de gedeelde smart, slechts halve smart was. En mijn ouders, die vele kritische vragen stelden en hebben geholpen het engelstalige niveau van het rapport te verhogen. Als laatste zijn er nog de vele vrienden die deden alsof ze mijn verhalen precies begrepen. De afleiding kwam van deze mensen. Afleiding, die nodig is om daarna weer geconcentreerd aan de slag te gaan.

Wat ik ga doen na mijn presentatie? Hier kan ik heel kort over zijn. Zeilen! Er is nu even tijd om hier een inhaalslag te maken! En dan is er 's avonds alle tijd voor vrienden en vriendinnen om een welverdiend biertje te drinken.

Contents

Pr	Preface									
Su	mma	ry								
1	Intr	troduction								
	1.1	Background	1							
	1.2	Over-Actuation	1							
	1.3	Problem statement	2							
	1.4	Outline								
2	Tope	ology Optimization	3							
	2.1	Principle of over-actuation	3							
	2.2	Over-actuation of a wafer chuck	5							
	2.3	Topology Optimization Procedure								
	2.4	Mechanical layout								
3	Dvn	amic properties of the wafer chuck	11							
_	3.1	Modal Analysis								
	3.2	Problem description								
	3.3	Dynamic analysis								
		3.3.1 Suspension modes	_							
		3.3.2 Plate springs								
		3.3.3 Gravity compensators								
		3.3.4 Actuators								
		3.3.5 Chuck								
	3.4	Model improvements								
	3.5	Improvements in the Current Setup								
		3.5.1 Added mass	28							
		3.5.2 Damping	_							
		3.5.3 Over-Sensing								
	3.6	Conclusions								
4	Con	trol and Performance of the wafer chuck	36							
•	4.1	Performance specification	36							
	4.2	PID control of the wafer chuck	37							
		4.2.1 System CoG control formulation	38							
		4.2.2 PID control and performance	39							

CONTENTS iv

	4.3	Chuck deformation due to the added actuator	44		
		4.3.1 Static deformation of the chuck	45		
		4.3.2 Deformation of the chuck at high frequencies	46		
		4.3.3 Conclusion	46		
	4.4	Model Based control performance	47		
		4.4.1 Dynamic Error Budgeting analysis tool	47		
		4.4.2 Disturbances	48		
		4.4.3 Disturbance propagation	50		
		4.4.4 \mathcal{H}_2 control as a performance measure	51		
		4.4.5 Optimal control of the wafer chuck	53		
	4.5	Control of the over sensed system	55		
		4.5.1 Active damping	55		
		4.5.2 Conclusion	60		
	4.6	Conclusion	61		
5	Design rules for over-actuated systems				
	5.1	Guide for creating an over-actuated system	63		
		5.1.1 Step 1: Work towards symmetry in the geometry	63		
		5.1.2 Step 2: Material choice	64		
		5.1.3 Step 3: Define actuator locations and chuck cavity	64		
		5.1.4 Step 4: Define the positions of the sensors	66		
6	Conclusions and Recommendations				
	6.1	Conclusions	68		
	6.2	Recommendations	70		
A	Add	itional measurements on the chuck	72		
	A.1	Measured mode shapes of the chucks	72		
	A.2	Actuators and their mounting	75		
		A.2.1 Balance masses	75		
		A.2.2 Actuators	75		
В	Add	itional measurements on control of the chuck	78		
	B.1	Transfer functions of the system	78		
	B.2	Transfer function of the decoupled system including damping channel	80		
	B.3	Analytical addition of damping of the second eigenmode	80		
C	Exp	eriment Description	85		
_	C.1	Starting the control system	85		

Summary

One of the future challenges in the design of semi-conductor manufacturing equipment is the introduction of 450 mm wafers. The wafer chuck supporting the 450 mm wafer is controlled in an active position feedback loop. It is assumed the wafer chuck behaves as a rigid body. In order to limit internal flexibility, the eigenfrequencies of the chuck are kept high, leading to a thick chuck with a large mass. With the continuous demand for higher throughput, this results in enormous acceleration forces leading to large power consumption and heat dissipation. The high acceleration forces may also perturb accurate machine components.

The topic of this thesis is the analysis of a lightweight 450 mm chuck with low stiffness. It uses over-actuation to deal with the flexible modes. The chuck is optimised so that the four actuators of the system do not excite the first five flexible modes of the chuck. With this lightweight system, the same performance can be achieved as with a thick and heavy chuck. The result is shown in Fig. 1(a). It can be seen that the eigenmodes are excited less than in the conventional situation. The expected result was no excitation of the first five eigenmodes. This report describes the research that has been carried out on the cause of the unwanted mode excitation. The performance of the chuck has been examined as well.

A lack of symmetry proved to be an important factor in the mode excitation. Masses added to the chuck in an a-symmetrical way caused the modes to be excited by the actuators. This however doesn't fully explain the excitement of the modes. Further research is recommended on the excitation of the eigenmodes. The mode excitation can be reduced by increasing the damping of the internal modes, making the system less sensitive to actuator placement.

The standstill servo error STD of the over-actuated system is 4.4 nm in Z-direction, the conventional system has an error STD of 26 nm in Z-direction. This result is accomplished with three decoupled SISO PID controllers. An extra sensor is added to the system. The extra sensor enables the first eigenmode to be distinguished from the rigid body movement. This allows the first mode to be damped by using the four actuators. The over-actuated system in this configuration has a servo error STD of 2 nm.

As a recommendation for the design of future over-actuated systems a step by step guide is presented. The most important conclusions on the future design of over-actuated systems are the necessity of adding internal damping and optimizing the positioning of the sensors.

CONTENTS vi

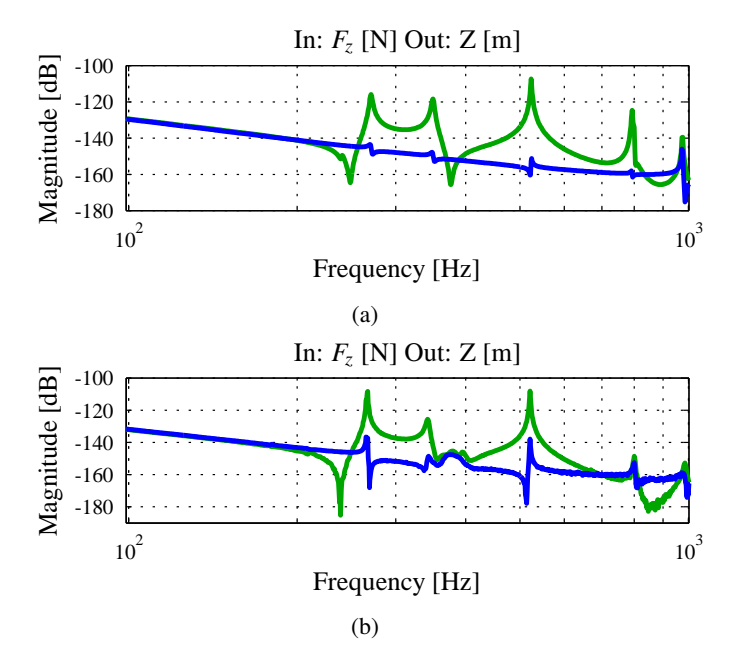


Figure 1
Transfer function of a chuck using conventional (—) actuation and over-actuation (—). The excitation of the first eigenmodes is significantly reduced in the over-actuated system. The FEM model of the system is given in (a), the measured system is given in (b). The excitation of the eigenmodes in the measured system is bigger than in the model.

Chapter 1

Introduction

1.1 Background

In the semi-conductor industry, chips are produced on wafers. A wafer is a thin slice of silicium that is used as base material for the production of chips. The currently used wafers, are 300 mm in diameter. A wafer has to be positioned with nanometer precision in several high-precision manufacturing equipment for the production steps. The need for cost reduction and increased throughput introduces the necessity of considering the production of 450 mm wafers.

One of the future challenges in the design of semi-conductor manufacturing equipment is the introduction of the 450 mm wafers. In these machines the wafer is generally held and positioned on a wafer chuck with nanometer precision. The position of the wafer chuck is controlled in an active position feedback loop, where it is assumed that the wafer chuck behaves as a rigid body. As the wafer area increases, so does the chuck's surface. To limit internal flexibility and keep internal eigenfrequencies at high levels, the chuck's thickness has to be increased as well. Increasing the dimensions of the chuck with a factor 1.5, means a volume increase of 1.5 to the third power. This leads to a significantly increased mass. In combination with the continuous demand for higher throughput, this results in enormous acceleration forces. High acceleration forces risk perturbing accurate machine components, leading to large power consumption and heat dissipation.

1.2 Over-Actuation

A first alternative of rigid body control is to deal with the chuck's flexible modes in the position control loop directly, so called modal control [3]. In modal control the number of actuators (over-actuation) and sensors (over-sensing) are increased with respect to the rigid body degrees of freedom (DoFs). Combined with a high order controller, the internal stiffness of the flexible chuck can be improved through control technical means. This method leads to additional control complexity and to added component costs.

A second alternative is to control the chuck with four instead of three actuators. The actuators are positioned at an optimized location in a mechanically optimized chuck. The smart optimization procedure and actuator placement increase the system's

performance with only one additional actuator and no increased control complexity.

The purpose of this project is to do a feasibility study on the second alternative. This concept uses over-actuation of a thin chuck. This means that more actuators than necessary are used to control the chuck. In this case, four actuators control three degrees of freedom (DoFs). The actuators are positioned such, that they do not excite the first five internal eigenmodes of the chuck. A test setup is built by MI-Partners to demonstrate the principle of over-actuation.

1.3 Problem statement

The over-actuated test setup, built by MI-Partners, proved that the concept of over-actuation is promising and indeed results in a better standstill performance in the controlled degrees of freedom. The system is designed such, that the first five internal eigenmodes should not be excited. In the over-actuated test setup the modes are excited by the actuators. This means there is a mismatch between the model and the test setup. However, the excitement of the eigenmodes in the over-actuated system is less than when using the conventional system with three actuators. The mode excitation in the over-actuated system can be seen in the system transfer function as small resonance peaks at the resonance frequencies that should not be excited.

The purpose of this thesis is:

- Study the behaviour of the chuck and identify the causes of the model mismatch
- Study the control and performance of the wafer chuck
- Create design rules for the design of future over-actuated systems

1.4 Outline

This thesis is a part of research performed to introduce over-actuated systems in industry. The research has been done on the first over-actuated test setup at MI-Partners. In Chapter 2 an overview is given of the optimization theory and the procedure that is used to design the test setup. Chapter 3 consists of the dynamic properties of the test setup. In this chapter the model mismatch observed is researched. The control strategies will be given in Chapter 4. In Chapter 5 a step by step procedure will be introduced to design an over-actuated system.

Chapter 2

Topology Optimization

The motion of a flexible structure can be described in modal coordinates using (among others) the eigenfrequencies and mode shapes of the structure. There are several eigenfrequencies in a flexible structure. At each eigenfrequency the structure moves harmonically with the same pattern of deformation. This deformation pattern is called the mode shape, or eigenmode. The mode shapes are different for each eigenfrequency. Since the mode shapes are uncoupled, they can be excited separately. The total structure response can be modelled by the sum of the responses of the individual modes [3].

In Sec. 2.1 the principle of over-actuation will by explained, using a one-dimensional example. The over-actuated principle in the case of a wafer chuck will be discussed in Section 2.2. The optimization performed to design the wafer chuck will be explained in Section 2.3. Finally the mechanical layout of the test setup will be given in Section 2.4.

2.1 Principle of over-actuation

Active control of a simple beam (e.g. Fig. 2.1(a)), generally consists of a beam, a sensor and an actuator. The sensor measures the position of the beam with respect to a metro frame. The actuator creates a force on the beam with respect to a force frame. The system is positioned by a controller. The beam presented here can be controlled in the indicated Z direction. The performance of the beam is limited by the eigenmodes of the beam. When the beam is excited with a frequency that is equal to the resonance

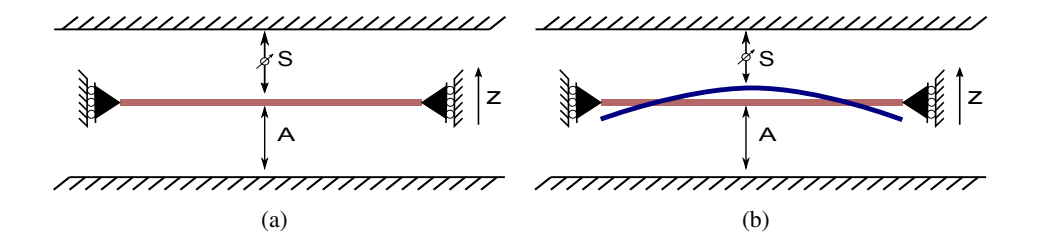


Figure 2.1

Typical control of a simple beam with one sensor and one actuator (a), excitation of the first eigenmode by the actuator (b).

frequency, the beam behaviour no longer corresponds to pure rigid body motion. The motion of the beam is determined by the rigid body motion and mostly the mode shape that is linked to that resonance frequency. Figure 2.1(b) shows the excitation of the first eigenmode due to the actuator. The dynamics of the beam can be expressed by its rigid body modes and all the internal eigenmodes of the beam [3]. The displacement of the beam at sensor location D(s), due to force F(s) can be described by a combination of it's rigid body modes and internal modes:

$$\frac{D(s)}{F(s)} = \sum_{i=1}^{\infty} \frac{c_{mi} \cdot b_{mi}}{m_i s^2 + d_i s + k_i}$$
 (2.1)

Where:

m_i: Modal Mass

 k_i : Modal stiffness

di: Modal damping

 c_{mi} : Modal sensor contribution

 b_{mi} : Modal actuator contribution

In this case, i=1 indicates the rigid body mode. The modal sensor contribution, c_{mi} , can be seen as the relative gain of the deflection of the beam at the sensor location. A sensor placed in the middle (Fig. 2.1(b)), is placed at the position where the deflection of the beam due to the first mode is at its maximum. The modal sensor contribution will therefore be one. If the sensor would be placed at the position where the deflection of that mode is zero, the so called node of the eigenmode, the modal sensor contribution will be zero. In this case the particular eigenmode would not be visible in the transfer function of Eq. 2.1.

The modal actuator contribution is, like the modal sensor contribution, proportional to the mode shape at the actuator location. When the actuator is positioned at the node of the eigenmode the actuator contribution of that eigenmode will be zero. The eigenmode will not be excited by the actuator and therefore will not be visible in the transfer function. Another way of not exciting a mode is when more actuators are used with opposite modal contributions. The total contribution of that mode cancels out and the mode is not excited. This actuation principle, called symmetric actuation, is another way of not exciting a flexible mode. A graphical representation of this effect can be seen in Fig. 2.2.

Figure 2.2 and Eq. 2.1 show two ways of making sure that a flexible mode is not visible in the transfer function. The first is to make sure the specific eigenmode is invisible for the sensors (unobservable). The eigenmode may be excited by the actuators, but can not be seen by the sensors. The second is to make sure the actuators are unable to excite the eigenmode (uncontrollable). The eigenmode can be observed by the sensors, but since the actuators will not excite the mode, the eigenmode will be absent in the transfer function.

The second method, the method to position the actuators in the node of the eigenmodes, is used in the over-actuated concept. The position of the actuators is optimized,

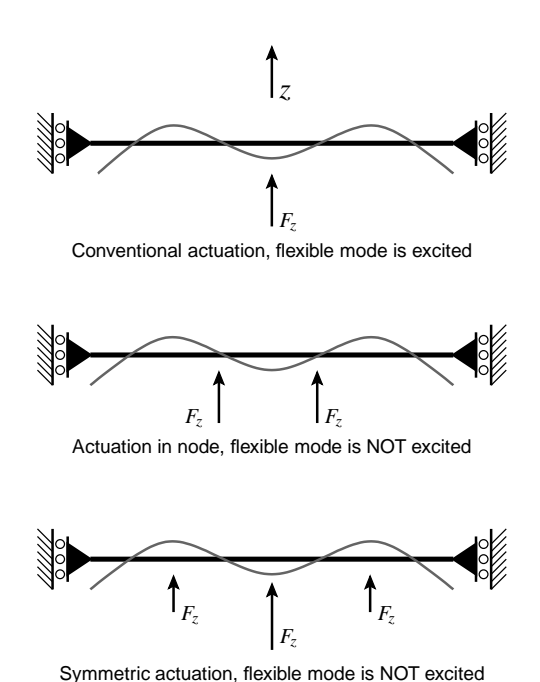


Figure 2.2 *Effect of actuator location on excitation of a flexible mode.*

in order to significantly reduce the excitation of specific eigenmodes. This allows actuation of large, flexible structures without exciting critical flexible modes. To limit the number of actuators required, the mechanical structure can be optimized such, that node locations of several modes coincide.

2.2 Over-actuation of a wafer chuck

Symmetrical actuation and actuation in the nodes of the eigenmode is also possible with a multi-DoF system. The flexible modes of a wafer chuck have a performance limiting influence in the planes perpendicular to the wafer surface $(Z, R_x \text{ and } R_y)$, since these directions contain the eigenmodes with the lowest eigenfrequencies. Overactuation in these degrees of freedom will be useful. The first five eigenmodes of a wafer chuck are presented in Fig. 2.3. In order to place the actuators in a manner that they do not excite the internal eigenmodes, the actuators have to be placed on the node lines. The node lines of the first five eigenmodes are indicated in Fig. 2.3(f).

Placing actuators on the diagonals has the effect that the first eigenmode is not excited due to symmetrical actuation and the second eigenmode is not actuated either, because the actuators are placed on the node lines of the second eigenmode. It is impossible to simultaneously avoid excitation of the first five modes, because there is no location where all the node lines coincide. An optimization procedure can be performed in order to shift the node lines such that they do coincide on the diagonals.

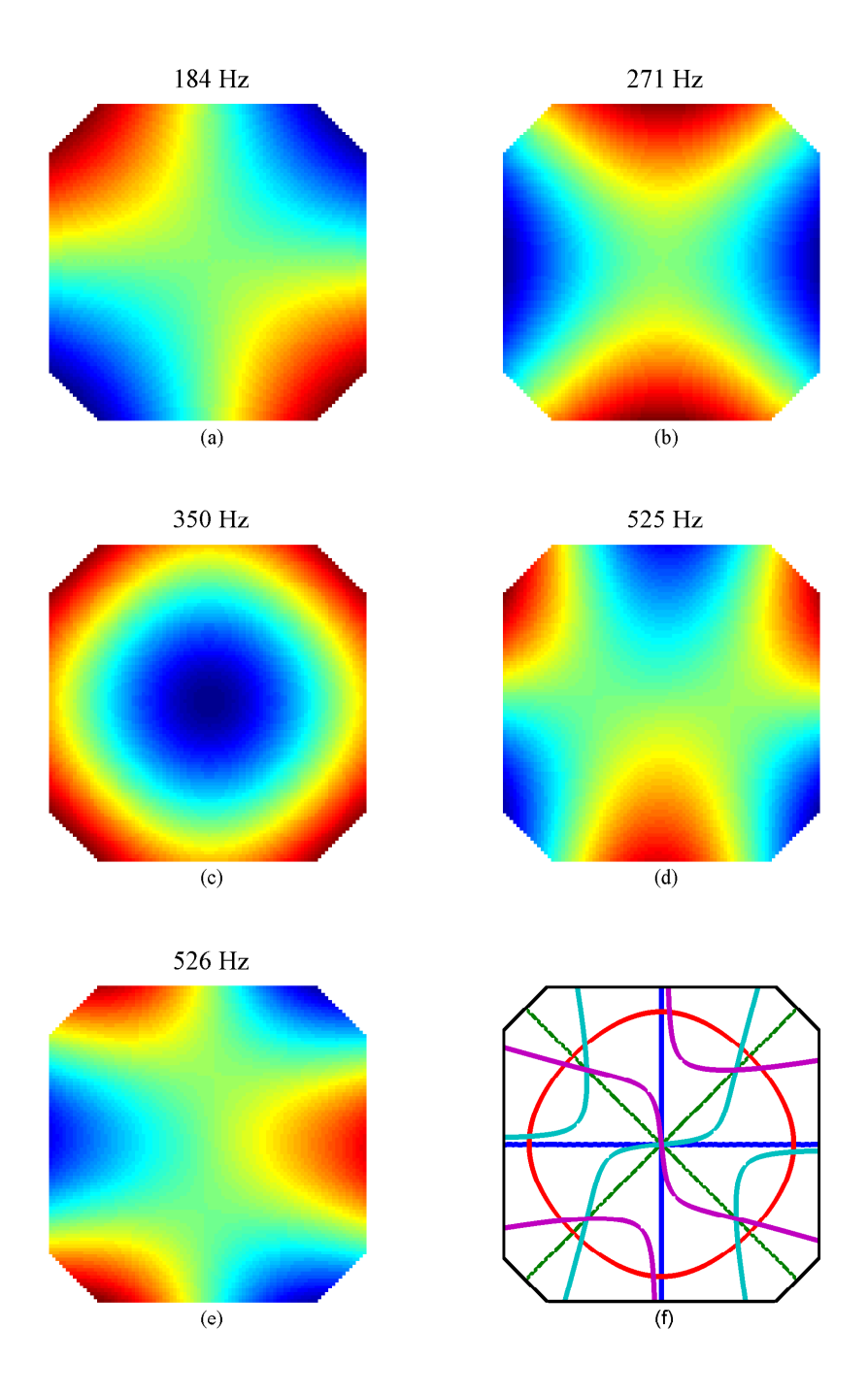


Figure 2.3

First five eigenmodes of the 450 mm wafer chuck (a-e), red means positive deflection, blue means negative deflection. The node lines of these eigenmodes are given in (f).

2.3 Topology Optimization Procedure

A conventional linear mechanical system with low proportional damping is described by Eq. 2.2. This system can be transformed into modal coordinates using the modal eigenvectors [9].

$$M_g \ddot{\mathcal{X}}_g + D_g \dot{\mathcal{X}}_g + K_g \dot{\mathcal{X}}_g = \vec{F}_g \tag{2.2}$$

The general eigenvalue problem of Eq. 2.3 gives the eigenfrequencies and corresponding eigenvectors.

$$K_{\varrho} \cdot \vec{\phi}_i = \omega_i^2 \cdot M_{\varrho} \cdot \vec{\phi}_i \tag{2.3}$$

The matrix of eigenvectors, Φ , decouples the coupled equation of motion of Eq. 2.2 into decoupled modal equations.

$$M_q \ddot{\vec{q}} + K_q \vec{q} = \vec{F}_q \tag{2.4}$$

Where $M_q = \Phi^T M_g \Phi$ and $K_q = \Phi^T K_g \Phi$ are diagonal matrices. The modal damping matrix is defined equally and is diagonal, because proportional damping is assumed [3]. Figure 2.4 graphically illustrates the modal decomposition of a mechanical structure.

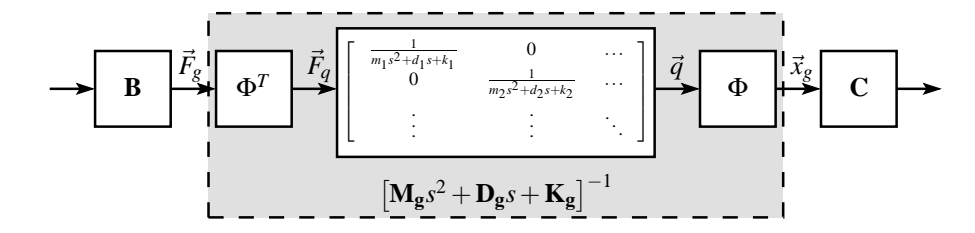


Figure 2.4 Conventional mechanical system of the form $M_{\vec{g}}\vec{x}_g + D_{\vec{g}}\vec{x}_g + K_g\vec{x}_g = F_g$ and its modal representation. Where $\bf B$ is the input matrix, $\bf C$ the output matrix and Φ the matrix of eigenvectors.

The node lines of the wafer chuck, as shown in Fig. 2.3(f), do not coincide. The eigenvector, Φ , containing the mode shapes, has to be changed so that the node lines do coincide. In order to change the node lines of the first five eigenmodes, the topology of the chuck has to be changed. By inserting a cavity in the middle of the plate, the node lines of modes three to five will change [8]. By varying the input matrix, **B**, the location where the eigenmodes coincide is found. The optimization procedure consists of the wafer chuck with a cavity with varying diameter, d. The actuator locations are varied along the diagonals to search for an optimal actuator location for each cavity diameter.

In order to find this optimal actuator location and cavity diameter, a criterion is created. The criterion to be minimised is based on the input matrix \mathbf{B} and the eigenvector Φ . The product of input matrix and eigenvector gives a measure of mode excitation.

Taking the norm for the five first eigenmodes and minimizing this norm, gives the optimal actuator location and cavity diameter. Since there are three load cases (j = 3; Z, R_x , R_y) there are three norms, one for each load case. The total norm of these three load cases will be used for the optimization criterion. This means that for each load case the actuators will excite the chuck in the nodes of the first five eigenmodes. The total excitation norm is given in equation 2.5.

$$N_j^2 = \sum_{i=1}^5 (\phi_i^T \cdot B_j)^2 \qquad N_{total}^2 = \sum_{j=1}^3 (N_j)^2$$
 (2.5)

The optimization of the chuck was focused on the degrees of freedom that are perpendicular to the wafer surface (Z, R_x, R_y) . The other DoF are constrained using plate springs. The dynamics of the chuck are calculated using Finite Element Method with Ansys[©] software. A Matlab[©] script automatically generates an Ansys[©] input file and retrieves the modal parameters from Ansys[©]. The calculation of the excitation norm is performed by Matlab[©]. In order to find the excitation norm, the eigenmode vector created by Ansys[©] is multiplied by the actuator vector. The actuator vector is a vector of zeros with a one at the positions where an actuator is placed. All the items that could have influence on the position of the node lines have to be included in the optimization. The Ansys[©] model therefore consists of the wafer chuck including the plate springs, actuators and gravity compensators. The complete optimization procedure can be found in [2].

The result of the optimization can be seen in Figure 2.5(a). The node lines coincide at four points on the diagonals. This is the position where the actuators will be placed. The cavity diameter is 446 mm and the position of the actuators is at (134,134) mm on the diagonals.

2.4 Mechanical layout

The over-actuated system built to demonstrate the over-actuated concept will be briefly described here. A report of the design and build progress can be found in [2]. The test setup consists of a base frame, positioned on the floor via spring-damper systems. The spring damper system should provide a low, well damped, suspension frequency of the base frame in the order of 10 Hz. On top of this base frame a glass plate, representing a wafer chuck is mounted with three plate springs. The plate springs provide constraints in X, Y and R_z directions and eigenfrequencies in Z, R_x and R_y directions in the order of 10 Hz. Figure 2.5(b) shows the base frame with the wafer chuck made of glass.

Five 'moving magnet' actuators are mounted on the chuck. The coils of the actuators are mounted to 1 kg balance masses. The balance masses are mounted on the base frame. The well-damped eigenfrequency of the balance masses are around 50 Hz. Four actuators are placed at the optimized actuator positions. The fifth actuator is positioned at the conventional actuator location. This test setup can therefore be controlled by an over-actuated controller, or a conventional controller.

Three linear encoders are mounted on the base frame and monitor the position of the chuck at the two top corners and in the middle at the bottom of the chuck. A schematic view of the wafer chuck is shown in Fig. 2.6. Based on the information of the linear encoders, the Centre of Gravity (CoG) movement can be reconstructed.

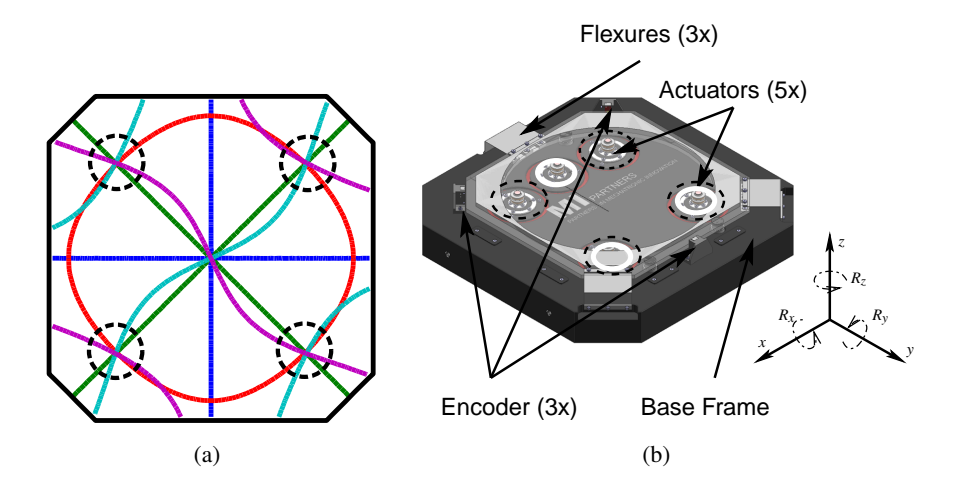


Figure 2.5
(a) Resulting nodal lines of the first five flexible modes. The optimized cavity diameter is 446 mm. The actuators are positioned in the four points on the diagonals where the node lines intersect. (b) Realised test setup. The chuck can be actuated using the four actuators at the optimized locations (dashed lines), or the chuck can be actuated by conventional three-point actuation (white lines)

The controller outputs for the Z, R_x and R_y directions are converted to proper actuator forces by a static transformation matrix.

The transfer function of the traditional actuated wafer chuck in Z-direction contains the first five eigenfrequencies. In the over-actuated wafer chuck the eigenfrequencies can not be seen in the transfer function. Figure 2.7 shows the transfer functions of the traditional and over-actuated system from actuator force to Z-direction. A measured result is also presented. The over-actuated system model excites the first five eigenmodes in the transfer functions around 30dB less than the traditional actuated model. The measured excitation is higher than expected from the model. The difference between the measured over-actuated system and the conventional actuated model is reduced to 20dB. In order to reveal the causes of this unexpected behaviour, an extensive research will be performed in Chapter 3.

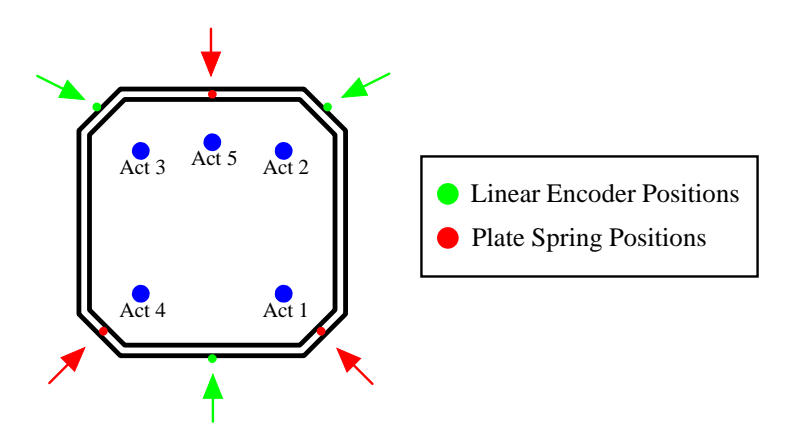


Figure 2.6 Schematic overview of the wafer chuck. The red dots indicate the positions where the plate springs are mounted. The green dots represent the sensor positions. The actuators are numbered 1 to 5.

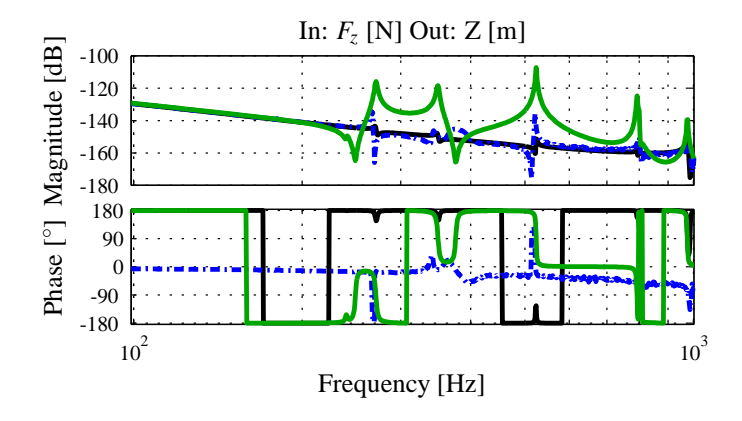


Figure 2.7

Transfer function of actuator force to chuck displacement in Z-direction. The modelled traditional actuated chuck (--) shows a higher mode excitation than the modelled over-actuated chuck (--). A measured result of the over-actuated controlled chuck (--) shows more mode excitation than modelled.

Chapter 3

Dynamic properties of the wafer chuck

The test setup, created by using the optimization procedure in Chapter 2 shows promising results. The excitation of the first five eigenmodes has reduced significantly. The expectation was that the first five eigenmodes will not be excited at all. The first measurements show that the first five eigenmodes are still excited, although less than the conventional system. The transfer function of the conventional and the over-actuated system is shown in Fig. 3.1. The excitation of the internal eigenmodes of the system is reduced significantly, but the excitation is still visible. In an active control loop the excitation of the eigenmodes is still performance limiting.

In this chapter a closer look will be taken at the system in order to study the dynamical behaviour of the over-actuated system. This includes the identification of possible causes for the excitation of the eigenmodes. A modal analysis of the chuck will give a clear indication of the problem in Section 3.1. In Section 3.2 the problem is described and the possible causes are given. In Section 3.3, the different parts that may cause the problem are studied. The model of the system is reviewed in Section 3.4. Research to improve the current setup is decribed in Section 3.5.

3.1 Modal Analysis

In order to identify the mode shapes and node lines of the first five eigenmodes of the chuck, a modal analysis is performed on the chuck. To reconstruct the dynamics of the chuck, the modes have to be excited properly and many sensors will have to be placed on the chuck. The actuators present in the system can be used to excite the chuck. Especially the fifth actuator is able to excite the flexible modes. Lightweight accelerometers are used as sensors for this measurement. They have little mass and therefore have a minimal influence on the mode shapes.

Glass chuck

Figure 3.2(a) shows a schematic overview of the glass chuck with the actuator and accelerometer positions. Four accelerometers are used to measure the accelerations of the glass chuck at the indicated positions. Based on the measured frequency responses

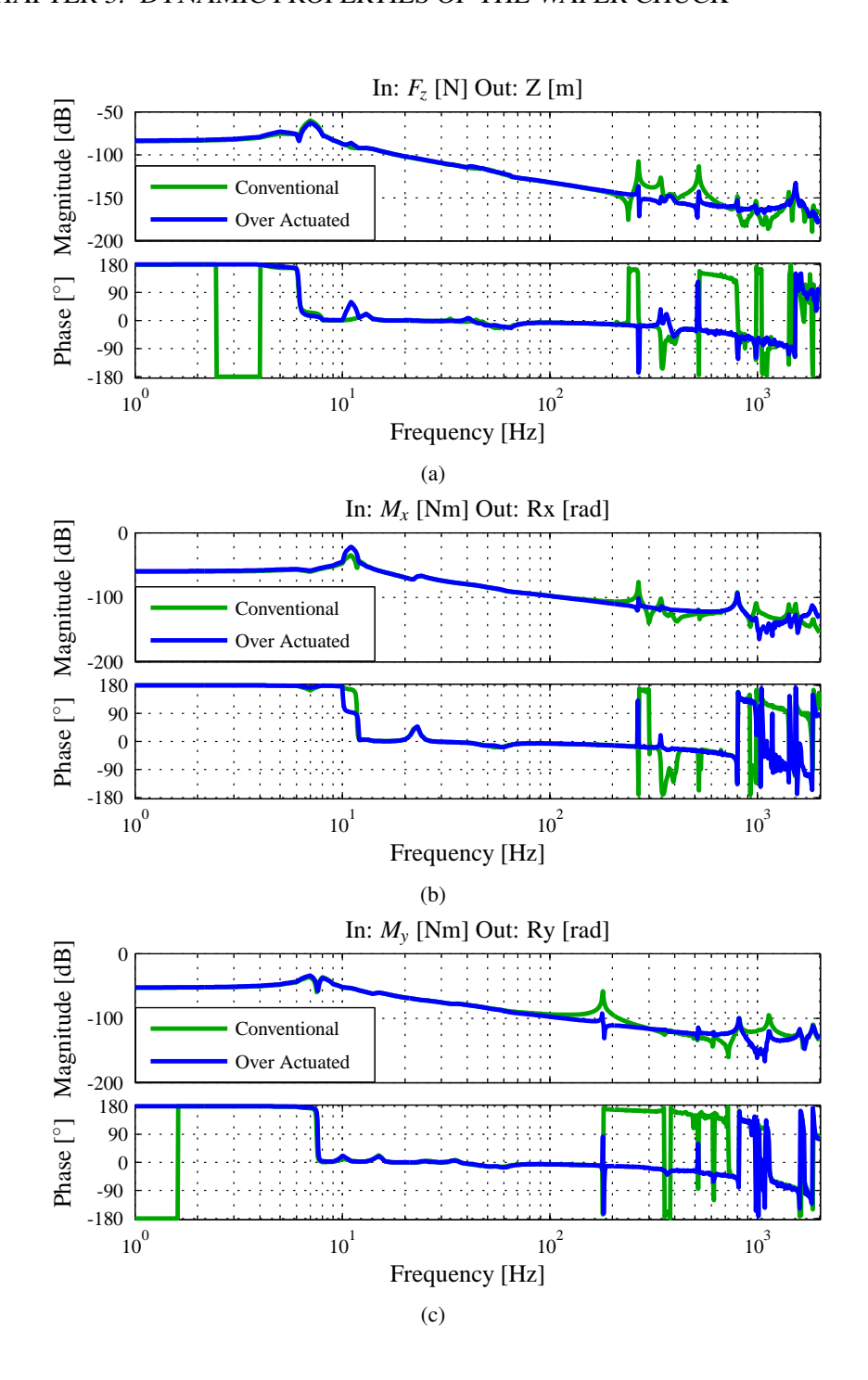


Figure 3.1 Transfer function of the overactuated (—) and conventional (—) system in Z, (a), R_x (b), and R_y , (c) direction. The conventional actuated system excites the internal eigenmodes. The over-actuated system shows less mode excitation than the conventional system. The over-actuated system is designed not to excite the first five eigenmodes. In this chapter effort has been made to investigate the reason for the mode excitation by the over-actuated system.

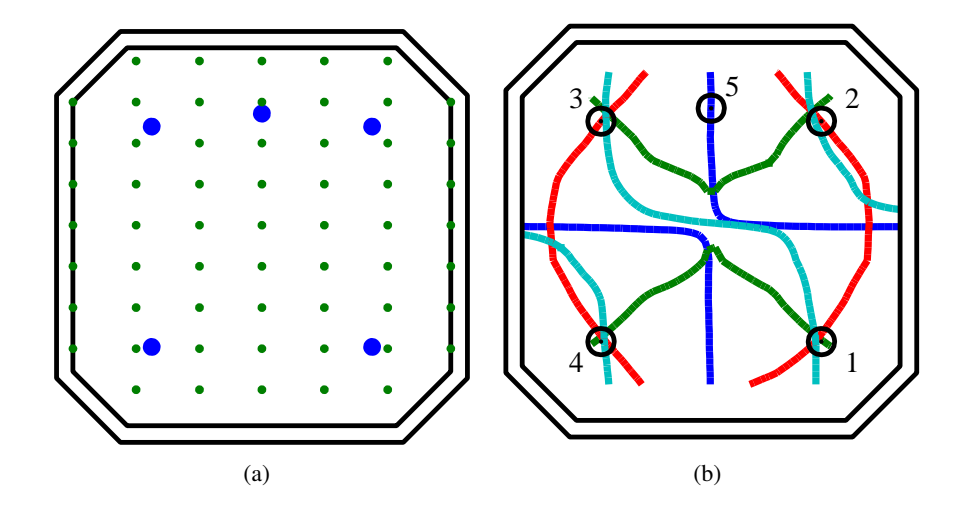


Figure 3.2
(a) Schematic overview of the glass chuck with indicated actuator positions (•) and accelerometer positions (•) . (b) Measured node lines of the first four eigenmodes. The optimized actuator positions are indicated.

the modeshapes can be reconstructed. The measured modeshapes can be found in Appendix A.1, Fig. A.1 on page 73. The first three modeshapes are relatively easy to spot. The fourth and fifth modeshape are only visible as a superposition of each other because these eigenmodes occur at about the same frequency. The node lines of the extracted eigenmodes are given in Figure 3.2(b).

The node line belonging to the first eigenmode (—) is located as predicted on the axes of the glass chuck. Note that a good measurement of the centre of the chuck is difficult, as almost all the eigenmodes have zero deflection at the centre. The second eigenmode should have it's node line on the diagonals of the chuck (—). Again, the information at the centre of the chuck is difficult to measure and therefore not very accurate. At the lower half of the chuck, the node lines are indeed at the diagonals and the actuators will therefore not excite this eigenmode. At the upper half of the chuck, the node lines are not at the diagonals of the chuck, which means that the second eigenmode is excited by actuators 2 and 3. The node lines of modes three (—) and the combined fourth and fifth mode (—) show a small offset of the calculated optimal position at different actuator locations.

The most unexpected difference in the positions of the node lines is the position of the node line of the second eigenmode (—). The mode shape of this eigenmode is unaffected by the cavity being cut out of the chuck, as was intended in the optimization procedure [2, 8]. The mode shape is expected to be symmetric along the diagonals, because the chuck is symmetric. The difference in symmetry can also be seen in the transfer function of different actuator forces to the upwards (Z) movement of the chuck, Figure 3.3. The second eigenfrequency, at 267 Hz, is hardly excited by actuators 1 and 4. Actuators 2 and 3, excite this eigenfrequency a factor 3 (10 dB) more. The third (340 Hz) and combined fourth and fifth (520 Hz) eigenfrequencies are also more excited by the top actuators.

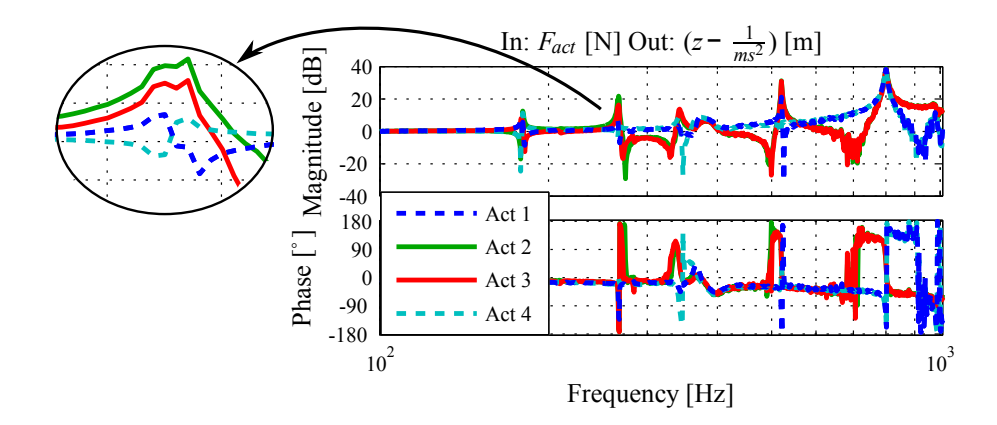


Figure 3.3

Transfer Function of the Z-movement of the glass chuck due to the different actuator Forces.

Aluminium chuck

The node lines of the first five eigenmodes are measured the same way as the glass chuck. They are expected to pass through the actuators. Figure 3.4(a) shows the measured node lines. In general the shape matches the expectation quite well, but when a closer look is taken at the position of actuator 2, it can be seen that the node lines coincide at another position. The actuator position is measured to be about one cm off. This is a large difference in comparison to the FEM calculations where the actuator position error was less than one millimeter.

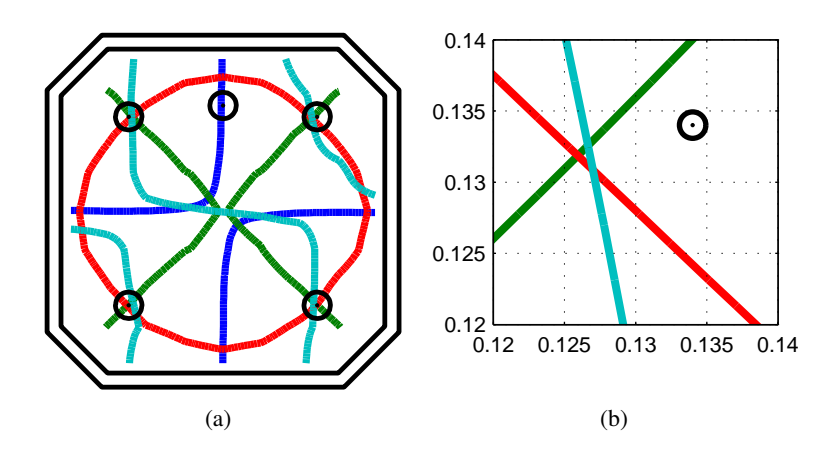


Figure 3.4 Measured node lines of the first four eigenmodes of the Aluminium chuck. The optimized actuator positions are indicated (a). Detailed view around the second actuator (b).

Conclusion

The modal analysis of the glass and aluminium chuck show mismatch between the calculated locations of the node lines and the measured node lines. Figures 3.2(b) and 3.4 indicate that the symmetry the chucks are supposed to have, is absent. The reason for this mismatch has to be studied. In section 3.2 the problem is described and research topics are given.

3.2 Problem description

The modal analysis of the chuck shows that actuators two and three excite the internal eigenmodes of the chuck, while actuators one and four are positioned so that the eigenmodes are not excited. The node lines of the five first internal eigenmodes do not intersect at the position of the top two actuators. This leads to the following research challenge:

Study the dynamics and properties of the over-actuated wafer chuck in order to find possible causes for the excitation of the eigenmodes by the actuators.

The following parts of the system will be studied in order to find out the influence on the node lines of the chuck:

• Suspension

The suspension is designed to provide a low-stiffness support of the chuck. If the rigid body frequencies of the chuck are too high-frequent, the suspension may influence the flexible modes of the chuck.

Plate Springs

The plate springs are mounted in a position that is not symmetric. One clearly visible effect of the plate spring positions can be seen in the rigid body modes. The rigid body mode in R_x direction shows a rotation around a fictitious line with function y = c, where c > 0. The internal dynamics of the chuck may also be affected by the plate springs

• Gravity compensators

The chuck is supported in Z-direction with four gravity compensators. These gravity compensators causes a-symmetry in the chuck. The four gravity compensators may influence the node lines of the chuck.

• Actuator

The position of the fifth actuator may cause the node line to change. The fifth actuator also causes a-symmetry in the chuck.

• Chuck

One chuck is made of two pieces of glass that are glued together. Tolerances in the glueing process, or different contact pressure during the glueing process may have influenced the node lines of the glass chuck. The other chuck is made of aluminium. In this chuck, the mechanical tolerances are more tight. However, the aluminium chuck shows some plate warp perpendicular to the surface. This might have influence on the internal eigenmodes.

3.3 Dynamic analysis

In this section, the suspicious parts of the system are studied. Two wafer chucks are available for testing. A glass chuck and an aluminium chuck. The glass chuck is manufactured from two pieces of glass. The bottom piece with the cavity and a top piece. The two pieces are glued together. The aluminium chuck is fabricated of one solid piece of aluminium. The tolerances of this chuck are more tight and therefore the chuck is expected to be more symmetric. The aluminium chuck has extra options to include additional gravity compensators and actuator masses. It has mounting holes for the plate springs in different positions, so that it can be mounted on the base frame in any possible orientation.

3.3.1 Suspension modes

Modal analysis of the base

To find the suspension modes of the base frame, a modal analysis will be performed using a modal impact hammer and accelerometers. The (black) base frame is shown in Figure 2.5(b). The suspension modes in Z, R_x and R_y directions are most important since these directions are measured by the sensors. Accelerometers are placed at the middle of the base frame, at the right end, on the X-axis and at the bottom, on the Y-axis. The modal impact hammer will excite the system at the same points.

The R_x eigenfrequency is assumed to be symmetric with respect to the X-axis and therefore the base frame movement due to the R_x eigenfrequency at the right sensor position is zero. The accelerometer at the right position will therefore only measure the Z and R_y eigenfrequency. The bottom sensor only measures the Z and R_x eigenfrequency and the sensor in the middle only measures the Z eigenfrequency. Exciting the base at the right side results in movement of the frame in Z and in R_y direction. Exciting the base frame at the bottom results in movement of the frame in Z and R_x direction. Out of these three measurements the eigenfrequency of the base frame in Z, R_x and R_y direction can be deducted.

Figure 3.5 shows the acceleration due to the impact hammer with co-located hammer and accelerometer positions. The eigenfrequency in Z-direction of the base frame is just below 6 Hz. The R_x and R_y eigenfrequencies are 21 and 14 Hz respectively. The coherence at the position of the eigenfrequencies is close to 1. This means that the eigenfrequencies can be well deducted out of this figure. With the wafer chuck attached, the eigenfrequencies lower a little bit due to the added mass of the chuck.

The first internal eigenfrequency of the base frame is at 490 Hz. This internal eigenfrequency is of no influence on the measurement of the chuck, because this mode is not excited by the actuators.

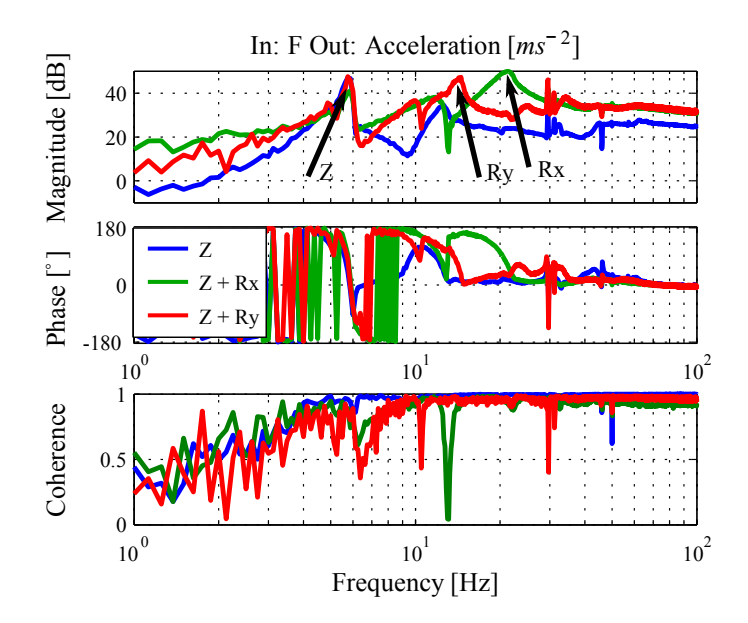


Figure 3.5
Modal Analysis of the base frame without the wafer chuck attached. Sensor and Hammer locations are around the same position in the centre, on the X-axis on the right and on the Y-axis at the bottom of the base frame.

Suspension modes of the chuck on plate springs

The wafer chuck is attached to the base frame with plate springs. The suspension frequency of this system can be monitored by the linear encoders available. The chuck will be actively controlled in two directions. There will be no control in the third direction. The eigenfrequency of the uncontrolled direction will be clearly visible in the output of the sensors. A Fourier transformation will be performed in order to identify the exact eigenfrequency of the chuck. The resulting movement of the chuck is a superposition of the eigenfrequency of the chuck and of the base frame.

Figure 3.6 shows the power spectral densities (PSDs) of the chuck movement in the indicated directions. The eigenfrequencies of the chuck due to the plate springs are 7, 11 and 7.5 Hz in the Z, R_x and R_y directions respectively. The base suspension in Z-direction is clearly visible in the PSD. The base is hardly excited in these rotational directions, therefore the base suspension in R_x and R_y direction are hardly visible. The suspension frequencies are summarised in Table 3.1.

Direction	Base suspension	Chuck suspension
	Frequency [Hz]	Frequency [Hz]
Z	5.2	7
R_{x}	21	11
R_{y}	15	7.5

Table 3.1 Suspension frequencies visible in the wafer chuck and their sources.

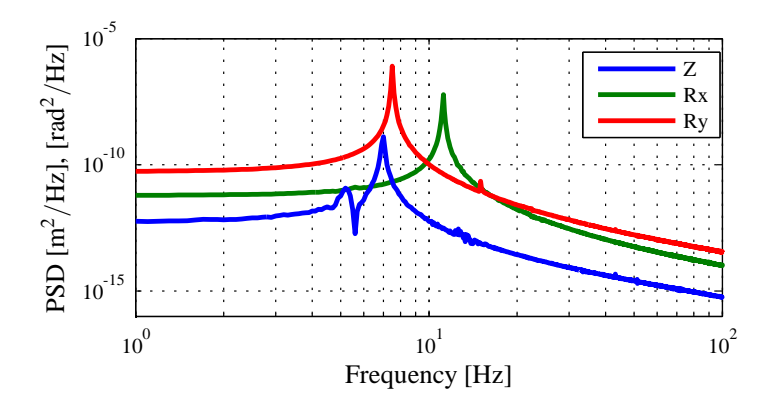


Figure 3.6

Power Spectral Densities of the wafer chuck displacement. The chuck is in control in the two degrees of freedom that are not the direction of measurement

Conclusion

The suspension modes of the chuck are low frequent. This means that the influence of the suspension on the high frequent internal modes is negligible. The internal modes of the base frame are not excited by the actuators, because the balance masses between the actuators and the base frame decouple the movements of the actuator to the base frame.

3.3.2 Plate springs

The chuck is mounted on the base with three plate springs. One plate spring is mounted on top, the other two are mounted at the corners on the bottom of the chuck. The plate springs limit movement in X, Y and R_z directions [6]. The plate springs are mounted so that the node line of the rigid body mode of the wafer chuck in R_x direction doesn't go through the middle of the chuck. The plate springs show no symmetry around the X-axis. The plate springs should provide a low frequency suspension for the wafer chuck. The influence of the plate springs at the resonance frequencies is always assumed to be negligible. On the other hand, the plate springs are a part of the system that make the chuck asymmetric. The excitation of the eigenmodes of the over-actuated system may therefore be caused by the influence of the plate springs.

The plate springs used are made of 0.4 mm thick steel. The first two eigenfrequencies in the constrained directions are Y-translation at 248 Hz and a combination of X translation and Rotation around Z at 325 Hz. The 248 Hz suspension frequency is close to the second eigenfrequency of the chuck at 267 Hz. Movement of the chuck in Y direction may have an influence on the excitation of the second eigenmode. In order to verify that the plate springs have no influence on the internal eigenmodes of the chuck, different plate springs are produced. The 0.4 mm thick steel plate springs will be replaced by aluminium plate springs lowering the two first eigenfrequencies in the constraint direction to respectively 150 Hz and 210 Hz. A comparison of two plate springs in a model shows no significant differences in the frequency region of the first five eigenmodes. Figure 3.7 shows the transfer functions of the modelled over-

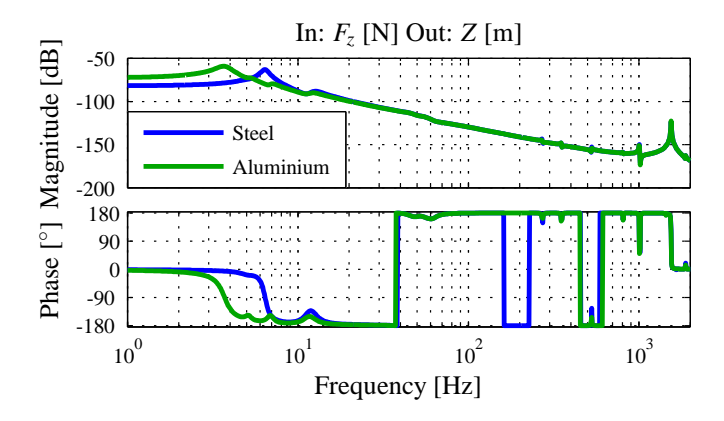


Figure 3.7

Transfer function of the modelled system in Z-direction with two different plate springs. Apart from a lower suspension frequency there are no significant changes.

actuated system in Z-direction. A measured transfer function of the chuck with the different plate springs is given in Fig. 3.8(a). As expected, the suspension frequency of the chuck has been lowered. A second resonance has shown in the transfer function at 6 Hz. The suspension of the base frame at 7 Hz is still dominant.

Figure 3.8(b) shows a detailed view of the transfer function from Actuator 1 and 2 to the Z-direction around 267 Hz, the second resonance frequency. All the actuators excite the second eigenmode. With aluminium plate springs mounted, the excitation of the mode by the different actuators gets around 5 dB lower. The aluminium plate springs have therefore slightly less impact on the excitation of the eigenmodes than the steel plate springs. The gain of the actuators at the second resonance frequency is compared when using different plate springs. The gain of actuator 5 is added for clarity. Table 3.2 shows the comparison.

	Steel pla	te spring	Aluminium plate spring	
	Magnitude [db]	Frequency [Hz]	Magnitude [db]	Frequency [Hz]
Actuator 1	-142	266	-142	267
Actuator 2	-125	267	-126	268
Actuator 3	-123	267	-123	268
Actuator 4	-142	266	-141	267
Actuator 5	-100	267	-100	268

Table 3.2 Actuator gains at the second resonance frequency using different plate springs.

No plate springs

The different plate springs have not given a clarification on the source of the difference in mode excitation by the four actuators. In order to see the effect when there are no plate springs, the chuck can be supported on foam and then tested. The chuck will be supported on foam at each corner for symmetry. The gravity compensators are

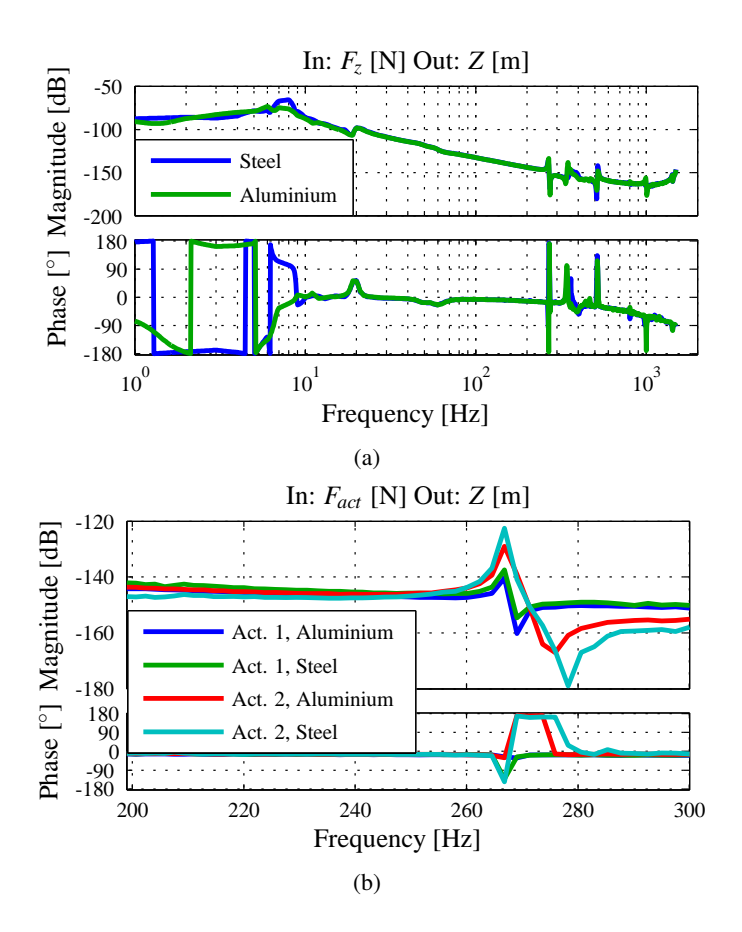


Figure 3.8

Transfer function of the measured system in Z-direction with two different plate springs (a). Detailed view of the excitation of the second eigenfrequency by actuators 1 and 2 with different plate springs (b).

removed on the base, so no static force will be present on the chuck at that position. With no plate springs, the influence of the plate springs on the chuck can't be present.

Because of alignment difficulties with the chuck supported on foam, only the lower encoder is used. The measurement will be performed without actuator 5 attached. Removing the fifth actuator creates symmetry in the actuators. The transfer function from each actuator to the bottom encoder in the frequency region of the second resonance is given in Fig. 3.9. There is a gain difference at all frequencies except the eigenfrequencies. This makes sense, since actuator 1 and 4 are positioned closer to the sensor than actuator 2 and 3. Actuators 2 and 3 still show a higher peak response than actuators 1 and 4. Since the influence of the plate springs is absent, the excitations of the eigenmodes is not due to the plate springs.

Conclusion

With no plate springs attached, the eigenmodes are still excited as much as when the plate springs are attached. The plate springs therefore do not influence the excitation

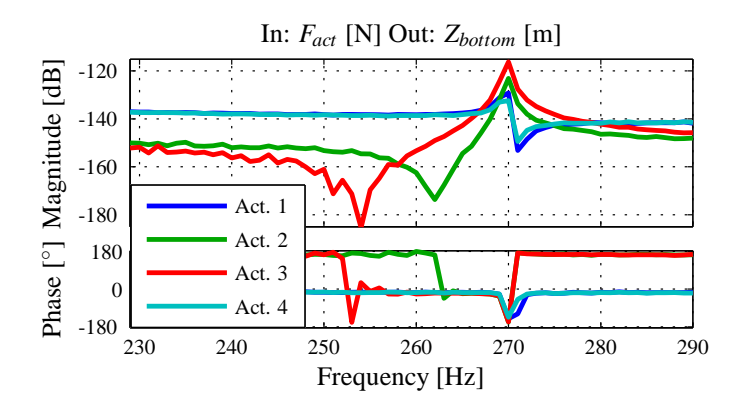


Figure 3.9

Transfer function of the actuators to the bottom sensor. The glass chuck is supported on foam. The plate springs have been removed.

of the internal eigenmodes of the chuck.

3.3.3 Gravity compensators

The aluminium chuck is build with added options to obtain symmetry. The parts that are not symmetric in the chuck are the gravity compensators and the fifth actuator. The gravity compensators can be removed, or extra gravity compensators can be mounted on the chuck. Figure 3.10 shows an overview of the locations of the gravity com-

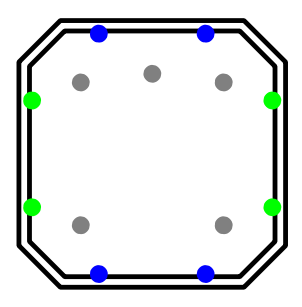


Figure 3.10 Overview of the chuck with gravity compensators in blue, optional extra gravity compensator positions in green. The actuators are plotted in grey.

pensators. With eight gravity compensators mounted, the chuck is more symmetric and the node lines of the second eigenmode should move towards the diagonals. The transfer function of the chuck with four and eight gravity compensators is given in Fig. 3.11(a). It can immediately be seen that the excitation of the second eigenmode hasn't changed. This means that the node line of the second eigenmode hasn't shifted when more gravity compensators are used. The excitation of the third eigenmode has improved significantly with eight gravity compensators. The added mass of the gravity compensators did change the node lines here. The excitation of the first eigenmode,

only visible in R_y direction (Fig. 3.11(b)) has also improved with eight gravity compensators. The symmetry of the gravity compensators proved to be important here.

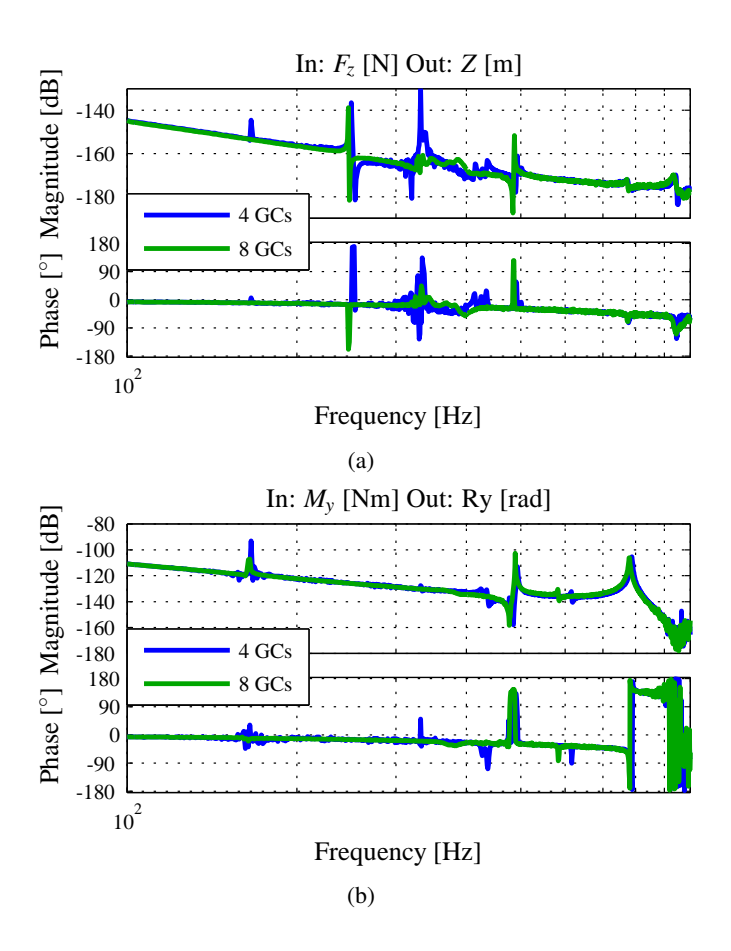


Figure 3.11 Transfer function of the Aluminium chuck with 4 and 8 gravity compensators (GCs) mounted. Z-Direction (a) and R_y direction (b).

Conclusion

The gravity compensators do influence the node lines of the chuck. With eight gravity compensators mounted, the excitation of the first and third mode is reduced. The eigenmodes are still excited when eight gravity compensators are mounted. This indicates that there is still another source that causes the change in node lines.

3.3.4 Actuators

The fifth actuator causes an a-symmetry in the chuck. This a-symmetry changes the node lines of the eigenmodes of the chuck. The node line of the second eigenmode, the green line in Fig. 3.2(b), is likely to move towards the fifth actuator. In this section

the influence on the excitation of the eigenmodes, caused by the addition of the fifth actuator, is determined.

The chuck can be made symmetric by removing the fifth actuator, or by adding three more actuators at the bottom and at the left and right side of the chuck.

Removing the fifth actuator. Removing the fifth actuator results in a symmetric chuck. Figure 3.12 shows the transfer function of the chuck with four and five actuators mounted on the chuck. With only four actuators mounted, the second and fifth

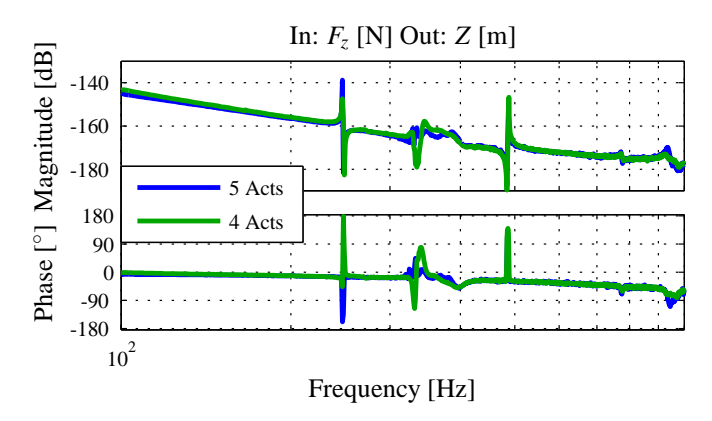


Figure 3.12
Transfer function of the Aluminium chuck in Z direction with four and five actuators mounted. In both situations 8 gravity compensators are mounted

eigenmodes are excited by the actuators. The excitation of the eigenmodes is reduced when four actuators are used.

Eight actuators. Another possibility to create symmetry is to mount extra actuators at the bottom, and the right and left side of the chuck to create symmetry with the fifth actuator. The extra actuators can't be used because an actuator also needs a coil which is absent. The extra actuators therefore act purely as dummy masses to create symmetry. Figure 3.13 shows the transfer function of the aluminium chuck with four and eight actuators mounted. The modes are excited in both situations. The situation with eight actuators shows a small reduction in mode excitaion.

Conclusion

The fifth actuator is a source of a-symmetry and has therefore influence of the position on the node lines. Without the fifth actuator, or with eight actuators mounted, the excitation of the eigenmodes is reduced. The eigenmodes are still excited, meaning there is another cause of the change of the position of the node lines.

3.3.5 Chuck

Two different chucks are used in this research. A glass chuck and an aluminium chuck. Both chucks are designed to be symmetrical. The glass chuck consists of two parts.

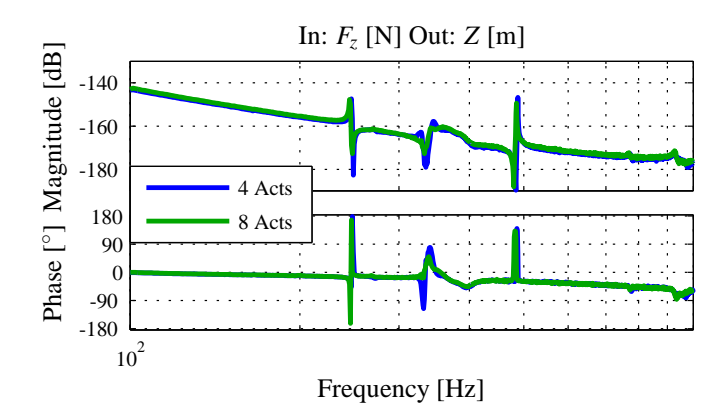


Figure 3.13

Transfer function of the Aluminium chuck in Z direction with 4 and 8 actuators mounted. In both situations 8 gravity compensators are mounted.

The bottom part has the cavity in it and on top, the second part is glued. This glueing process can influence the symmetry of the chuck. The two parts may be misaligned, causing the eigenmodes to change. The glue may also have a different thickness at different positions causing different characteristics. The aluminium chuck is constructed out of one solid peace of aluminium. All the dimensions of the aluminium chuck are referenced from the centre of the chuck to make it symmetrical.

With all the external parts of the system in symmetry, the internal eigenmodes are still excited. In the following section, the properties of the two chucks are analysed.

Glass chuck

The glass chuck is possibly a-symmetric because of its construction method. Figure 3.9 shows the excitation of the second eigenmode of the glass chuck without plate springs attached. The two top actuators, 2 and 3, excite the second eigenmode more than the two bottom actuators. If the excitation of the eigenmodes is due to an asymmetrical chuck or to a problem in the manufacturing of the chuck, the excitement of the eigenmodes in the rotated position should be higher on the bottom of the chuck.

Actuator five will be removed from the glass plate for symmetry purpose and only the bottom sensor will be used, due to alignment difficulties. The transfer function of the rotated chuck, of the four actuators to the bottom sensor, around the second eigenfrequency, is shown in Fig. 3.15. It shows that the actuators at the bottom of the chuck now excite the eigenmode. This indicates that the problem exists in the chuck.

The excitation of the eigenmode is dependent on the actuator location on the chuck, and not on the rotation of the chuck. This becomes evident when a comparison is made between actuator 1 and 3. Actuator 3 in the rotated position, excites the same part of the chuck as actuator 1 in the normal position. The maximum peak height of actuators 1 and 3 in the different rotations are equal to each other. See Fig. 3.16.

The analysis of the glass chuck shows that the glass chuck is not symmetric as it was designed to be. As a result the eigenfrequencies, designed not to be excited by the actuators, still are excited.

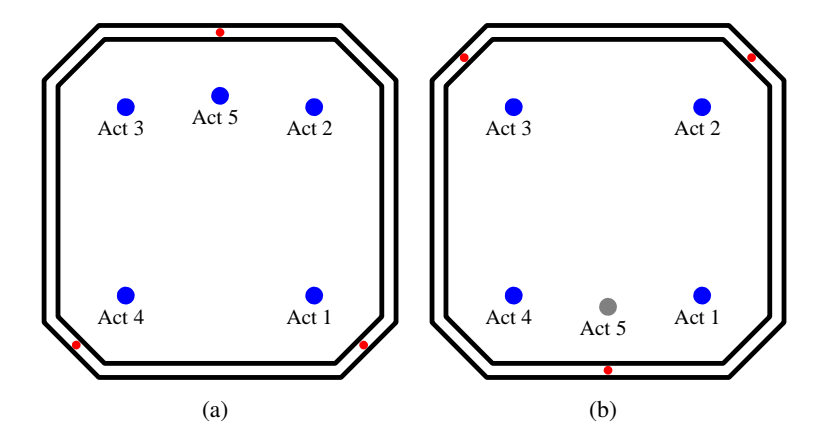


Figure 3.14
Schematic overview of the glass plate in original (a) and rotated(b) position. The red dots indicate the position of the plate spring mounts not attached.

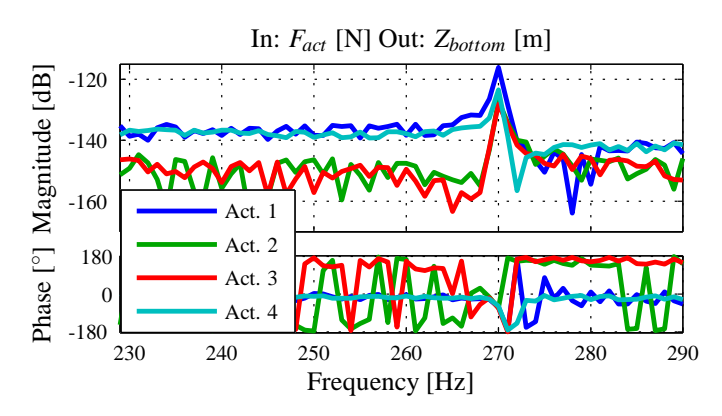


Figure 3.15
Transfer function of the actuators to the bottom sensors with the rotated chuck.
The chuck is supported on foam and the plate springs are not attached.

Aluminium chuck

The second chuck is build in aluminium and all the dimensions are referenced from the centre. The tolerance errors will be the same in each direction and don't add up. The chuck has interfaces to position actuators in eight locations and the plate springs can be mounted in different ways. The chuck can therefore be mounted on the base in 4 different positions, each 90 degrees rotated. A preference position is absent and the chuck can be measured in each mounting position. The gravity compensators can be mounted in 8 positions. With these modifications, the system can be build fully symmetrical.

The difference in the transfer functions between the glass and the aluminium chuck in Z-direction are shown in Fig. 3.17. The first thing to be noticed is the shift in the resonance frequencies. This is due to a different mass and E-modulus. A detailed view shows there is no improvement in the excitation of the eigenmodes. The excitation of

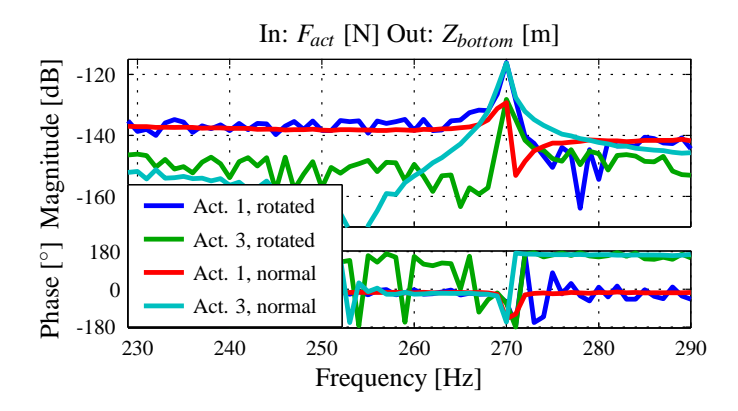


Figure 3.16
Comparison of the transfer functions of actuators 1 and 3 in the normal and rotated situation. This figure indicates that the excitation of the eigenmode is dependent on the position of the chuck and not on the rotation of the chuck.

the second and third eigenfrequencies, around 250 and 330 Hz, became worse. The fourth and fifth eigenfrequencies are less visible at the aluminium chuck. There is no influence of the rotation of the aluminium chuck on the mode excitation. The mode excitation of the aluminium chuck is still present.

Conclusion

The different chucks do have influence on the mode excitation. The glass chuck shows a clear position dependence. The aluminium chuck, designed to be better in symmetry, has less position dependence. The eigenmodes are still excited by the actuators. An explanation for the difference in position of the node lines has not been found. A possible cause for this is plate warp perpendicular to the chuck surface. The aluminium chuck shows a lot of plate warp. This influences the excitation of the eigenmodes of the aluminium chuck.

3.4 Model improvements

The results of the aluminium chuck are not as expected. The node lines of eigenmodes 2-5 should all go through the same point at the location of the actuators. The excitation of these eigenmodes, visible in the transfer functions, indicate that the node lines are not at the position of the actuators. The FEM calculations performed may be erroneous. It appeared that the density of the actuators and gravity compensators were not correctly implemented in the model. Figure 3.19(a) shows the node lines of the chuck. Figure 3.19(b) shows a detailed view of the node lines around the actuator position. In the original calculation all these lines should be on top of each other within one millimeter accuracy. The corrected densities in the Ansys calculation give a slightly different result. From geometry and symmetry point of view the green line should always go through the diagonals. In this case it doesn't, which shows the influence of the gravity compensators and the fifth actuator.

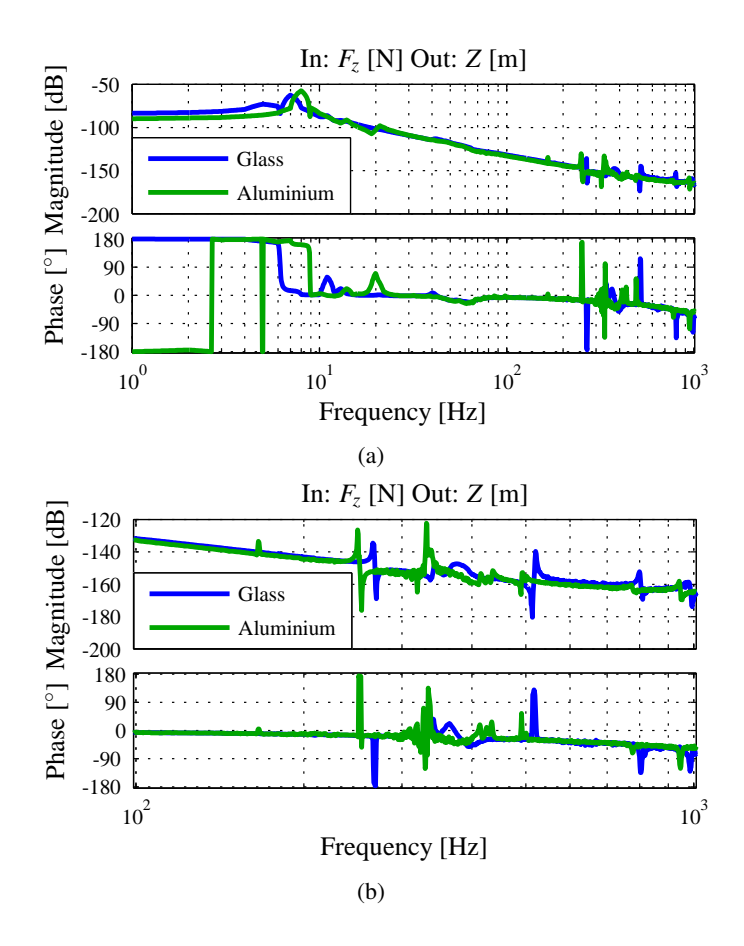


Figure 3.17
Transfer function in Z-direction of the Glass chuck and Aluminium chuck (a). Detailed view between 100 and 1000 Hz (b).

Mounting eight gravity compensation magnets and eight actuators to the wafer chuck would create a symmetrical situation. Figure 3.20(a) shows the node lines of the wafer chuck when 8 gravity compensators are mounted. The green node line is still not exactly diagonal. When also 8 actuators are mounted, Fig. 3.20(b), the green node line is exactly diagonal. The other node lines have also shifted a little bit.

The Ansys calculation used for the optimized wafer chuck contained an error. The difference in the position of the node lines with the improved model is very small. Calculations with an increased number of gravity compensators or actuators show that the node lines do change a little bit. In the test setup, the addition of actuators and gravity compensators is also observed by less mode excitation. In the test setup (Fig. 3.13), the modes are excited, whereas in the model, no excitation occurs. The position of the node lines changes so little when adding masses for the gravity compensators and actuators that it can't explain the position of the node lines of the test setup.

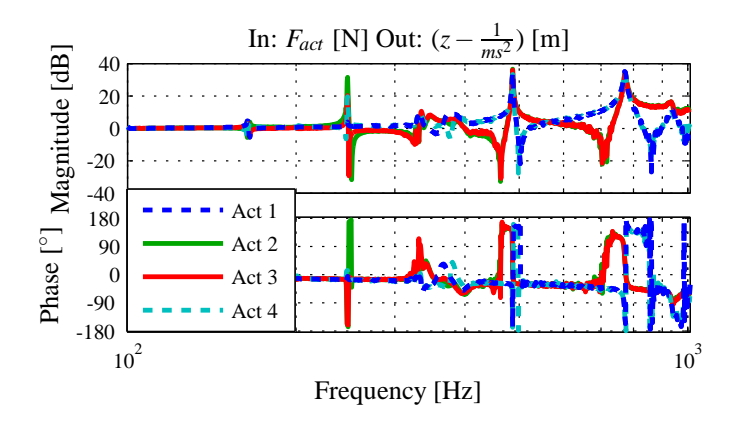


Figure 3.18

Transfer Function of the Z-movement of the aluminium chuck due to the different actuator Forces. Actuators two, three and four excite the eigenmodes. Actuator one doesn't excite the second eigenmode.

3.5 Improvements in the Current Setup

The two test setups, the glass chuck and the aluminium chuck, both have the node lines of the first five eigenmodes at locations that were not expected. Analysis of the chuck has showed that the position error of the node lines is so big that the eigenmodes which should not have been excited by the four actuators, still are excited. In this section improvements on the test setup will be proposed.

3.5.1 Added mass

The masses of the gravity compensators have an influence on the node lines of the eigenmodes. This means that an extra added mass may change the node lines back. In the model, the sensitivity of the mode excitation when mass was added proved to be quite low [2]. The test setup shows mode excitation in every situation, no matter how many effort is put in creating symmetry. In order to find out the sensitivity of the test setup to added mass a modal analysis is done with a 100 gram added mass. The mass is added at a position perpendicular to the second node line in order to have maximum effect on this node line. The added mass is also positioned near the third (—) node line to have a minimal effect on this eigenmode.

The node lines have changed position as shown in Fig. 3.21. Especially the second eigenmode, the green node line, has shifted towards the actuator. The second eigenmode is not excited by the second actuator. The influence of this large mass is small however, the 100 gram mass only changes the node line of the second eigenmode by a few millimeter. This means that in the chuck there is something big that is causing the symmetry to be wrong. It can only be corrected by a relatively large 100 gram mass. The gravity compensators are only 26 gram.

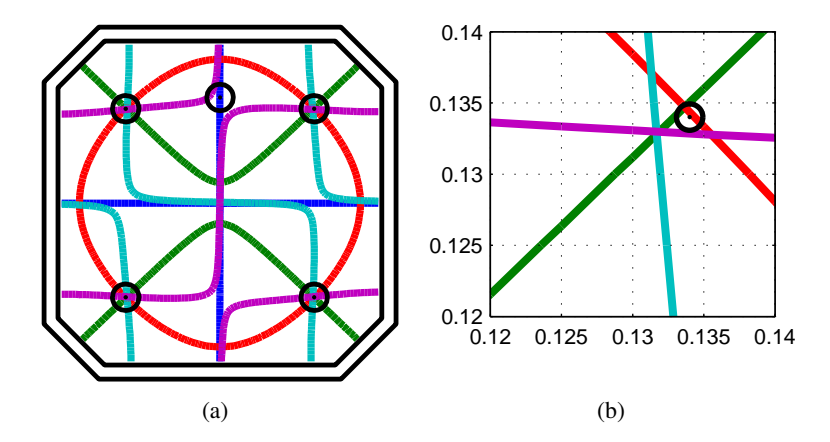


Figure 3.19 Node lines of the optimized wafer chuck model with correct densities of the four gravity compensators and five actuators (a), detailed view around the second actuator location (b).

3.5.2 Damping

The total system consists of a chuck, attached with three plate springs to a base frame. The chuck is made of aluminium and the plate springs are made of steel. The materials used have a low internal damping. This means that the internal modes show highly underdamped behaviour. The maximum amplitude of the eigenfrequency is dependent on damping. Increasing the damping could reduce the amplification of the eigenmodes, making the system easier to control. The amount of damping needed in order to make the eigenmode invisible in the transfer function, is estimated using a modal leaver representation [11]. Secondly, the modal damping parameters will be estimated using a circle fit-method [7, 4].

Estimating the minimal damping coefficient required in the chuck

A question that arises is how much damping is needed in the chuck in order to make the eigenfrequencies invisible. An estimation is made by using a modal leaver representation [11]. The modal movement of an eigenmode can be represented by a second order system with modal mass M_m and modal stiffness k_m . The position where the mass is attached to the leaver will be considered as the point of maximum modal deflection. In order to excite the eigenmode at another point, a different equivalent mass is calculated. If for instance the mode is excited by F_2 at distance d as indicated in Fig. 3.22, the equivalent modal mass is derived from the modal mass based on energy equivalence [11]:

$$M_{eq} = M_m/d^2 \tag{3.1}$$

The equivalent spring constant is calculated in the same way.

The actuators in the chuck are supposed to actuate at the pivot point of the modal leaver, being unable to excite the eigenmode. In the test setup the actuators are not

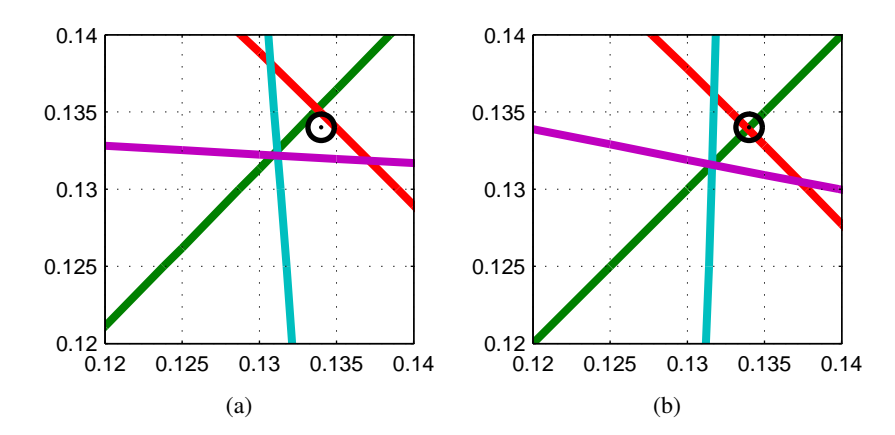


Figure 3.20

Detailed view of the node lines of the optimized wafer chuck model with (a) 8 gravity compensators mounted and (b) 8 gravity compensators and 8 actuators mounted.

exactly positioned in the pivot point, but at a small distance, d, from this point. If the modal mass of the second eigenmode is estimated to be one fourth of the total mass and the position of the actuators to be 1/10 of the position of maximum deflection, then the equivalent mass at the actuator position is estimated to be 1/400 of the total mass. The mass line of the second eigenmode, actuated by the over-actuated configuration will therefore be around 52 dB lower than the mass line of the rigid body mode. The peak response of this eigenmode should be more than 52 dB for this eigenmode to be visible in the transfer funcion. The maximum amplitude of the response is given by [12]:

$$M_{\text{max}} = \frac{1}{2\zeta\sqrt{1-\zeta^2}} \tag{3.2}$$

Where M is the amplitude ratio and ζ the damping ratio. When a maximum amplitude ratio of 400 is allowed, the damping ratio of the chucks second eigenmode should be higher than about 0.15 %.

Damping measurement of the chuck

The damping coefficient of the internal eigenmodes will be measured using a circle fit method [7, 4]. The circle fit method is a single degree of freedom method based upon the fact that the frequency response function of a single degree of freedom system describes a circle in the Nyquist diagram. The influence of other modes is approximated by a complex constant. The damping ratio is estimated with the use of the phase difference between the two points next to the resonance frequency:

$$\zeta = \frac{\omega_2 - \omega_1}{\omega_r \left(\tan \left(\frac{\theta_1}{2} \right) + \tan \left(\frac{\theta_2}{2} \right) \right)}$$
(3.3)

Where:

 ω_1, ω_2 : two frequency points at both sides of the resonance frequency ω_r ,

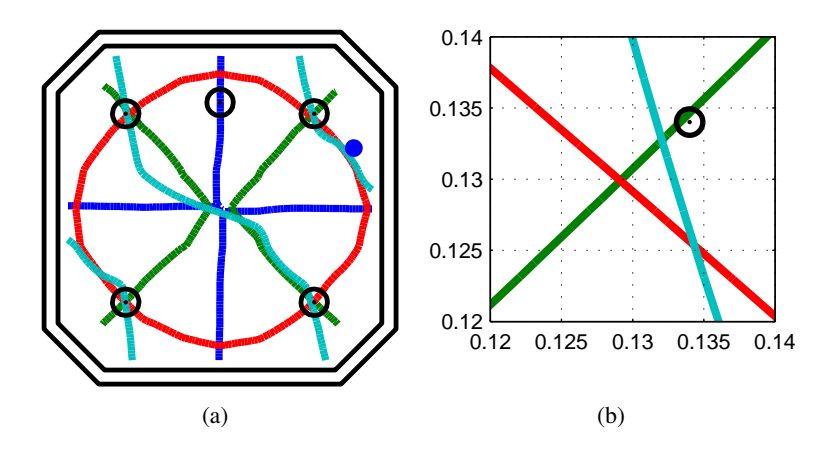


Figure 3.21 Node lines of the Aluminium chuck with an added mass at the position indicated by the blue dot (a), detailed view around the second eigenmode (b).

 θ_1, θ_2 : the corresponding angles between the frequency points ω_1 , ω_2 and the resonance frequency ω_r .

The damping is measured in two different situations. The first situation is the normal situation, where the chuck is attached to the plate springs and no additional damping measures have been taken. In the second situation a stroke of rubber material is placed between the plate springs and the chuck. This should provide extra damping, this situation is called the lightly damped chuck. The damping material works best in the position where the deflection of the eigenmode is largest. The first eigenmode is damped by material on two positions (the corners) and the second eigenmode is damped by material on only one position (the top). The damping of the second eigenmode will therefore be less than the first eigenmode. In order to increase the damping of the second mode, damping material is added at all the middle sections on the rims of the chuck. The effect is called the "medium damped chuck". The damping percentage of the second eigenmode is significantly increased. The damping ratios are given in the Tab. 3.3.

	Damping percentage mode 1	Damping percentage mode 2
Undamped chuck	0.17 %	0.09 %
Lightly damped chuck	0.22 %	0.11 %
Medium damped chuck	0.22 %	0.20 %

Table 3.3

Damping factors of the chuck

From this table, it shows that the chuck is very lightly damped. The excitation of the eigenmodes reduce when more damping is present. This means that in an industrial system when the damping ratio is designed to be, say 1 %, the over-actuated system doesn't excite the first five eigenfrequencies enough to be performance limiting in the control system. Efforts have been made to increase the damping percentage of

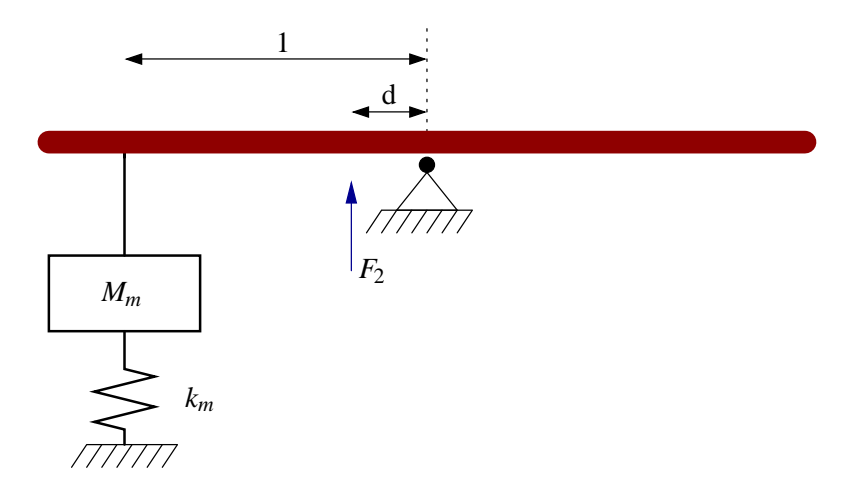


Figure 3.22 modal leaver representation of an eigenmode with the effective mass and effective spring constant as indicated in [11].

the chuck. This has only limited influence on the damping percentages. Increasing the damping even further lowers the excitation of the eigenfrequencies, leading to a standstill performance increase.

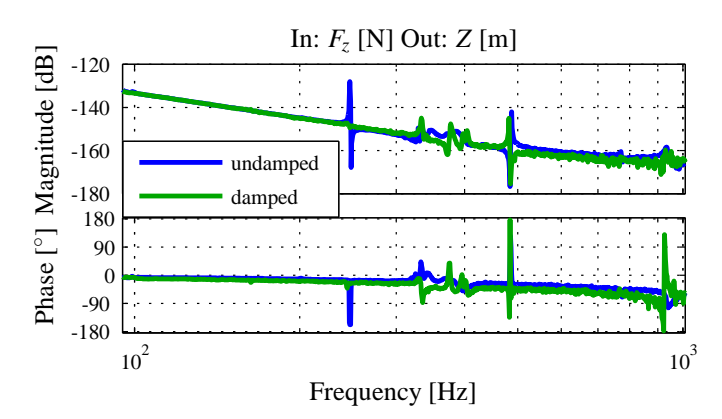


Figure 3.23
Transfer function of the aluminium chuck in Z-direction of the undamped and medium damped system. The improved damping reduces the excitation of the second eigenmode at around 250 Hz.

Figure 3.23 shows the transfer function in Z-direction of the medium damped and undamped situation. The small increase in damping decreases the amplification factor of the eigenmode, enough to make the eigenmode disappear in the transfer function. This is in analogy with the calculation of the minimum required damping ratio. Unfortunately, adding damping also adds mass at positions which dod not occur in the optimization. This means that other modes, the third for instance, get amplified, not because of the added damping, but because of the changed node lines.

3.5.3 Over-Sensing

The current setup uses over-actuation to reduce the excitation of the first five eigenmodes. The location of the sensors is chosen arbitrarily. The current sensor location has a few disadvantages. The first eigenmode is solely detected by the two sensors on top. The result is that the first eigenmode is interpreted as R_y movement by the CoG transformation. Excitation of the first eigenmode by actuator action in Z or R_x direction leads to movement in the R_y direction. This cross coupling effect is hard to control using decoupled PID control.

The second eigenmode is solely detected by the bottom sensor. The sensor is placed exactly at the point where the deflection caused by the eigenmode is maximum. This makes the sensor extremely sensitive for deflection by the second eigenmode. The sensor placement can be optimized in the same manner as the actuator placement. A sensor norm can be defined like the actuator norm. Positioning a sensor at the same place as the actuator will lead to a further reduction of the resonance peaks. This results in a further increased standstill performance. The first five eigenmodes are not excited by the actuators, and if they are excited, they are not sensed by the sensors. The used linear encoders can only be mounted at the same position as the actuators with a redesign of the setup. Another idea is to place the sensors in a different position along the rims. Figure 3.24 shows a sensor setup with four sensors, which are used to measure the three degrees of freedom.

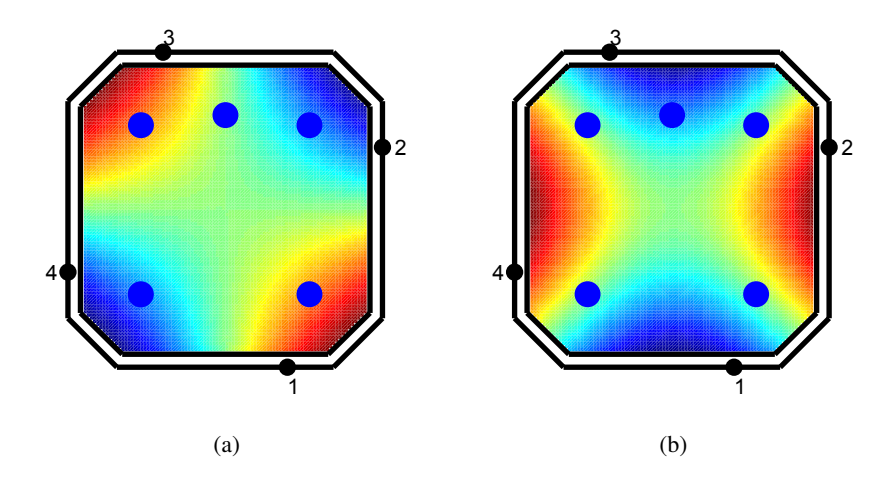


Figure 3.24

Over-sensed sensor positioning with the first eigenmode visible (a) and the second eigenmode visible (b). These two eigenmodes will be unobservable by the CoG movement reconstructed by the sensors.

The sensors measure symmetric displacement of the first two eigenmodes e.g. if sensor 1 and 3 measure upward movement caused by to the first eigenmode (Fig. 3.24(a)), sensor 2 and 4 measure downward movement. No Z, R_x , or R_y movement is reported, because for Z-movement all the sensors should measure upward movement and so on. The transfer functions in Z, R_x and R_y directions are shown in Fig. 3.25. Over-sensing makes the first two modes invisible in the over-actuated situation and hardly visible in

the classic actuated situation. The third mode can be observed by the sensors and can therefore be seen in the transfer functions.

3.6 Conclusions

The two wafer chucks that are available in the test setup both excite the first five eigenmodes. The analysis of the chuck shows that symmetry is highly important. The influence of the gravity compensators and the fifth actuator proved to be bigger than in the model. Even with extra gravity compensators and extra actuators mounted, the first five eigenmodes were excited by the actuators. The node lines of the eigenmodes were still not at the modelled positions. An added mass did move the node lines, but the added mass was so large that the problem can't be explained by the mass of the gravity compensators and actuators alone. Different causes have been studied, especially the fifth actuator and gravity compensator proved to have an influence on the mode excitation. With these elements corrected, the modes are still excited. There remains an unknown source of the change in node lines that can't be explained.

The chucks are sensitive for actuator misplacement. This is because of the low internal damping of the chucks. A chuck with higher internal damping would be less sensitive for this actuator placement. A chuck with an internal damping coefficient of 1 %, which is feasible, would be insensitive to the actuator misplacement present in the chuck. A small amount of extra damping is added to the chuck which showed an immediate improvement in the mode excitation of especially the first and second mode. Adding too much damping material in the current chuck has a counter effect. All the added mass moves the node lines of the eigenmodes, meaning the modes get more excited by the actuators. A new designed chuck should include damping material in the optimization procedure. The optimization can be performed with all the extra masses, leading to correct actuator locations when the damping material is attached to the chuck.

When the over-actuation concept is combined with over-sensing, the eigenmodes are not visible in the transfer functions. With the eigenmodes invisible in the transfer functions, higher control bandwidths can be achieved. One drawback is that the eigenmodes might be present in the chuck, although not detected by the sensors.

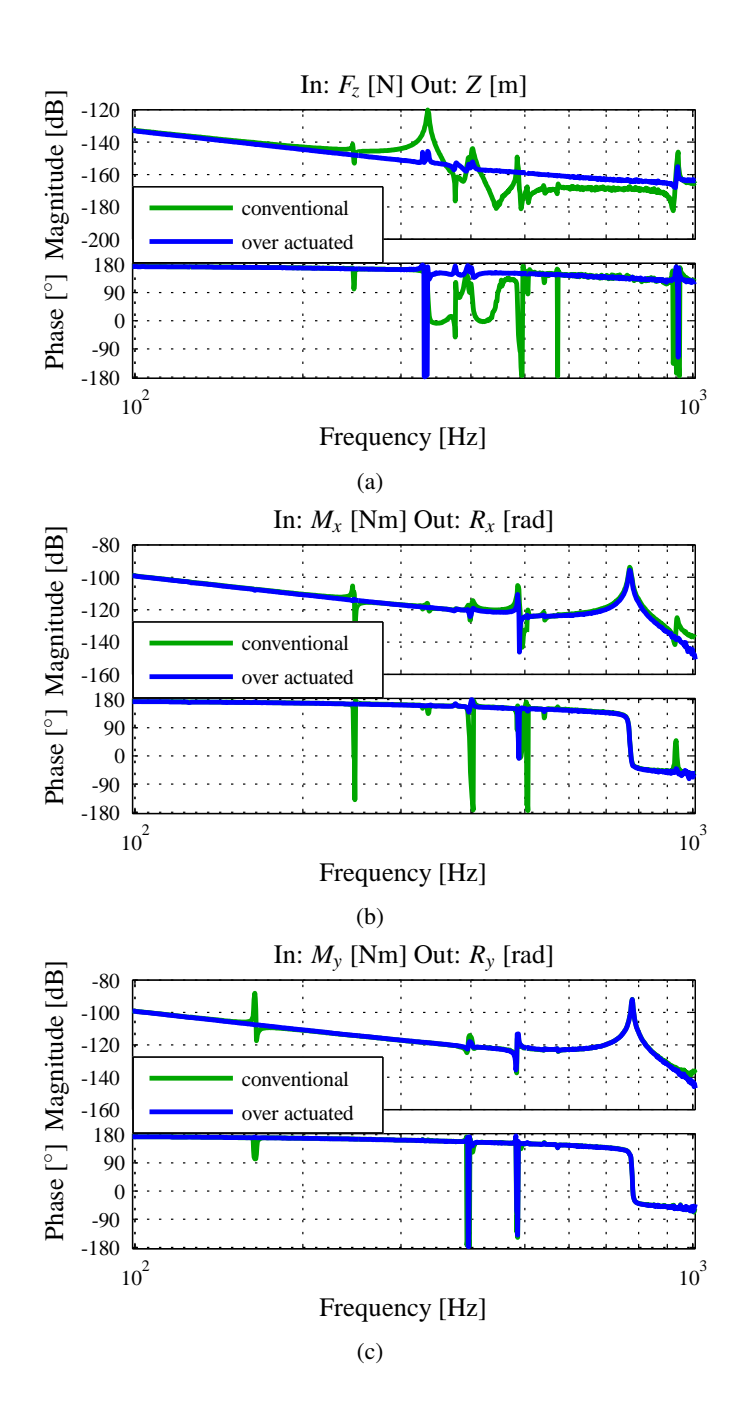


Figure 3.25 Transfer functions of the conventional actuated and over-actuated system in Z, R_{x} and R_{y} direction using over-sensing.

Chapter 4

Control and Performance of the wafer chuck

A traditional control system contains a number of actuators equal to the degree of free rigid body modes. If the system to be controlled is supposed to behave only as a rigid body, or if the desired control bandwidth of the structure is much lower than the structure flexible eigenfrequencies, then this is a plausible choice.

When the control bandwidth of the flexible structure has to be improved, additional actuators can be placed. In order to provide extra damping for the internal modes, actuators can be placed at positions where controllability is high for the specific internal modes [3, 15]. These methods require extra sensors and actuators and additional control complexity.

The over-actuated system has four actuators and three sensors to control three degrees of freedom. The actuators are positioned on an optimized chuck, such that the first five internal eigenmodes are (almost) not excited by the actuators. The information of the sensors will be used for the reconstruction of the CoG movement allowing for decoupled control. The chuck will be actuated as a rigid body. An analysis is performed on the validity of rigid body actuation.

A performance specification for the wafer chuck is specified in Section 4.1. The decoupled PID control of the system will be covered in Section 4.2. In Section 4.3 the deformation of the chuck, due to the over-constraint situation of the over-actuated system is described. Notes on model based control of the system will be covered in Section 4.4. Finally a control system for the system with an extra sensor will be analysed in Section 4.5. At the end of the chapter the conclusions on the control of the chuck will be presented.

All the tests are performed during day time in the MI-Partners lab environment. The equipment used is described in Appendix C.

4.1 Performance specification

The wafer chuck is basically used to support a wafer on an industrial machine. The standstill performance requirement of the wafer is determined by the operation that has to be done. For example, a laser cutting process requires standstill in Z-direction to keep the laser beam in focus. R_x and R_y movements of the wafer are less critical,

since this only affects the cutting direction which has to be more or less perpendicular to the surface. A wafer stepper requires standstill in all directions in order to keep the light beam on focus and the patterned image within tolerances.

A performance specification in terms of Z, R_x or R_y movements has no influence on the optimization procedure. The mode excitement is performance limiting in all directions, which means that every industrial machine will benefit of the over-actuated system. The optimization parameters can change due to a performance specification (e.g. the thickness of the chuck). The performance specifications are met by the design of the system and by tuning the controllers of the system. There will only be a small difference in the obtained controllers. The performance specification that is chosen here, is standstill performance in Z, R_x and R_y directions.

With the over-actuated system, the challenge is to create a controller with a bandwidth that is higher than the first eigenfrequency of the system. For this system, it means that the control bandwidth has to be 200 Hz in all directions.

In order to compare the standstill performance of the system, the standard deviation of the positioning error is used. The standstill performance of a system can be expressed in terms of a standard deviation, because the assumption is made that the disturbances acting on the system are random stationary processes (see sec. 4.4). The position error will therefore be normally distributed [5].

The standard deviation (STD) of the servo error and of the sensor signals will be used as a performance measure. There can be a big difference in these two STDs due to the deformation of the flexible modes.

This system is mainly created to demonstrate the difference in standstill performance between the conventional and over-actuated system. The absolute value of the standstill performance was of less interest in the design of the system. The standstill performance of the over-actuated and conventional system will therefore be made as small as possible.

4.2 PID control of the wafer chuck

The wafer chuck consists of three sensors and three or four actuators. This plant is a coupled Multi Input Multi Output (MIMO) plant. This means that the three sensors all measure the combined Z, R_x and R_y movement of the chuck and all the actuators produce a combined F_z , M_x and M_y force / momentum. Decoupling the plant gives the opportunity to apply Single Input Single Output (SISO) controllers seperately for each degree of freedom. The use of SISO controllers for the control of the decoupled degrees of freedom has several advantages [9, 2, 14]:

- Straightforwardness of individual SISO design
 The SISO control design techniques are straightforward, well known and easy interpretable. The controller can be improved manually if the performance specification is not achieved.
- Simple implementation on a digital computer

 Automated control design procedures, like \mathcal{H}_2 methods, generate high order controllers. These controllers increase computation time on a computer. A

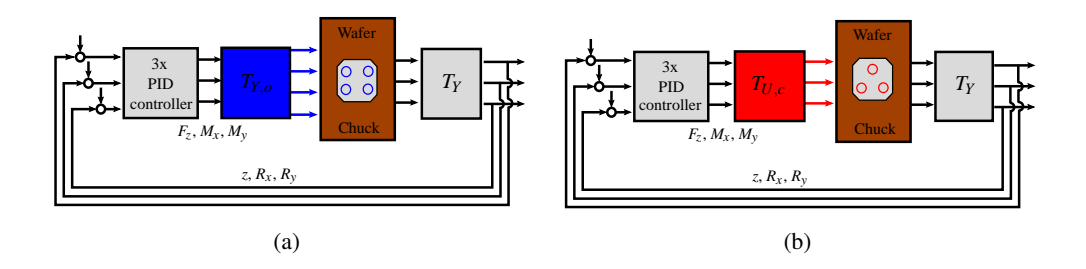


Figure 4.1 Decoupled control formulation of the over-actuated (a) and conventional actuated (b) system.

shorter computation time due to a simpler digital controller, allow enhancements like signal tracing.

- Less accurate model of the chuck is needed

 Automated control design procedures, like \mathcal{H}_2 methods, require an accurate model of the plant. The available model of the wafer chuck, shows less excitation of the eigenmodes and therefore a controller based on this model will be of no use in the plant.
- Simple implementation on commercially available controllers

 Standard controllers, such as the NYCe4000[©] controller by Bosch Rexroth[©], are designed to work on a SISO based plant. With the decoupled plant, implementation of three SISO controllers is possible on this industrial system.

4.2.1 System CoG control formulation

The system has to be decoupled in order to apply three SISO PID controllers. The decoupling of the plant involves transforming the local coordinates of the inputs and outputs of the plant to the Centre of Gravity (CoG) coordinates. In order to decouple the plant, the sensor and actuator signals can be multiplied with in- and output decoupling matrices. Figure 4.1 shows the decoupling scheme of the over-actuated and conventional system. The coupled outputs of the plant are decoupled, using transformation matrix T_Y . The CoG output of the three controllers is transformed in to local inputs of the plant by transformation matrix T_U .

Figure 4.2(a) shows the positions of the three linear encoders with respect to the CoG. The positions of the actuators with respect to the CoG are shown in Fig. 4.2(b). The relationship between the local sensor positions and the CoG movements is given in Eq. 4.1. Equations 4.2 and 4.3 give the relationship between the local actuator forces and the forces and torques acting on the CoG. The assumption $sin(\theta) \approx \theta$, and $cos(\theta) \approx 1$ is made in these equations, as the angles made remain small.

$$\begin{bmatrix} s_1 \\ s_2 \\ s_3 \end{bmatrix} = \mathbf{T_{sens}} \cdot \begin{bmatrix} Z \\ R_x \\ R_y \end{bmatrix} = \begin{bmatrix} 1 & -l_2 & 0 \\ 1 & l_1 & l_1 \\ 1 & l_1 & -l_1 \end{bmatrix} \cdot \begin{bmatrix} Z \\ R_x \\ R_y \end{bmatrix}$$
(4.1)

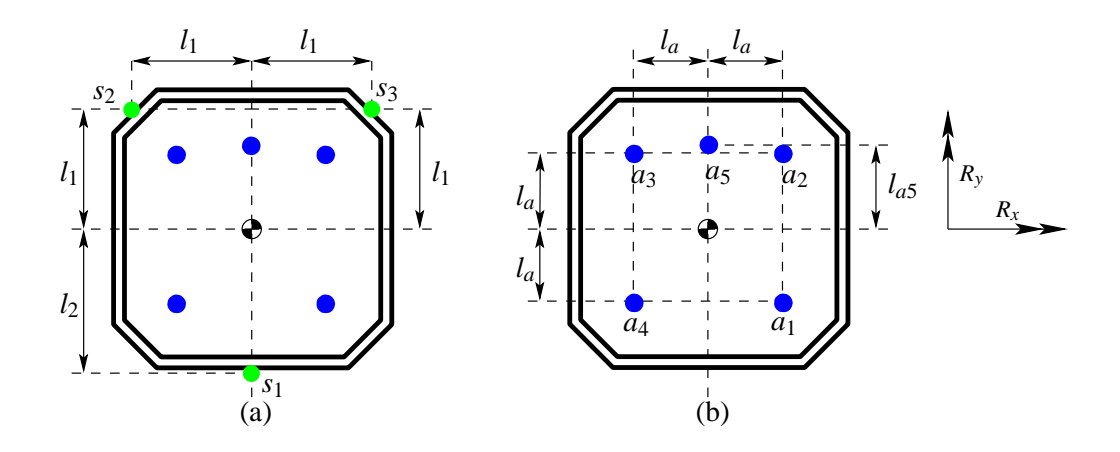


Figure 4.2 Overview of the wafer chuck showing the positions of the sensors (a), and actuators (b).

$$\begin{bmatrix} F_z \\ M_x \\ M_y \end{bmatrix} = \mathbf{T_{overact}} \cdot \begin{bmatrix} a_1 \\ a_2 \\ a_3 \\ a_4 \end{bmatrix} = \begin{bmatrix} 1 & 1 & 1 & 1 \\ -l_a & l_a & l_a & -l_a \\ -l_a & -l_a & l_a & l_a \end{bmatrix} \cdot \begin{bmatrix} a_1 \\ a_2 \\ a_3 \\ a_4 \end{bmatrix}$$
(4.2)

$$\begin{bmatrix} F_z \\ M_x \\ M_y \end{bmatrix} = \mathbf{T_{conv.act}} \cdot \begin{bmatrix} a_1 \\ a_4 \\ a_5 \end{bmatrix} = \begin{bmatrix} 1 & 1 & 1 \\ -l_a & -l_a & l_{a5} \\ -l_a & -l_a & 0 \end{bmatrix} \cdot \begin{bmatrix} a_1 \\ a_4 \\ a_5 \end{bmatrix}$$
(4.3)

The decoupling transformation matrices are formed by taking the inverse of the matrices in equation 4.1, 4.2 and 4.3.

$$T_Y = T_{sens}^{-1}, \quad T_{U,o} = T_{overact}^{-1} \quad \text{and} \quad T_{U,c} = T_{conv.act}^{-1}$$
 (4.4)

Where the subscript o stands for over-actuated and c for the conventional actuated system. The decoupled transfer functions in Z, R_x and R_y direction are given in Fig. 4.3. The transfer function of the entire 3x3 decoupled plant can be found in Appendix B.1, together with the Relative Gain Array (RGA).

4.2.2 PID control and performance

PID controllers are created for the conventional and over-actuated system. The controllers are designed through an iterative procedure. First PD controllers are designed using Ziegler-Nichols tuning rules. With these simple controllers the bandwidth of the system has been increased by including notches in order to make a higher controller gain possible. With integral action included, the servo error of the three controllers was traced at standstill. From these error traces, Power Spectral Densities (PSD) and Cumulative Power Spectra (CPS) are constructed to identify the system performance. The frequency region where the error buildup is significant can be deducted from the CPS.

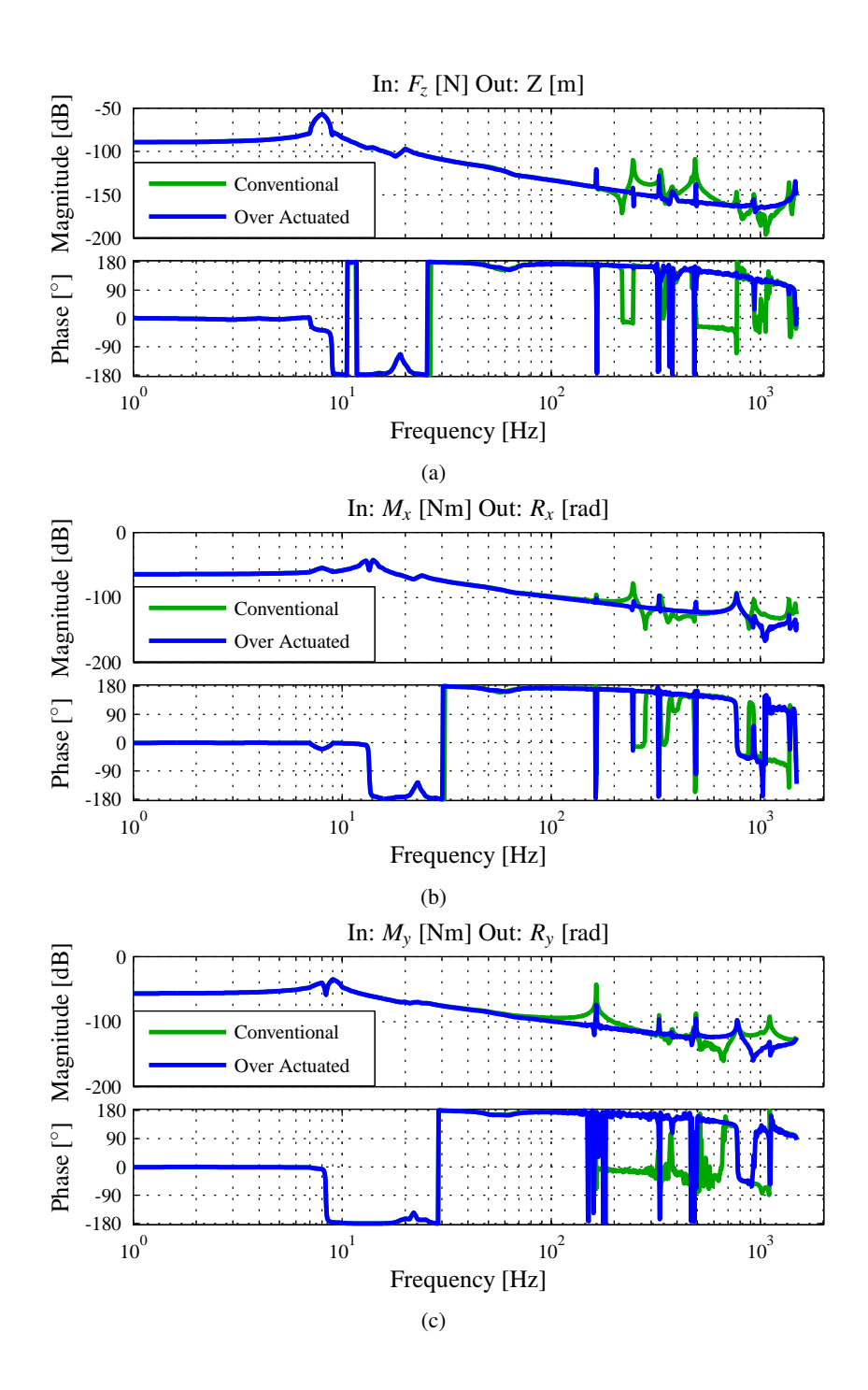


Figure 4.3 Transfer function of the decoupled overactuated (—) and conventional (—) plant in Z, (a), R_x (b), and R_y , (c) direction. The wafer chuck used in this system is the aluminium chuck.

Control of the conventional actuated wafer chuck. The internal eigenfrequencies (Fig. 4.3) of the system have a large impact on the control of the conventional system. Without the use of a notch filter, a bandwidth of around 20 Hz will be possible in all directions. With the use of up to four notch filters the gain of the control loop can be increased. Figures 4.4 and 4.5 show the open loop transfer function and the transfer function of the controllers. The realised bandwidths of the tuned controllers are around 50-60 Hz in all directions.

Control of the over-actuated wafer chuck. The internal eigenmodes of the chuck are less excited by the over-actuated system. This immediately leads to a system that is easier to control. A bandwidth of 60 Hz in all directions is easy to obtain without the use of notch filters. The bandwidth of the over-actuated system without notches is already equal to the bandwidth of the conventional system with notches. This makes the over-actuated system more robust, since notch filters are commonly regarded as not robust.

By applying notch filters to the controllers, the control bandwidth of the system is increased to 100 Hz for each direction. From the open loop transfer function of Fig. 4.4, the bandwidth of the system in Z and R_x directions could be easily increased to 150 Hz. The standstill performance of the system in R_y direction decreases with the increased bandwidth. This is because of the presence of the first flexible mode at 164 Hz.

The excitation of the chuck with a frequency of 164 Hz in the Z and R_x directions will excite the first eigenmode of the chuck. The reason that it can't be seen in the transfer functions in these directions is, that the transformation matrix decouples all the motion of the first eigenmode to the R_y direction. This can also be seen in the cross-coupling term from input F_z to output R_y in the total plant, Fig. B.1 on page 79.

Performance of the wafer chuck with conventional and over-actuated control. The realised control bandwidths of the conventional and over-actuated systems are summarised in Tab. 4.1. The control bandwidth of the over-actuated system is roughly twice as large as the control bandwidth of the conventional actuated system.

Direction	Conventional system Over-actuated system		
	Bandwidth [Hz]	Bandwidth [Hz]	
Z	30	60	
R_x	30	60	
R_y	30	60	
	With notch filters		
Z	57	100	
R_{x}	55	100	
R_{y}	50	100	

Table 4.1 Closed loop bandwidth of the conventional actuated wafer chuck with and without the use of notch filters.

The cumulative power spectrum of the servo error of the conventional actuated

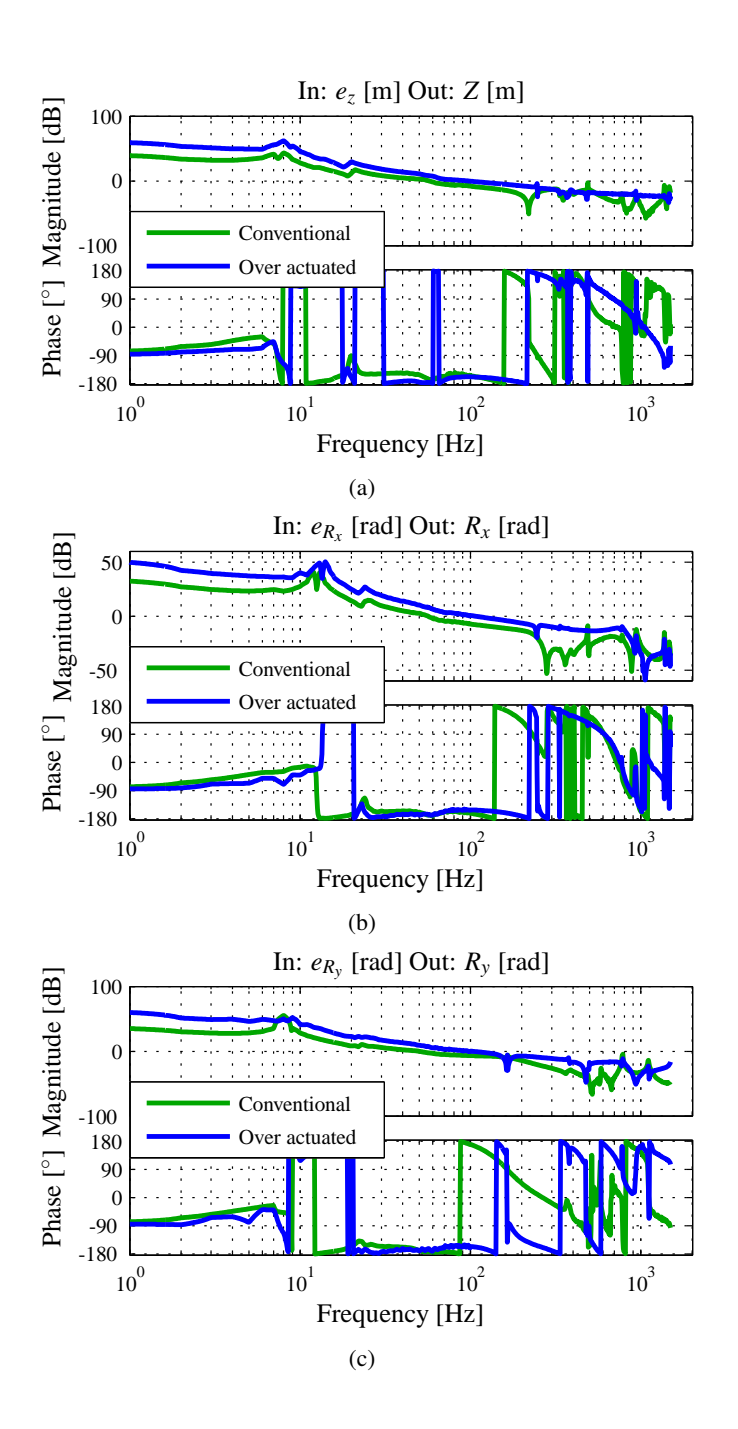


Figure 4.4 Measured open-loop transfer function from controller input to plant output. The over-actuated system is able to achieve higher bandwidths.

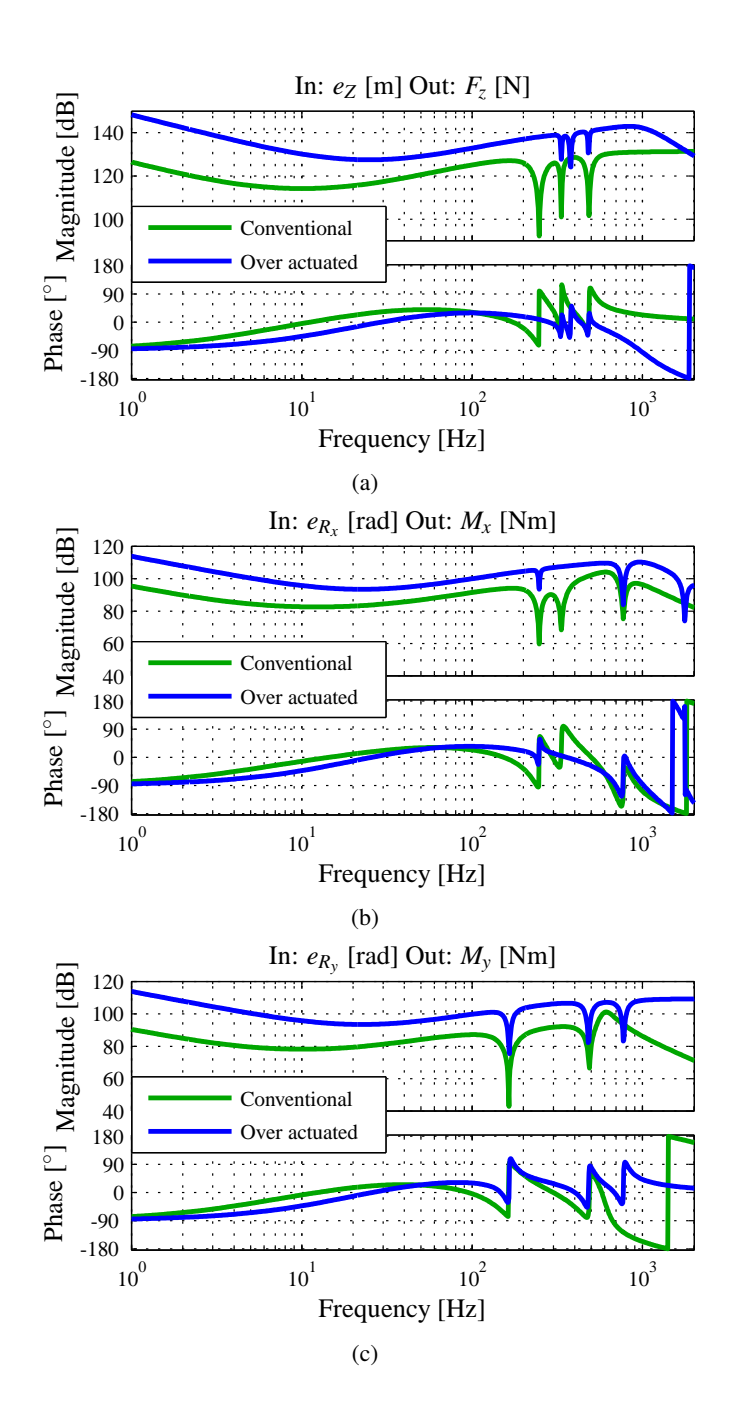


Figure 4.5

Transfer function of the conventional controllers. Notches were implemented to increase the bandwidth of the system for both the conventional and the overactuated setup.

wafer chuck is given in Fig. 4.6. The servo errors that are measured are mostly low

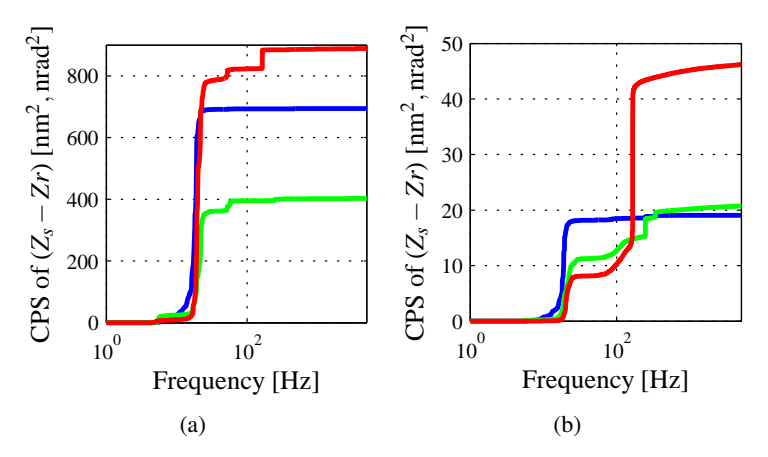


Figure 4.6 CPS of the servo error of the conventional actuated wafer chuck (a). CPS of the servo error of the over-actuated wafer chuck (b). Given are Z (—), R_x (—) and R_y (—) directions.

frequent and occur between 15 and 20 Hz. The standard deviation of the servo error of the conventional system and over-actuated system is given in Tab. 4.2

Direction	Conventional system	Over-actuated system
	Standard deviation	Standard deviation
Z	26 nm	4.4 nm
R_{x}	20 nrad	4.6 nrad
$R_{\rm y}$	30 nrad	6.7 nrad
Sensor nr.	Standard Deviation	Standard deviation
1	24 nm	4.0 nm
2	28 nm	4.8 nm
3	31 nm	5.3 nm

Table 4.2 Standard deviations of the servo errors and the standard deviations at sensor positions of the of the conventional and over-actuated wafer chuck.

4.3 Chuck deformation due to the added actuator

The over-actuated actuator configuration creates the possibility of static chuck deformation when the actuator gains are not equal. The deformation can be static, due to the over-constrained situation and it can be high frequent, where deformation is caused by the excitation of the eigenmodes. In this section the deformation of the chuck due to the addition of an actuator is studied.

In order to identify the deformation of the chuck an extra sensor will be placed at the rim of the chuck. The sensor is located at the position of the fourth sensor of the over sensed setup of Sec. 3.5.3. The difference between the calculated movement and the measured movement is analysed. This gives the deformation of the chuck. In order to identify high frequent position differences, the CPS of the individual sensor signals is calculated.

4.3.1 Static deformation of the chuck.

Static deformation of the chuck occurs when four actuators are used to control three degrees of freedom. A static force, with different actuator gains, applied in the Z-direction, like in Fig. 4.7(a), results in static deformation of the chuck. In the conventional system of Fig. 4.7(b), the actuator gain difference results in a tilting action that will be corrected by the controller. In order to test the static deformation of the

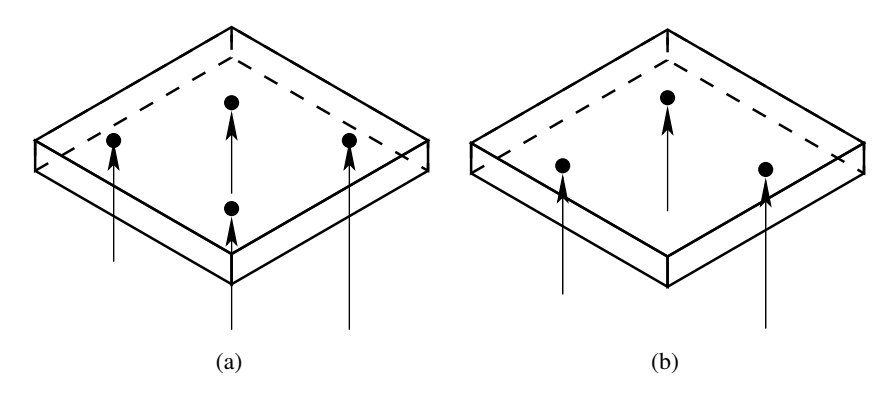


Figure 4.7
Situation of actuator gain difference in an over-actuated (a) and conventional actuated (b) system. The gain difference in (a) results in static chuck deformation, the gain difference in (b) in a tilting error that will be corrected by the controller.

chuck, the deformation of the chuck is analysed in the conventional and over-actuated situation at different chuck heights. A high setpoint in Z-direction results in a large actuator force and therefore a large deformation.

The chuck is supported by plate springs. The plate springs also exert a force on the chuck, which creates a deformation. The gravity compensators deform the chuck as well. The deformation of the over-actuated chuck is compared with the deformation of the conventional actuated chuck to find the deformation caused by the additional actuator of the over-actuated setup. Table 4.3 gives the deformations encountered in both situations.

The static deformation error caused by the additional actuator is significant. The error stemming from the additional actuator is maximum 30% of the total deformation measured. There are two possible ways to deal with the chuck deformation.

1. Perform high accuracy tasks at the stationary position

The system can be supported by three gravity compensators. The high accuracy tasks will be performed at a chuck height where the actuators exert little force on the chuck, the deformation of the chuck will remain low.

Chuck height	Conventional system	Over-actuated system	Deformation caused by
μm	deformation [nm]	deformation [nm]	additional actuator [nm]
0	0	0	0
20	58	67	9
40	81	118	38
60	131	177	46
80	188	239	51
100	204	283	79

Table 4.3 Static deformation of the chuck with different chuck heights.

Compensate for the deformation of the chuck
 The deformation of the chuck is static. A setpoint in Z-direction can change the height of the chuck at the position where the accuracy is needed at that particular moment.

4.3.2 Deformation of the chuck at high frequencies

The maximum difference between the calculated position and the sensor position due to non static deformation is 5 nm. The main contribution to this error is the deformation of the chuck due to the first and second eigenmode. The sensor position is important for the amount of deflection detected. The sensors used to measure the CoG movements are sensitive to the deflection caused by the first and second eigenmode. The position of the extra sensor is less sensitive to deflections caused by these eigenmodes. That is the reason that the calculated position is larger than the real position. A small part of the signal trace is given in Fig. 4.8(a).

At high frequencies, the transformation of the local sensor coordinates to the CoG coordinates introduces a bigger positioning error to the system than the presence of four actuators. The CPS of the error between the calculated and the real movement of the chuck at the position of the fourth sensor is given in Fig. 4.8(b). The error between measured and calculated position is mainly the source of the first and second eigenmode of the chuck. The transformation matrix doesn't handle these deformations well.

4.3.3 Conclusion

The static deformation of the chuck increases with the addition of an extra actuator. This is a complication in the system that has to be dealt with. The high frequent deformation shows that the plant is not decoupled at the eigenfrequencies, leading to a mismatch between calculated position and measured position. In this case the calculated position is over estimated because the deformation of the chuck is measured as a rigid body mode.

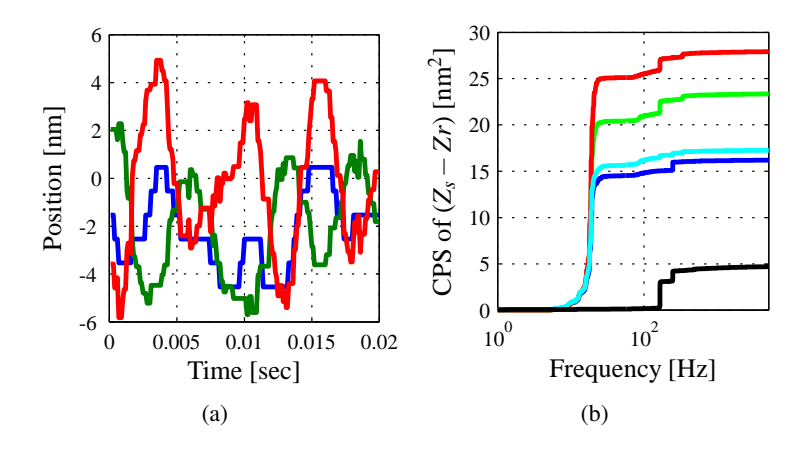


Figure 4.8
(a) Signal trace of the chuck. The blue line (—) represents the measured signal at the extra sensor position. The green line (—) gives the calculated movement of the chuck at the position of the extra sensor. The positioning error is given in red (—). It shows that the position calculation is bigger than the real position. This is because the deformation of the chuck due to the first and second eigenmode is interpreted as a rigid body mode. The frequency of the largest error contribution is 164 Hz.

(b) CPS of the different sensor signals with subtracted means, sensor 1 (—) (bottom), sensor 2 (—) (upper left), sensor 3 (—) (upper right) and sensor 4 (—). The CPS of the error signal is given as well (—). The biggest error source of the error signal is at the chucks first and second eigenfrequency.

4.4 Model Based control performance

As in many mechatronic systems, disturbances acting on the system influence the system performance. In order to take all the disturbances into account, and to identify the contribution of each error source to the system performance, the Dynamic Error Budgetting (DEB) technique [10, 5] is used.

4.4.1 Dynamic Error Budgeting analysis tool

In DEB, the disturbances acting on the system are assumed to be random stationary signals. The stochastic nature of the noise sources allows the source to be modelled by their Power Spectral Densities (PSDs). The propagation of each disturbance through the system can be computed using linear system theory [9]. A complete overview of the DEB analysis tool can be found in [5] and [10]. The DEB analysis gives a good indication of the maximum performance of the modelled system.

The PSD of the total performance measure in the closed loop system is the weighted sum of the contributions of each disturbance to the performance channel. A closed loop transfer function of the plant, $H_w(s)$, from the disturbance source w, to the output y, is constructed. Using this transfer, the propagation of each uncorrelated stochastic

disturbance source w_n can be computed using Eq 4.5.

$$PSD_{y}(f) = \sum_{n=1}^{N} |H_{w_{n}}(f)|^{2} \cdot PSD_{w_{n}}(f)$$
(4.5)

The DEB analysis can be extended to include quantization errors from sources such as the DA converter and linear encoder. The general assumptions, redefined and supplemented for the quantization errors are:

- The error is a stationary random process
- The error is uncorrelated with the signal sequence
- The probability distribution is uniform over the quantization range.

These assumptions are generally valid if the signal is sufficiently complex and the quantization steps are sufficiently small so that the amplitude of the signal is likely to traverse many quantization steps from sample to sample.

4.4.2 Disturbances

In this section, the disturbances that act on the wafer chuck will be modelled

Floor vibrations

Floor vibrations have a significant impact on performance of nanometre precision machines. Floor vibration enters the system at the base frame as a force input due to ground acceleration. Measurements of the floor in the NTS lab show the frequency content in this region. The frequency content of the ground vibrations is significant below 200 Hz. Above 200 Hz the signal content of the floor vibrations was measured to be lower than the noise of the measurement system. The high frequent floor vibrations will not enter the system, since the suspension frequency of the base is between 6 and 21 Hz. The measurement is performed during 24 one-hour periods. The PSD of the measurement with the highest noise content is shown in Figure 4.9(a).

Current amplifier noise

The actuators of the system are current driven. The output signal of the DA convertor is fed through a Quanser linear current amplifier. The input of the amplifier is short-circuited and the output is connected to the coil of the actuator. The current noise is measured using a LEM module, allowing the current amplifier noise to be measured separately. The PSD of the current amplifier is shown in Figure 4.9(b).

DA converter noise

Most mechatronic systems utilize digital control. This means that the digital signal from the computer has to be converted to an analog signal that can be sent to the mechatronic system. This conversion introduces a noise in the system, called quantization noise. In literature, [5, 10] the quantization errors from sampling are considered as an additional noise signal at each sample.

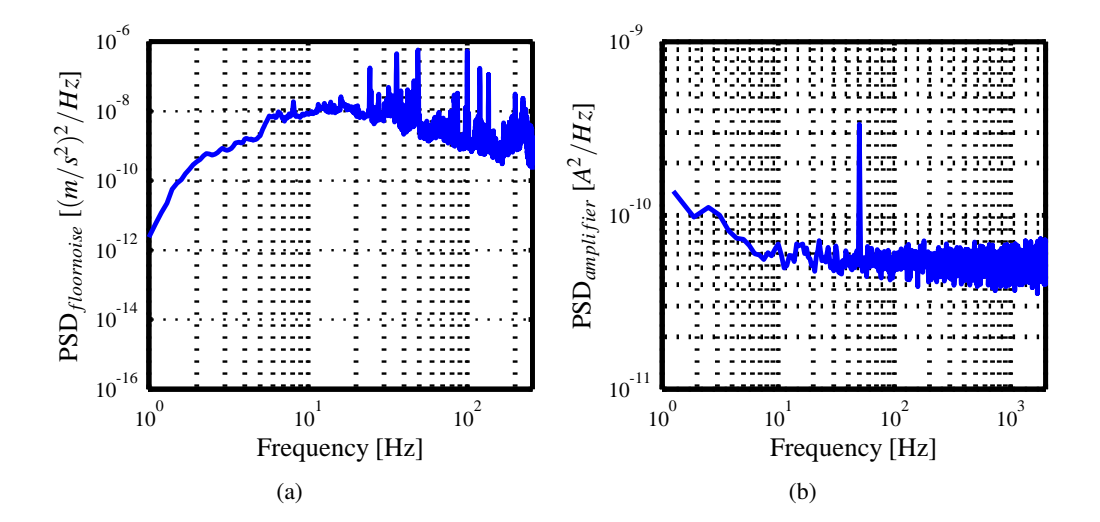


Figure 4.9
(a) Power Spectral Density of the floor vibrations. The PSD is obtained from the floor at NTS mechatronics during a busy period using a geophone. (b) Power Spectral Density of the amplifier noise. The PSD is obtained by measuring the current using a LEM module with a short-circuited input.

With the assumptions made to represent the quantization error as a stochastic signal, as given in Sec. 4.4.1, the quantization noise can be modelled as uniform distributed white noise with variance [9]:

$$\sigma^2 = \frac{q^2}{12} \tag{4.6}$$

With q the quantization interval, determined by the converter range and the number of bits (s):

$$q = \frac{range}{2^s} \tag{4.7}$$

The PSD of the DA quantization noise is white up to the Nyquist frequency f_N (half the sampling time):

$$PSD_{DA} = \frac{q^2}{12 \cdot f_N} \tag{4.8}$$

Linear encoder noise

The linear encoder has a digital quadrature output. The encoder scale has a pitch of $p_{linear} = 20 \ \mu \text{m}$ which is interpolated 20.000 times by an interpolator to get to the resolution of 1 nm. The electrical noise of the interpolator and sensor is not known. The quantization noise of the linear encoder can be calculated similar to the quantization noise of the DA converter:

$$PSD_{encoder} = \frac{p_{linear}^2}{12 \cdot n_i^2 \cdot f_N} = \frac{res^2}{12 \cdot f_N}$$
(4.9)

Where n_i is the interpolation factor and *res* is the resolution.

Acoustic noise

The chuck has a large area of 500×500 mm with a chuck thickness of only 10 mm in the middle and 20 mm on the sides. This makes the chuck sensible to acoustic noise. In order to estimate the error caused by acoustic noise, the sound is assumed to be stochastic. The sound intensity level is defined as:

$$L = 20\log\left(\frac{p}{p_0}\right) \tag{4.10}$$

Where p equals the pressure level of the sound and p_0 the reference pressure, $20 \mu Pa$ in air. Given the sound intensity level, the pressure level of the sound can be calculated. Assuming the acoustic noise is equally distributed over a certain frequency range f_{Δ} and the area of the plate sensitive to acoustic noise is A, the following PSD is found:

$$p_{U}(w) = \begin{cases} \frac{1}{b-a} & \text{if } a \le w \le b, \\ 0 & \text{if } w < a \text{ or } w > b. \end{cases}$$

$$(4.11)$$

$$PSD_{acc} = \begin{cases} \frac{\left(p_0 \cdot A \cdot 10^{\frac{L}{20}}\right)^2}{f_{\Delta}}, f \in f_{\Delta} \\ 0, otherwise \end{cases}$$
 (4.12)

A measurement on the chuck has shown that acoustic noise can be measured with frequency from 30 Hz. The upper limit is set to 5000 Hz, the Nyquist frequency. A sound intensity level of 70 dB is assumed for the disturbance PSD.

Process force

Some industrial systems may perform an action in which a force interaction exists between the machine and the chuck. In order to identify the propagation of a noise of this nature, the machine noise is added to the analysis. The machine noise is not present in all systems and is mainly added in order to get information about this kind of noise. The noise is modelled as a 30 Hz low pass filter with fourth order roll off. The RMS value of the machine force is 0.1 N. The PSD and CAS are shown in Figure 4.10(a) and 4.10(b).

4.4.3 Disturbance propagation

The disturbances that act on the system enter the control loop at the positions indicated in Fig. 4.11. The CPS of the servo error of the system is shown in Fig. 4.12. The biggest noise sources are the floor noise and the acoustic noise. The sensor noise is so small that the contribution of this noise source to the total error is negligible. It is therefore excluded from the figure. In the test setup, the main error contribution in the vertical (Z) direction was present in the frequency region between 10 and 20 Hz. These low frequent disturbances are assumed to be the source of the floor vibrations. The floor noise has a larger impact on the total system than predicted in the model.

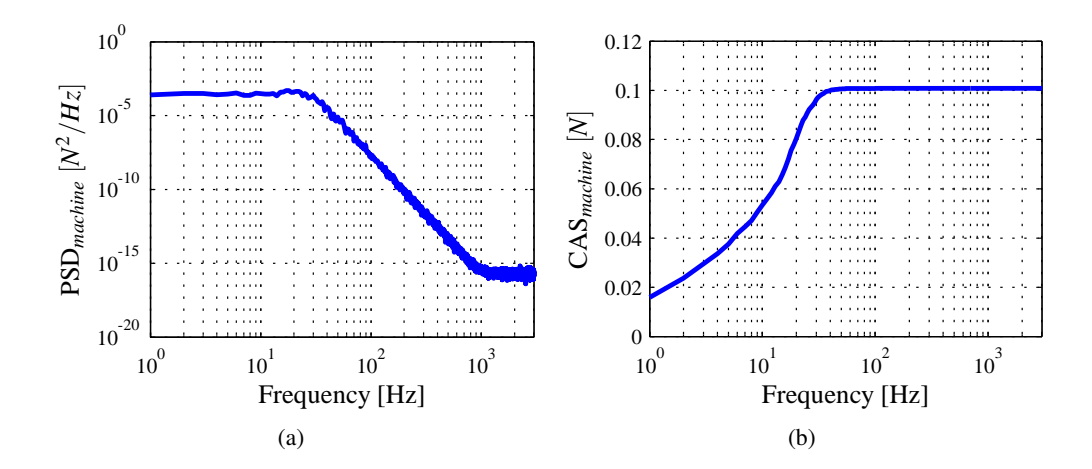


Figure 4.10

Power Spectral Density (a) and Cumulative Amplitude Spectrum (b) of the noise induced by machine actions on the chuck

The mismatch between the model and the test setup can be found in the supports of the test setup. The base frame of the test setup is supported on a simple 19 inch rack. This rack is not included in the model and may amplify the low-frequent noise. The second difference between model and test setup is the floor noise data. The floor noise data is an averaged measurement of the noise of the floor in the NTS lab. The test setup proved to be sensitive to impacts on the floor, such as doors slamming and people marching by. The averaged data of the floor measurement contains less of these impact shocks.

Conclusion

The DEB analysis performed, shows the influence of the different disturbance sources. The analysis showed that a controller should consist of increased disturbance rejection between 10 - 20 Hz. This can be accomplished by the use of an inverse notch filter.

The DEB analysis also shows the importance of an accurate model of the plant and an accurate model of the disturbances for this approach. The model used is corrected for the actuator locations which were not in the optimal position. However, even with the improved model, the CPS of the analysis is different than the CPS of the test setup.

4.4.4 \mathcal{H}_2 control as a performance measure

When different system concepts are designed by a system designer, the concept which is most promising has to be found by a performance comparison. Other influences may affect the choice of the concept. The over-actuated test setup was build to demonstrate an increased standstill performance of the chuck with one extra actuator, without implementing an advanced MIMO controller.

Comparing the realised PID controllers with a theoretically optimal controller can be beneficial to determine the quality of the PID controller. Model based \mathcal{H}_2 control is a control strategy, in which the output error is minimised given the system model

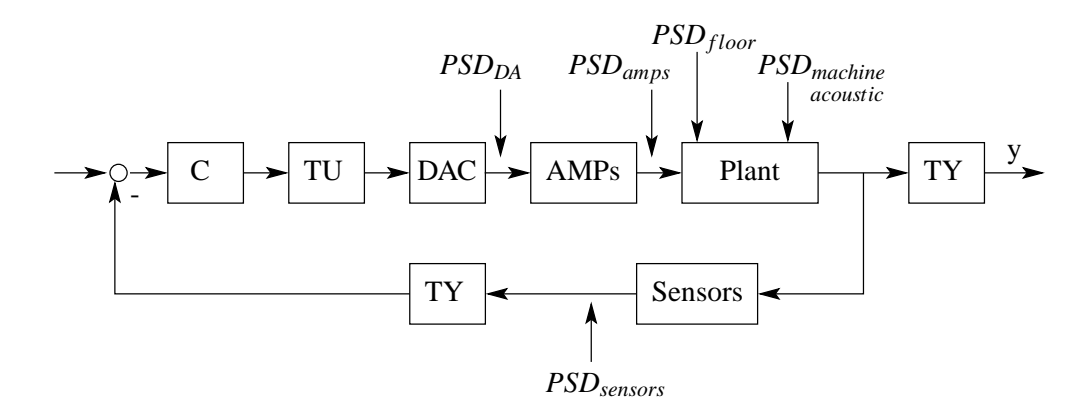


Figure 4.11 Closed loop representation of the wafer chuck plant with controller C, transformation matrices TU and TY, output y, amplifier and sensor positions. The position where different disturbance PSDs enter the system is indicated.

and its disturbances [16, 1]. The \mathcal{H}_2 controller is unique for the system and its disturbances and gives an upper bound on the achievable system performance. A detailed explanation of \mathcal{H}_2 control can be found in [16], more examples of the implementation and practical use of \mathcal{H}_2 control can be found in [5, 10].

The general plant configuration used in the \mathcal{H}_2 control field is shown in Fig.4.13. The system is described by eq. 4.13.

$$\begin{bmatrix} z \\ v \end{bmatrix} = P(s) \begin{bmatrix} w \\ u \end{bmatrix} = \begin{bmatrix} P_{11}(s) & P_{12}(s) \\ P_{21}(s) & P_{22}(s) \end{bmatrix} \begin{bmatrix} w \\ u \end{bmatrix}$$
(4.13)

Where: u are the control variables, v the measured variables, w the exogenous signals, such as disturbances and z the error signals to be minimised by the controller [16]. The disturbances, as described in sec. 4.4.2 are used as disturbance sources in the model. The PSDs of the disturbances are used to create weighting filters for the disturbance inputs in, order to create colored noise out the white noise inputs of the plant.

In order to balance the performance of the system and the controller output, the controller output is included in the performance channel of the controller. By weighing the controller output, the influence of the controller output in the performance channel can be influenced. The controller output in the performance is weighted with a weighting factor (α) in order to bound the controller action. By calculating the \mathcal{H}_2 optimal controllers for increasing controller output weight (α) , a Pareto curve is obtained between performance output and controller effort [5]. Each point on this curve is Pareto optimal, i.e. achieving a better system performance with less control effort is impossible.

The MIMO \mathcal{H}_2 controller will be used to create a Pareto curve in order to compare the PID controller with the Pareto optimal points. The resulting controller is a complex 4 x 3 MIMO¹ coupled controller. The analysis of this controller is of little use when the performance of the PID controller is to be increased. In order to create a \mathcal{H}_2 controller

¹A 4 x 3 controller has 3 inputs and 4 outputs.

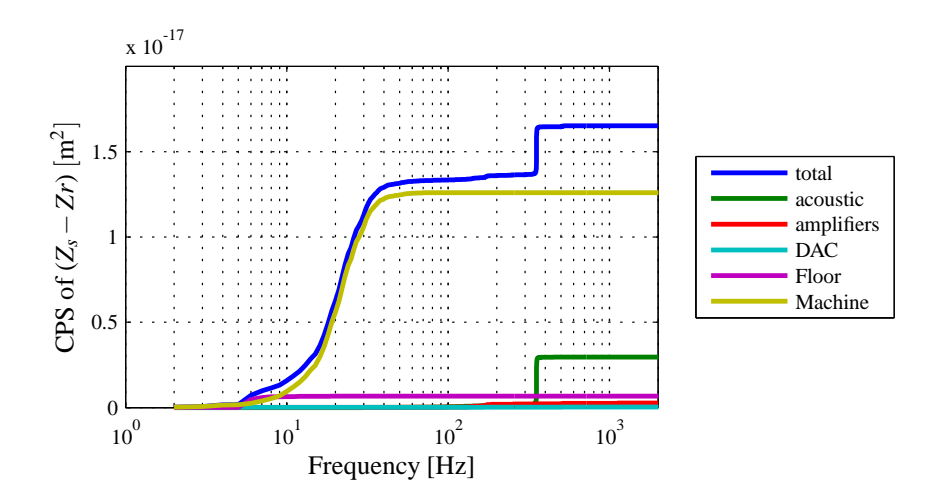


Figure 4.12 Cumulative Amplitude Spectra of the position error in Z-direction with a PID controller.

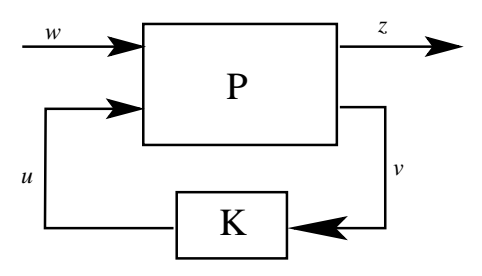


Figure 4.13
General control configuration

which can be compared with the PID controller, a \mathcal{H}_2 controller is created on the 3 x 3 decoupled plant. This controller, a 3 x 3 MIMO controller, is comparable to the PID controller. The diagonals of this controller can be analysed in order to increase the performance of the individual PID controllers.

4.4.5 Optimal control of the wafer chuck

The \mathcal{H}_2 controllers are calculated with the discrete \mathcal{H}_2 package from Matlab[©]. The \mathcal{H}_2 controllers can only be created when the generalised plant fulfils the standard assumptions. The standard assumptions are extensively discussed in [16] and [10] and will therefore not be repeated here.

The Pareto curves for the different systems are shown in Fig. 4.14. The norm of the performance, $||y||_{rms}$ is calculated at the rim of the chuck to include the error of the chuck due to the angular offset in nanometres. The controller effort is calculated as the norm of the actuator forces in Newtons². The maximum achievable performance,

²The controller effort of the decoupled \mathcal{H}_2 controller is scaled to the individual actuator forces

independent of the controller effort is the same in every situation. The over-actuated system uses less controller effort for the same performance, which makes sense, since the over-actuated system excites the internal dynamics of the chuck far less than the conventional system. The \mathcal{H}_2 controller designed for the decoupled plant has the same pareto curve as the over-actuated coupled system.

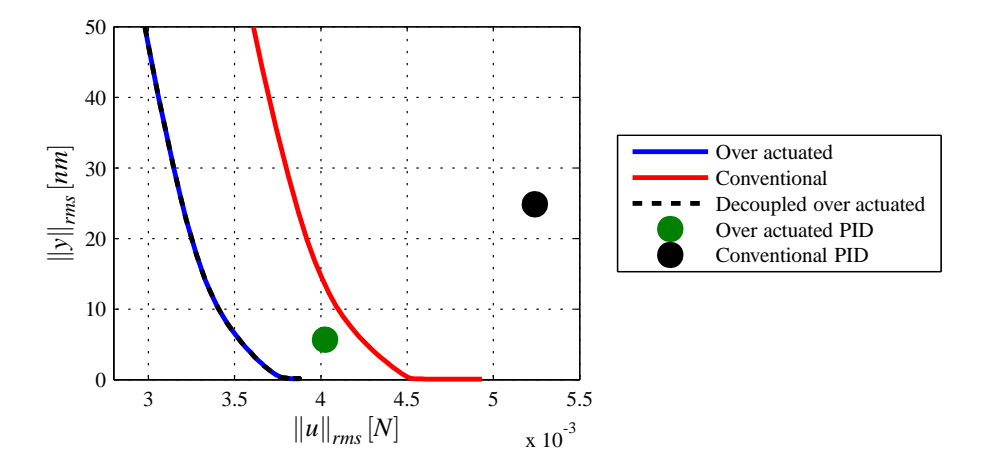


Figure 4.14 The Pareto curve for the wafer chuck model. The \mathscr{H}_2 controllers are based on a chuck with four actuators (—), a conventional chuck, with three actuators (—), and a chuck with four actuators with the decoupling matrices included (——). The Pareto points of the over-actuated (\bullet) and conventional actuated (\bullet) system model with PID controllers are included.

The controllers that have been created for the optimal control can't be compared to the PID controllers. Even the optimal controller for the decoupled plant can't be used. When only the diagonal terms of this controller are used, the system is unstable, which means that the cross terms of the controller are important.

The CPS of the decoupled controller with the same performance as the PID controller is given in Fig. 4.15 The standard deviation of the system with this controller is 5.5 nm. The biggest error stems from the machine and acoustic noise, which is as expected. The PID controller also shows the biggest error from these noise sources.

Conclusion

The model based control techniques described in this section create full MIMO controllers for the system. The decoupled \mathcal{H}_2 controller did not give any information about improving the PID controller, because the diagonal terms are still not the main part of the controller. The Pareto curve did show that the PID controller, created for the over-actuated system was close to the Pareto curve and that the controller was better than the conventional system can achieve with advanced control. This result shows the advantage of the over-actuated system once more.

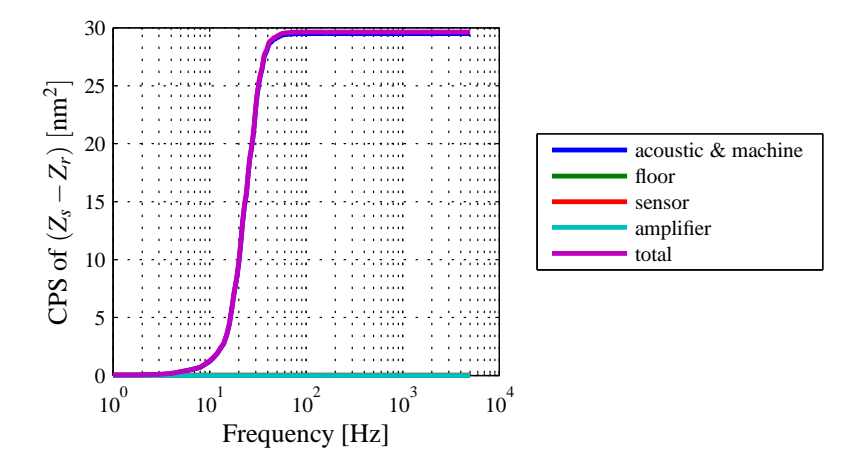


Figure 4.15 CPS of the decoupled over-actuated system using \mathscr{H}_2 control. It can be seen that the main contribution of the error in the system is due to the combined machine and accoustic noise.

4.5 Control of the over sensed system

One of the improvements of the test setup proposed in sec. 3.5 is the sensor configuration. With one extra sensor and a different sensor positioning, the chuck deformation due to the first two internal eigenmodes is cancelled out in the transformation matrix. In the transfer function of this setup, Fig, 3.25 on page 35, the excitation of the first two eigenmodes can not be seen. This allows the control bandwidth to be increased in both the conventional and the over-actuated configuration. The open loop transfer function in \mathbb{Z} , R_x and R_y direction is shown in Fig. 4.16, the controllers in Fig. 4.17.

The bandwidth of the controllers in the over-actuated setup can be set to 200 Hz for each direction. The conventional setup can have a controller with bandwidths of 100 Hz in each direction. Extra control effort has been placed around 18 Hz as concluded from the DEB analysis. This has been implemented as an inverse notch filter at 18.5 Hz.

The CPS of the servo error of this setup is shown in Fig. 4.18. The errors of both systems have been significantly reduced. The deflection of the chuck due to the first and second eigenmode is not visible in this CPS. The CPS of the individual sensors includes these deformations and is shown in Fig. 4.19. The standard deviations of the chuck at CoG and sensorposition are summarised in Tab. 4.4. It is shown in Fig. 4.19(b) that the first and second eigenmode are excited and that the deflection of the chuck due to these eigenmodes is the largest error source in the over-actuated system.

4.5.1 Active damping

The over sensed and over-actuated system consists of four actuators and four sensors to control three degrees of freedom. The conversion to CoG coordinates from the sensors cancels out the movement of the first and second eigenmode. This means that another

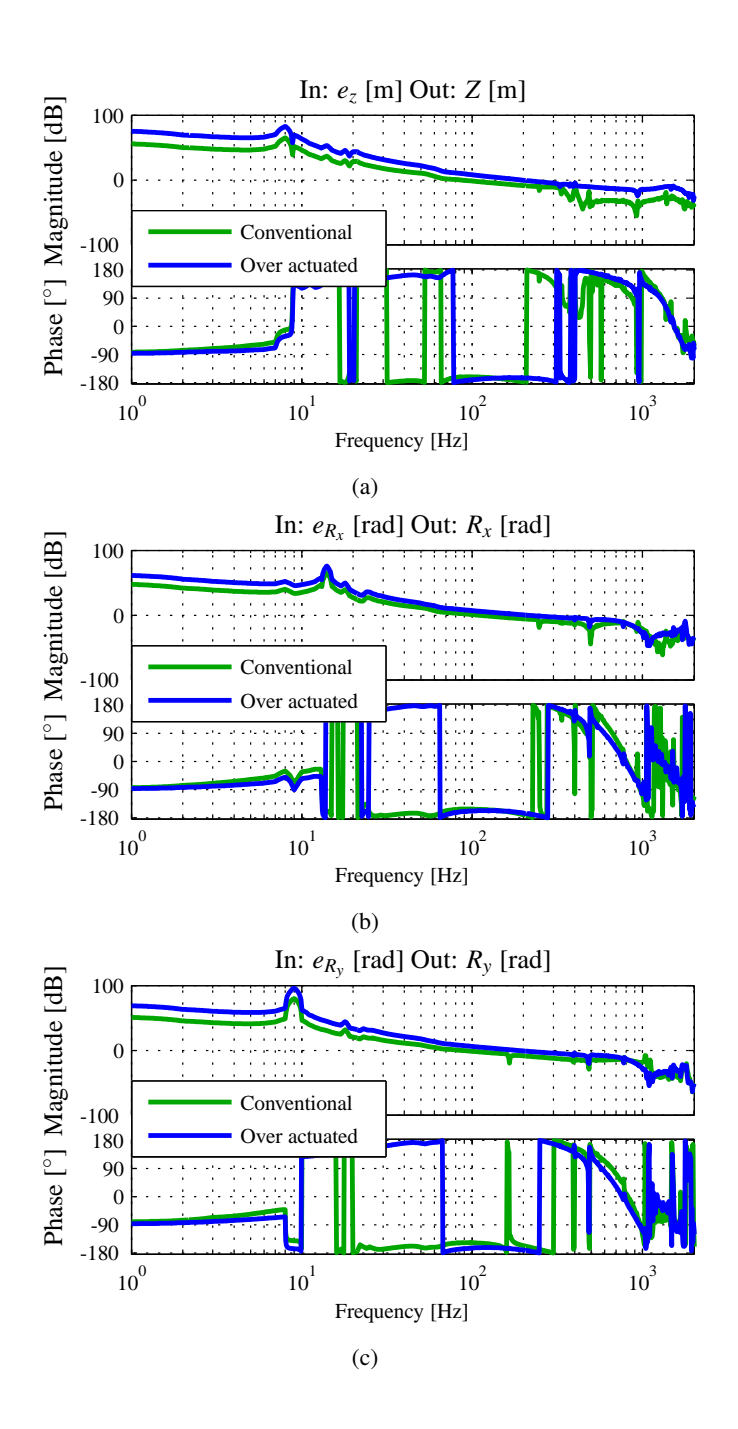


Figure 4.16
Measured open-loop transfer function from controller input to plant output. The Center of Gravity movement is reconstructed from four sensors. This makes the first two flexible modes invisible in this transfer function, allowing a higher control bandwidth for both the conventional and the over-actuated system.

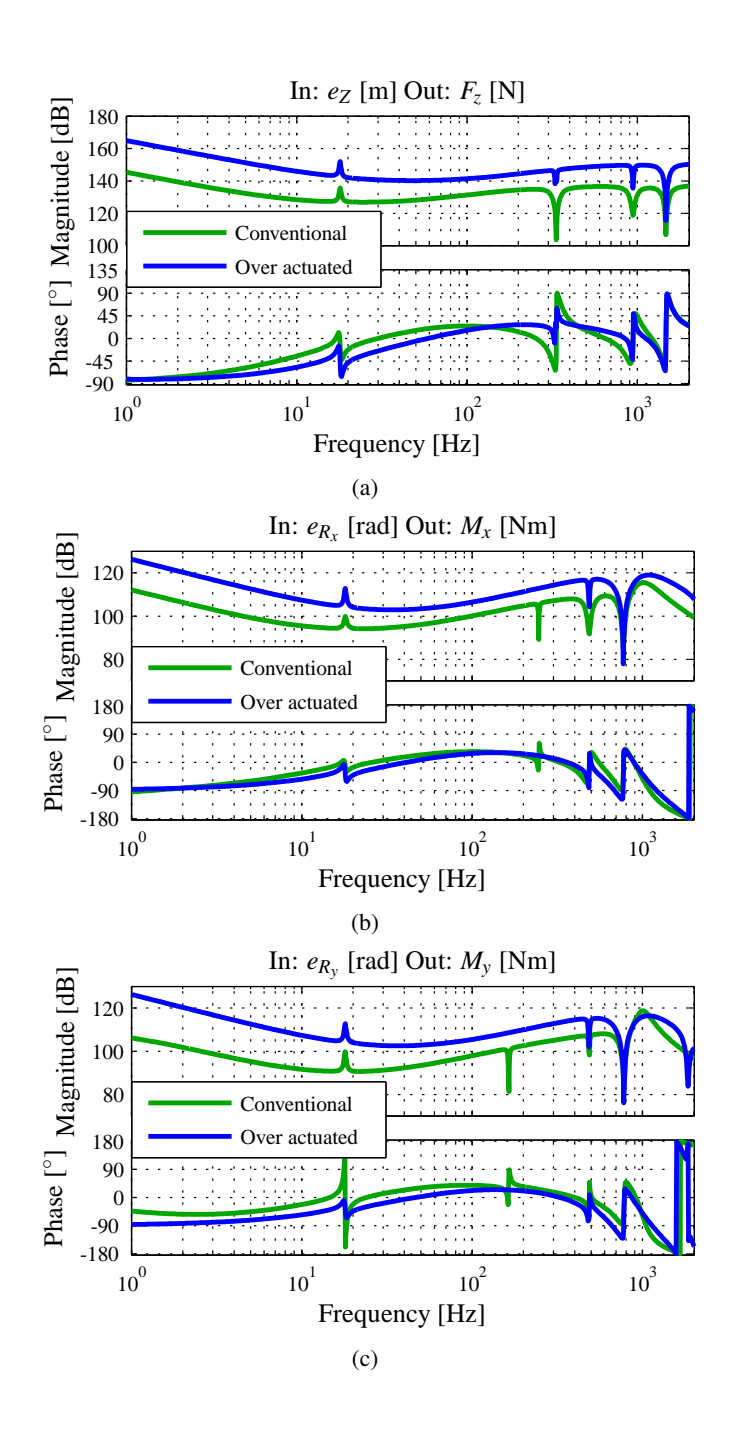


Figure 4.17

Transfer function of the conventional and over-actuated controllers. Four sensors are used for the measurement of the CoG, the resulting transfer function allows for a higher bandwidth controller.

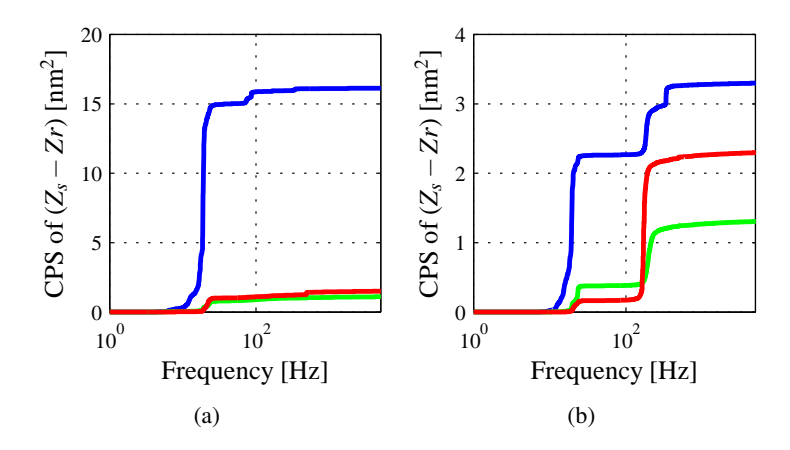


Figure 4.18 CPS of the servo error of the conventional (a) and over-actuated (b) wafer chuck with the use of four sensors. Given are Z (—), and the movement of the side of the chuck due to rotations R_x (—) and R_y (—).

Direction	Conventional system	Over-actuated system
	Standard deviation	Standard deviation
Z	4.0 nm	1.8 nm
R_{x}	4.2 nrad	4.6 nrad
R_{y}	4.9 nrad	6.0 nrad
Sensor nr.	Standard Deviation	Standard deviation
1	4.0 nm	2.5 nm
2	5.8 nm	2.8 nm
3	4.6 nm	2.5 nm
4	4.6 nm	2.6 nm

Table 4.4 Standard deviation of the servo error of the wafer chuck in the CoG and at sensor level using different actuation systems.

transformation of the sensor signals results in the measurement of the deflection of the chuck caused by the first and second eigenmode. The transformation matrix that is made for this measurement is given in Eq. 4.14.

$$\begin{bmatrix} Z \\ R_x \\ R_y \\ deflection \end{bmatrix} = \mathbf{TY_2} \cdot \begin{bmatrix} sens. \ 1 \\ sens. \ 2 \\ sens. \ 3 \\ sens. \ 4 \end{bmatrix} = \begin{bmatrix} 0.25 & 0.25 & 0.25 & 0.25 \\ -a & b & a & -b \\ -b & -a & b & a \\ -1 & 1 & -1 & 1 \end{bmatrix} \cdot \begin{bmatrix} sens. \ 1 \\ sens. \ 2 \\ sens. \ 3 \\ sens. \ 4 \end{bmatrix}$$
(4.14)

Where: b and a are the x and y coordinates of the sensors alternatively. The fourth channel of the decoupled system represents the deformation of the chuck caused by to the first and second eigenmode.

The four actuators are able to create the first mode shape. The first and third

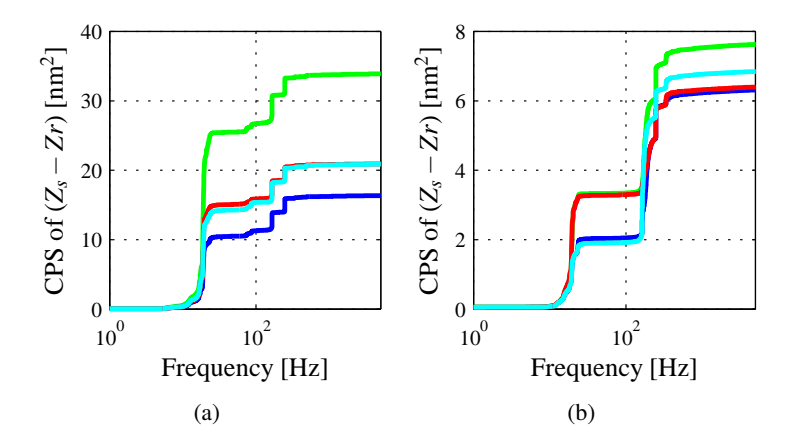


Figure 4.19
CPS of the four sensors used in the over sensed configuration with (a) conventional actuation and (b) over-actuation. This figure shows the CPS of the chuck at the sensor position, which includes the deflection of the chuck due to the first two eigenmodes, which are cancelled in the COG measurement (Fig. 4.18). Given are sensor 1 (—), sensor 2 (—), sensor 3 (—) and sensor 4 (—).

actuator have to create an opposite force to the second and fourth actuator. A fourth actuator channel in the decoupling output matrix is simply created by adding a column to the actuator matrix, TU, with a -1 for actuators 1 and 3 and +1 for actuators 2 and 4.

The resulting transfer function is shown in Fig. 4.20(a). Note that the damping ratio of this mode is low. The damping ratio, estimated from this figure is lower than 0.1%. The first eigenmode can be actively damped by a controller that adds damping action at this frequency. A controller that adds damping by means of a simple +1 slope will be able to damp the first eigenmode. The open loop transfer function of the deflection loop with controller can be seen in Fig. 4.20(b).

Figure 4.21 shows the CPS of the damped system. The first eigenmode disappeared in the CPS of the measurement at sensor level (Fig. 4.21(b)). Table 4.5 summarises the standard deviations of the controlled chuck. The standard deviation of the sensors is now 1.9 nm per sensor. The achieved performance is better than the system without active damping of the first eigenmode. The biggest error source now originates in the excitation of the second eigenmode. This eigenmode can not be damped with the four actuators, since the four actuators are positioned (almost) at the node line of the second eigenmode.

At this point, the cross terms in the transfer function of the system have impact on the system performance. Appendix B.2 shows the total transfer function of the 4 x 4 decoupled system, where the fourth channel is the deformation channel. From this transfer function it is clear that all the actuators excite the first and second eigenmode due to the non-diagonal terms in the transfer function. In order to achieve the performance of the system, a notch filter has been applied on all axes at the frequency of the second eigenmode. If the bandwidth has to be increased, it is clear that the cross terms in the decoupled system have to be taken into account for loop shaping.

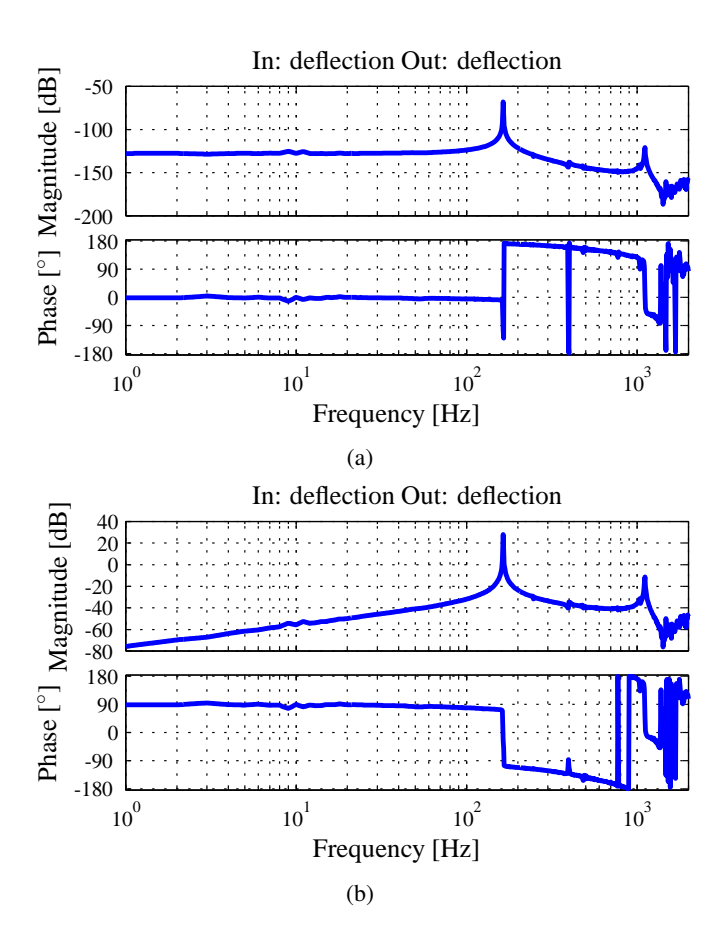


Figure 4.20 (a) Transfer function of the deflection measurement and actutation of the chuck. The first eigenmode, at 164 Hz, can be actively damped. (b) Open loop transfer function of the controlled deflection loop.

4.5.2 Conclusion

Over sensing gives an increase in performance for both the conventional and the overactuated system. The CPS values of the servo error give a somewhat misleading picture on the performance of the chuck, as the first two flexible modes of the chuck are cancelled out in the sensor transformation matrix. When comparing the CPS and standard deviation of the measurements at sensor position, the deformation due to the excitation of the flexible modes is included in the performance measure and it can be seen that these two flexible modes have an impact on the standstill performance of the chuck.

Active damping of the first eigenmode has been performed with the over-actuated system. The first eigenmode has disappeared in the transfer function, leading to a performance increase. The second eigenmode is the source of the largest error and thus limits the performance of the chuck.

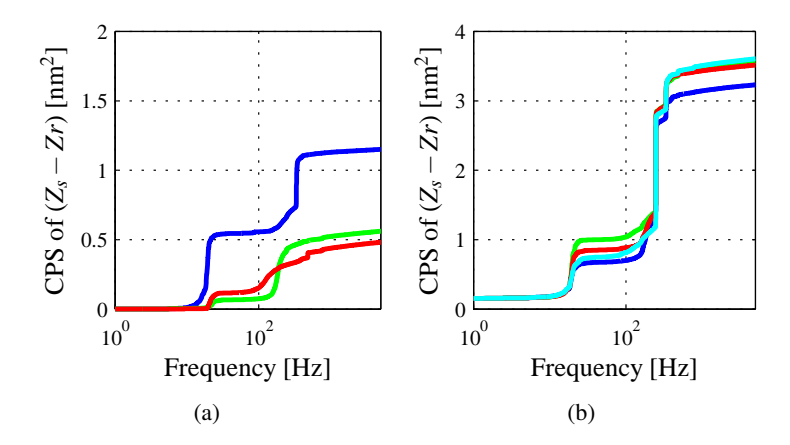


Figure 4.21 CPS of the over-actuated and over sensed wafer chuck with active damping of the first eigenmode. The CPS of the CoG measurement is given in (a) with Z (—), and the movement of the side of the chuck due to rotations R_x (—) and R_y (—). The CPS of the individual sensors is given in (b) with sensor I (—), sensor I (—), sensor I (—), sensor I (—) and sensor I (—). It can be seen that the first eigenmode is not the source of the biggest error. The excitation of the second eigenmode is.

Direction	CoG measurement	Sensor nr.	Sensor level
	Standard deviation		Standard deviation
Z	1.1 nm	1	1.8 nm
R_{x}	3.0 nrad	2	1.9 nm
$R_{\rm y}$	2.8 nrad	3	1.9 nm
		4	1.9 nm

Table 4.5
Standard deviation of the servo error of the wafer chuck in the CoG and at sensor level using different actuation systems.

4.6 Conclusion

The PID control of the system leads to a servo error STD of 4.4 nm with the over-actuated chuck and 26 nm with the conventional actuated chuck. The simple controllers that were created, perform well when compared to model based controllers. The use of a model based controller showed the maximum achievable performance. The performance of the PID controllers of the conventional and over-actuated setups can be further improved by adding extra control action around 18 Hz. This has been successfully implemented in the over sensed setup and can also be implemented in the normal setup with three sensors.

The static deformation of the chuck due to the presence of the extra actuator is significant. The static deformation has to be dealt with in an industrial system. The high frequent deformation of the chuck is over-estimated in the servo error. The deformation of the chuck by the excitation of the eigenmodes is interpreted as rigid body motion. The real deformation of the chuck is much smaller at most points of the chuck

than calculated, because the sensors that are used in the transformation matrix are positioned at the points where the deflection due to the first and second eigenmode is largest.

The performance of the system remains limited by the excitation of the first and second eigenmode. In the over sensed setup the deformation, due to these eigenmodes, is excluded in the transformation matrix. This leads to a performance increase. The position error STD in this situation is around 5 nm at sensor level for the conventional system and just below 3 nm for the over-actuated system.

The extra sensor can be used to create an extra channel that measures the deformation of the chuck due to the first and second eigenmode. With this extra channel a controller has been created in order to actively damp the first eigenmode. The position error STD with the active damping has been decreased to below 2 nm at sensor level. The performance limiting factor now mostly originates in the excitation of the second eigenmode. The second eigenmode can't be damped actively by the four actuators of the over-actuated system. By including the fifth actuator and a fifth sensor, this resonance can be actively damped. This results in an increase in standstill performance. The analytical decoupling of the second eigenmode is performed in the Appendix B.3.

Chapter 5

Design rules for over-actuated systems

In this chapter the experience gained during the design and testing of the over-actuated test setup is summarised in a general design strategy for future over-actuated systems. It is assumed that the choice for an over-actuated system has already been made and a performance criterion is specified by means of a standstill performance error standard deviation.

5.1 Guide for creating an over-actuated system

5.1.1 Step 1: Work towards symmetry in the geometry

The geometry of the chuck (or any other system) that will be designed is important for the optimization of the chuck. The choice for a square chuck instead of a triangular shaped chuck seems logical as on a square system, actuators which are placed on the diagonals are already placed symmetric w.r.t the first eigenmode and in the nodes of the second eigenmode.

Symmetry of the chuck is the most important aspect of the geometry. The more symmetric the system, the better the node lines will be on the diagonals. Extra added weight from tools, sensors and actuators, and damping measures should be included in the geometry in order to calculate the optimal cavity radius later on.

The thickness of the chuck has to be defined as well. The thickness determines the weight of the chuck and the eigenfrequencies. A trade off exists here between high internal modes and a high mass. The thickness of the chuck has to be specified taking into account the performance specification and the present disturbances.

Example The geometry defined in the test setup of this project is shown in Fig. 5.1(a). The geometry is defined as a square with removed corners and a large insert all around the rims of the chuck. The thickness is 20 mm at the thickness point and 10 mm everywhere else. Added masses from the gravity compensators, actuators and plate springs are indicated. In Fig. 5.1(b) a cross section of the chuck is shown with a cavity in the middle as will be described in step 3. The cross section shown is to scale.

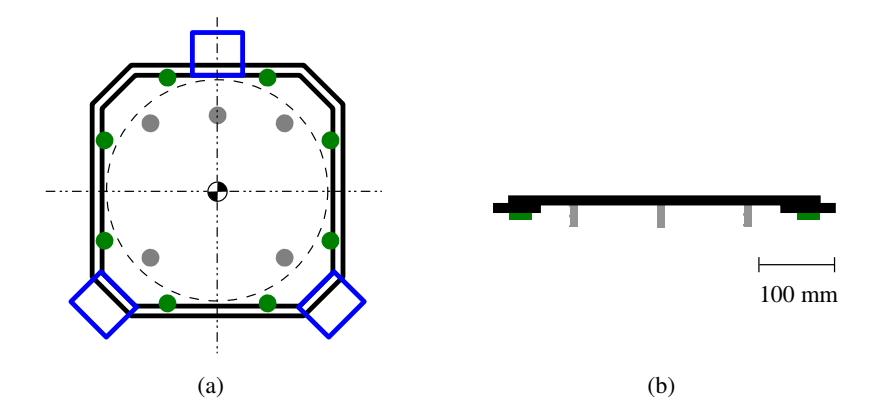


Figure 5.1
Geometry of the wafer chuck of the test setup. Included are added parts of the chuck that will be present on the chuck. The gravity compensators (\bullet) , actuators (\bullet) and plate springs (-) are indicated. (a) Top view with the cavity of the optimization (--), (b) Cross section.

5.1.2 Step 2: Material choice

One chuck used in the test setup is made of glass, the other is made of aluminium. Both chucks had several drawbacks which were one of the reasons why the chuck's first five eigenmodes are excited. The glass chuck is not homogeneous, the aluminium chuck is warped. Damping is low on both chucks.

In industry a wafer chuck is mostly made of zerodur. Zerodur is a material known for its low thermal expansion. A property important for a chuck with a surface area big enough to support a 450 mm wafer. Zerodur is a ceramic material. Warpage of a zerodur chuck will therefore be much smaller than an aluminium chuck.

The damping of the internal modes, discussed in Sec. 3.5.2, is an important property. A material with a high damping ratio of itself is advantageous, as less extra damping measures are needed to improve the internal damping of the chuck. An interesting list of damping properties of materials is given in [13].

5.1.3 Step 3: Define actuator locations and chuck cavity

When the geometry and the material of the chuck is defined, the optimization procedure as described in [2, 8], can be performed. The optimization criterion to minimise, is based on the actuator locations. The sensor location has an influence on the performance as well, but the actuator location has to be optimized in order to excite the first five eigenmodes of the chuck as less as possible. The performance criterion of Eq. 2.5 on page 8 is used in order to define the position of the actuators and the diameter of the cavity. The performance criterion is repeated in Eq. 5.1.

$$N_j^2 = \sum_{i=1}^5 (\phi_i^T \cdot B_j)^2 \qquad N_{total}^2 = \sum_{j=1}^3 (N_j)^2$$
 (5.1)

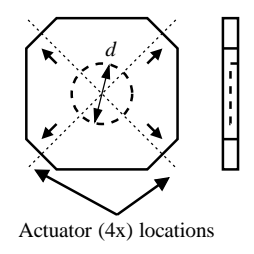


Figure 5.2

Optimisation procedure of the over-actuated setup. A cavity is created in the chuck with a diameter to be determined in order to change the node lines. The actuators are positioned on the diagonals, so that they act in the nodes of the first five eigenmodes. The optimization results in the diameter and in the actuator locations to be used.

The optimization procedure, used in [2] calculates the chuck's eigenmodes for every combination of cavity and actuator location on the diagonals. A schematic view of this procedure is shown in Fig. 5.2. This full grid scan proved to be time consuming. An optimized procedure is proposed here to decrease the calculation time. This procedure can be used because of the symmetry of the system.

- Calculate the eigenmodes of the chuck with different cavities, without actuators attached.
 - The impact of the added weight of the actuators placed on the node lines of the chuck is low. The calculation of the eigenmodes without the actuators attached will save time.
- Import the eigenmodes in Matlab[©] and find the chuck at which the node lines intersect at one point in the diagonals.
 Using the symmetry of the chuck, the node lines should intersect on the diagonals.
 - nals of the chuck. A simple Matlab[©] script can define which cavity makes the node lines of the chuck intersect at the diagonals. One way to accomplish this is to search for the location of the node line of the third and the fifth mode on the diagonals and subtract these locations. The smallest difference in location will be the position where the node lines intersect.
- Perform a full scan optimization with actuators in a region around the optimal point, found without actuators.
 - A full grid scan optimization procedure will be performed in order to make sure that the optimal actuator location and cavity diameter is found. This is done by using the performance criterion (Eq. 5.1).
- Check the position of the actuators using the node line representation in matlab. In order to double check the optimization procedure, a node line representation of the chuck, as in Fig. 3.19, can visualise the position of the node lines and the actuators.

5.1.4 Step 4: Define the positions of the sensors

The test setup has been used with two different sensor setups. The first sensor setup consists of three sensors, positioned at the point of maximum deflection of the first and second eigenmode. This has two consequences:

1. Observability of the eigenmodes as rigid body modes.

The eigenmodes are observed and transformed to rigid body modes of the CoG.

The excitation of the eigenmodes is visible in the transfer function and therefore bandwidth limiting.

2. Over-estimation of chuck movement.

Because the deflection of the chuck is interpreted as a rigid body mode, the movement of the chuck at positions other than the positions of maximum deflection caused by an eigenmode, is over-estimated. The standstill performance of the chuck, determined by the sensors, is therefore equal to, or worse than the real standstill performance of the chuck, depending on the excitation of the eigenmode.

These two consequences result in less standstill performance, because of consequence 1. The measured standstill performance is a good measure of the real standstill performance of the chuck.

The second sensor setup consists of four sensors, placed so that the first two eigenmodes are not visible as rigid body CoG movements. This has two consequences, opposite to the above consequences.

1. The first two eigenmodes are not measured as rigid body modes.

The first two eigenmodes are cancelled out in the transformation matrix to the CoG coordinates. The deformation of the chuck due to these eigenmodes, will therefore not be visible in the CoG transfer functions of the system, allowing a higher control bandwidth.

2. Under-estimation of chuck movement.

Because the deflection of the chuck caused by the first two eigenmodes is cancelled out in the CoG transformation, the actual movement of the chuck may contain deformations due to these eigenmodes. The real movement of the chuck will therefore be higher than measured.

The second sensor setup results in a higher control bandwidth. Disturbances acting on the system exciting the first and second eigenmode¹, may decrease the standstill performance. The sensors cannot measure this deflection, therefore the chuck movement may be under-estimated. A schematic representation, using a simple beam is shown in Fig. 5.3.

In the test setup, the use of four sensors proved to give the highest standstill performance. When the four sensors are properly positioned, the first eigenmode can be damped as well. A sensor position optimisation, like performed for the actuators, results in the same location as the actuators. The sensors will not be able to observe

¹The actuators themselves are one of the disturbances that excite the eigenmodes

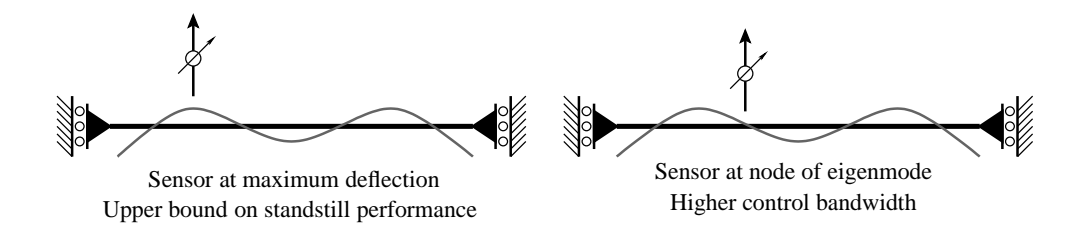


Figure 5.3

Schematic representation of the influence of the sensor location on the observation of eigenmodes.

deformations of the chuck caused by the second till fifth eigenmode. The first eigenmode can be distinguished and damped with an extra control loop. The best possible positioning of the sensors will therefore be a co-located positioning. This is not always possible. For example, the use of linear encoders in the test setup requires the positioning of the sensors at the rims of the chuck. A symmetrical setup, like the one explained in Sec.3.5.3 on page 33, is then preferred. The sensor setup will cancel out the deformation of the first and second eigenmode of the chuck by symmetry.

An optimisation criterion can be used along a specified boundary (e.g. the rims). The optimization should include the eigenmode, the sensor location and the transformation matrix in order to include the mode cancellation in the optimization. The optimization criterion is given in Eq. 5.2.

$$N^{2} = \sum_{i=1}^{5} (\phi_{i}^{T} \cdot T_{Y} \cdot C)^{2}$$
 (5.2)

Where T_Y is the transformation matrix, ϕ_i represents the ith eigenmode, and C is the nodal matrix containing the position of the sensors.

Chapter 6

Conclusions and Recommendations

6.1 Conclusions

This section provides the conclusions of the research performed on the 450 mm over-actuated lightweight wafer chuck. The main challenge of this research was to identify the dynamic properties of an over-actuated test setup. One of the analyses to be performed was to identify the causes of the excitation of the first five eigenmodes by the over-actuated actuators. The two wafer chucks available in the test setup showed the excitation of the eigenmodes. The actuators are not positioned exactly in the nodes of the eigenmode, since this was not in the model, there is a model mismatch.

Conclusions on the causes of the model mismatch

The analysis performed on the chucks shows that symmetry is essential. The system proved to be sensitive to a lack of symmetry. The influence of the gravity compensators and the fifth actuator, both items that are not mounted symmetrically on the chuck, proved to be bigger than in the Ansys model. Even with a symmetric mounting of the actuators and gravity compensators, the eigenmodes are excited, although less than without symmetry. Different aspects of the chuck have been studied in order to identify the remaining problem. However, no conclusive solution was found during the coarse of this research. The topic remains to be dealt with during future recommended studies.

The chucks proved to be sensitive for the actuator misalignment. The small misalignment of the actuators w.r.t the node lines of the first five eigenmodes has the effect that the eigenmodes are excited and therefore visible in the transfer function. In order to make the chuck less sensitive to such misalignment, the damping coefficients of the eigenmodes can be increased.

Conclusions on Control and performance

The chuck movement in Z, R_x and R_y directions are actively controlled with SISO PID controllers for every direction. A bandwidth of 100 Hz is achieved with the overactuation principle leading to a standstill STD of 4.4 nm in Z-direction. The conventional system, with three actuators to control the system in the same directions was

able to be controlled with controllers with a bandwidth of around 55 Hz. This leads to a standstill STD of the conventional system of 26 nm in z-direction.

A DEB analysis is performed to establish the best possible standstill performance. This analysis reveals that the performance of the system can be improved by adding an inverse notch filter around 18 Hz. Model based control has been applied to a model of the system leading to a Pareto curve. The performance of the PID controllers can be compared to an optimal controller. The over-actuated PID controllers provided improved performance compared to a conventional system that uses optimal control.

The performance of the over-actuated system is limited by the first and second eigenmode. The deformation of the chuck caused by these eigenmodes is measured as a rigid body movement and is therefore bandwidth limiting for the system. An over sensed setup is proposed that excludes the deformations due to the first and second eigenmode from the CoG movements. This allows a higher control bandwidth. The extra sensor addition can also be used to actively damp the first eigenmode. With a control bandwidth of 200 Hz and the active damping of the first eigenmode, the standstill STD of the over-actuated and over sensed setup is just below 2 nm at the sensor positions of the chuck. The calculated CoG movement STD is 1.1 nm in Z-direction.

The over sensed setup can also be used in the conventional setup. This also results in a higher bandwidth, because the deflections of the first and second eigenmode are absent in the control loop. Active damping of the first eigenmode is impossible in the conventional setup, since there are only three actuators available to control the three degrees of freedom. With the conventional over-sensed setup a bandwidth of 100 Hz is achieved which results in a standstill STD of 5.8 nm at sensor level. The calculated CoG movement STD is 4 nm in Z-direction.

The over sensed configuration with damping of the first mode shows that the second eigenmode is excited and the biggest part of the position error STD at the sensor position is due to the excitation of the second eigenmode. The control loops of the three degrees of freedom excite this eigenmode. The cross terms in the transfer function influence the performance. The performance of the chuck is therefore defined by the excitation of the next eigenmode. Active damping of the next eigenmode, if possible, is one of the ways to increase performance.

Conclusions on designing an over-actuated system

Throughout the research the symmetry of the system proved to be the most important factor in predicting the node lines on the diagonals and positioning the actuators on the node lines. A design of an over-actuated system should be designed symmetrically, including added weights mounted on the chuck, e.g. weights like equipment, gravity compensators etc.

Damping of the eigenmodes of the chuck leads to a lower sensitivity of the actuator location. Using a chuck with a higher internal damping coefficient, the offset of the actuators has less impact on the performance of the chuck.

The sensor positioning of the chuck has proven to significantly influence on the standstill performance of the system. The standstill performance of the over-actuated system has improved from 4.4 to 2 nm with the addition of an extra sensor. The sensor placement has to be included in the design of the system as a variable that can be

performance limiting.

The additional static deformation of the chuck caused by the added actuator proved significant. The static deformation is a part of the system that has to be dealt with.

6.2 Recommendations

This section provides recommendations for further research and the future design of over-actuated systems.

Further research

The dynamical analysis of the wafer chuck in Chap. 3 showed that the symmetry of all components of the chuck is important. The symmetry of the system enables the node lines to intersect on the diagonals, such that an actuator can be placed there. A symmetrical chuck showed that the excitation of the eigenmodes was less than an a-symmetric chuck. Notwithstanding, even while using a symmetrical chuck, the eigenmodes are excited. Further research has to be performed to identify the cause of this mode excitation. One aspect that has not been studied in this research is the warp of the chuck. The aluminium chuck shows warping which may influence the excitation of the eigenmodes. Figure 6.1 shows a beam in warped position. The actuator forces of the warped beam introduce a torque on the beam. This torque can excite the eigenmodes.



Figure 6.1 Influence of chuck warp on actuator force direction. The actuators create a force not perpendicular to the surface. This may excite eigenmodes.

The test setup consists of five actuators. Active damping of the first eigenmode has been successfully applied using four sensors and four actuators. The fifth actuator is positioned at a position where active damping of the second eigenmode can be accomplished. With an extra sensor and the fifth actuator, active damping of the second eigenmode can be achieved. Further research may indicate if this setup results in a further performance increase. In Appendix B.3 the analytical decoupling of this setup is provided.

Recommendations on the future design of over-actuated systems

This report is the result of research on the first over-actuated system available. The shortcomings and problems of this test setup can be used to design an improved over-actuated system in the near future. The most important recommendations for future design of over-actuated systems will be summarised here.

• *Create a symmetric system*The positions of the node lines of the eigenmodes are influenced by every mass

added to the chuck. Creating a symmetric system ensures the node lines are located on the diagonals.

• Add damping of internal modes

The sensitivity of the excitation of the eigenmodes due to the misalignment of actuators on the node lines can be lowered by adding damping. In order to create a robust system, a chuck with eigenmodes which are moderately damped (at least ζ bigger than say 0.3%) will be less sensitive for misalignment between the actuator position and the node lines.

• Optimise sensor locations

The sensor location proved an important factor when improving the standstill performance. When an optimisation is performed in a similar fashion as has been described for the actuators, the outcome would be that the sensors have to be placed co-located with the actuators. This indeed gives the lowest observability of the first five internal eigenmodes. The modes are hardly excited, and if they are excited, they are hardly measured. Using four sensors allows active damping of the first internal eigenmode.

Appendix A

Additional measurements on the chuck

A.1 Measured mode shapes of the chucks

In this section the measured mode shapes of the glass and aluminium chuck will be given. The mode shapes of the glass chuck are shown in Fig. A.1, the mode shapes of the aluminium chuck, including 3d view, in Fig. A.2.

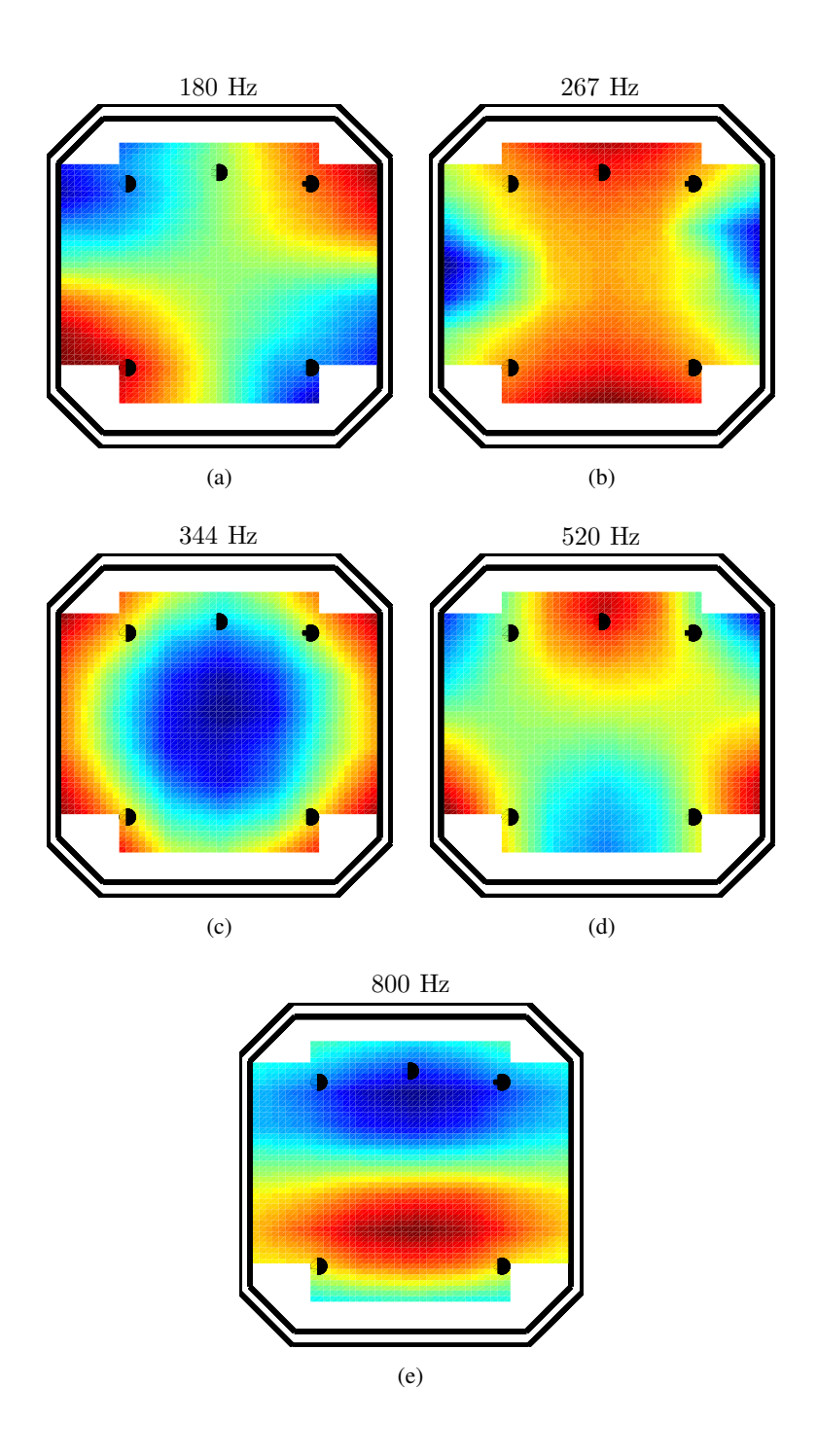


Figure A.1 Measured mode shapes of the glass chuck

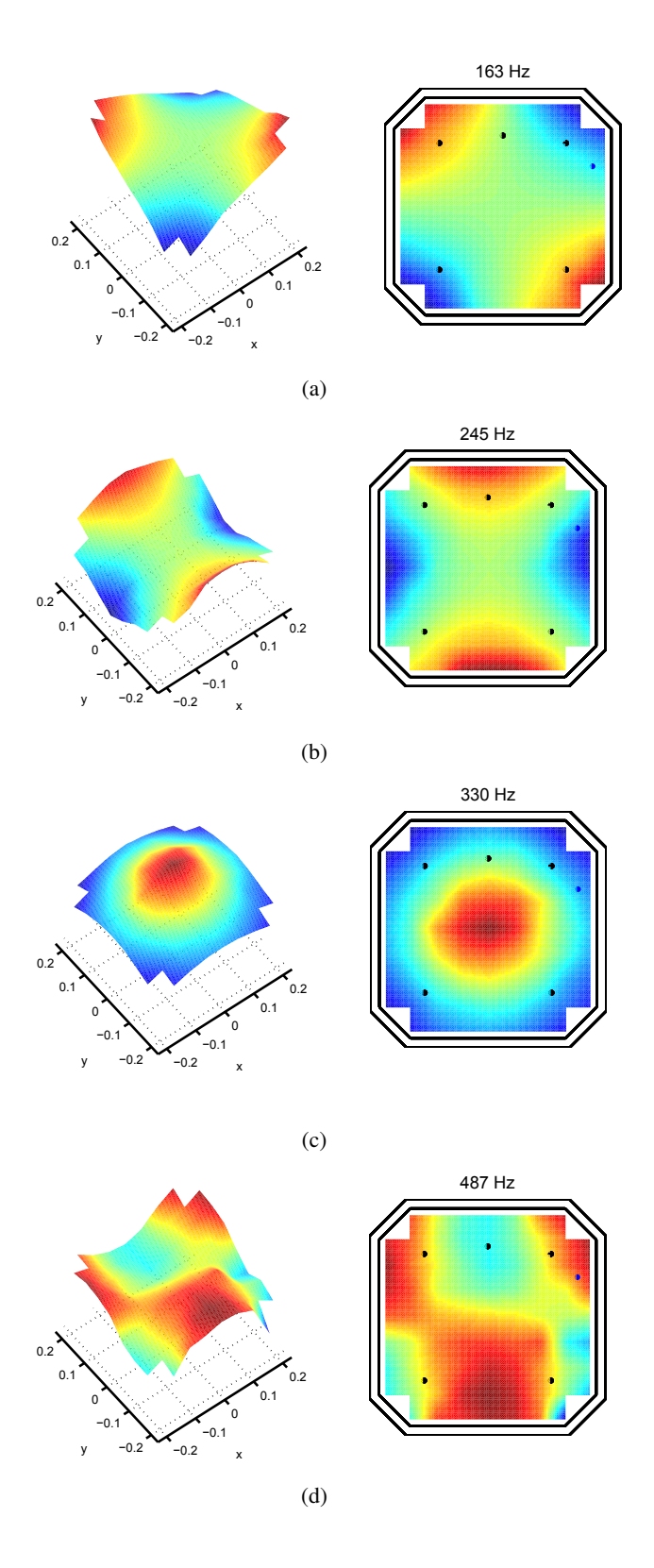


Figure A.2

Measured mode shapes of the aluminium chuck

A.2 Actuators and their mounting

This section describes efforts done to identify a gain difference between the different actuators. The actuator mounting on balance masses will be explained and measurements to identify possible parasitic forces are performed.

A.2.1 Balance masses

The actuators are mounted on the base frame with balance masses [2]. These balance masses are mounted on the base frame with high damping. The excitation of the eigenmode by the actuators is visible in the transfer function the system. Around 40 to 50 Hz the mass line of the chuck shows some disruptions. This is due to the balance masses. A modal analysis on the balance masses reveals the eigenfrequencies. The eigenfrequencies of the balance masses are given in Table A.1

Balance mass number	Frequency [Hz]
Balance mass 1	51
Balance mass 2	53
Balance mass 3	43
Balance mass 4	41
Balance mass 5	47

Table A.1 Eigenfrequencies of the balance masses. Numbering consistent to the actuator numbers of Figure 2.6.

A.2.2 Actuators

The actuators that are fitted in the system may have a different motor-constant. This means that they may give a slightly different force output per current input. The reason for this difference can be the uncertainty of the strength of the magnets, the position of the magnet in the coils and other tolerances. These differences can also introduce parasitic forces. If the actuator creates an additional torque, some eigenmodes will be excited even if they are acting at the nodes. It is therefore important that the actuator only creates a force in the Z-direction.

Actuator Gains

In order to measure the gain of every actuator, the influence of every actuator to the movement of the middle of the plate will be studied as well as the gain of the actuator measured with a sensor at the actuator position, a co-located measurement. These measurements will be done in a frequency region where the plate is moving freely, at 90 Hz. The influence of the different plate springs will therefore be negligible.

The Co-located measurement will be performed with actuators one to four and an accelerometer, positioned at the actuator locations. The gain of actuator 3 will be set to 1 and the other gains will be related to the gain of actuator 3. The choice of actuator 3 is arbitrary. The numbers calculated are correction factors to give the same gain

as actuator 3. Table A.2 shows the actuator gains and the corresponding correction factors. A five percent difference in actuator gains is observed with respect to actuator 3.

	Actuator 1	Actuator 2	Actuator 3	Actuator 4
Actuator gain	0.0607	0.0570	0.0597	0.0603
Correction factor	0.984	1.05	1.00	0.991

Table A.2

Actuator gains and correction factors for the Co-located measurement

The second measurement is a measurement to the linear encoders. When the input transformation matrix is applied the influence of each actuator to Z, Rx and Ry at the middle point is known. The movement that the plate makes when only one actuator is actuating with a sine wave of 90 Hz is a rotation around the diagonal of the plate. The Z movement of the centre of the plate is therefore very small. The Rx movement of the plate due to the different actuators should be the same for each actuator as is the case in the model. A gain difference in the actuators can be measured this way. Table A.3 shows the actuator gains for this measurement. The two measurements differ in correction factor. The difference in gain for actuator 2 is the highest. Actuator 1 seems to be most constant. The position of the chuck, and therefore the orientation

	Actuator 1	Actuator 2	Actuator 3	Actuator 4
Actuator gain	1.91	1.87	1.84	1.93
Correction factor	0.967	0.984	1.00	0.955

Table A.3

Actuator gains and correction factors for the Rx measurement

of the permanent magnets attached to the plate in their coils, might have influence on the performance of the actuators. In order to find out, the actuator gains will be tested with different plate positions.

Influence of chuck position

In order to find out the influence of the chuck position and tilt to the actuator gains the actuator gains will be tested with different chuck positions and tilt angles. The actuator gains can be seen in Fig. A.3. It can be seen that the gain of the actuators is constant in the range that the chuck can position itself. The average actuator gains are given in Tab. A.4. The constant actuator gain with the tilted chuck indicates that the force in

	Actuator 1	Actuator 2	Actuator 3	Actuator 4
Actuator gain	1.8948	1.8609	1.8553	1.9164
Correction factor	0.9792	0.9970	1.0000	0.9681

Table A.4

Average actuator gains

Z-direction is constant, independent of the chucks position. Any additional parasitic

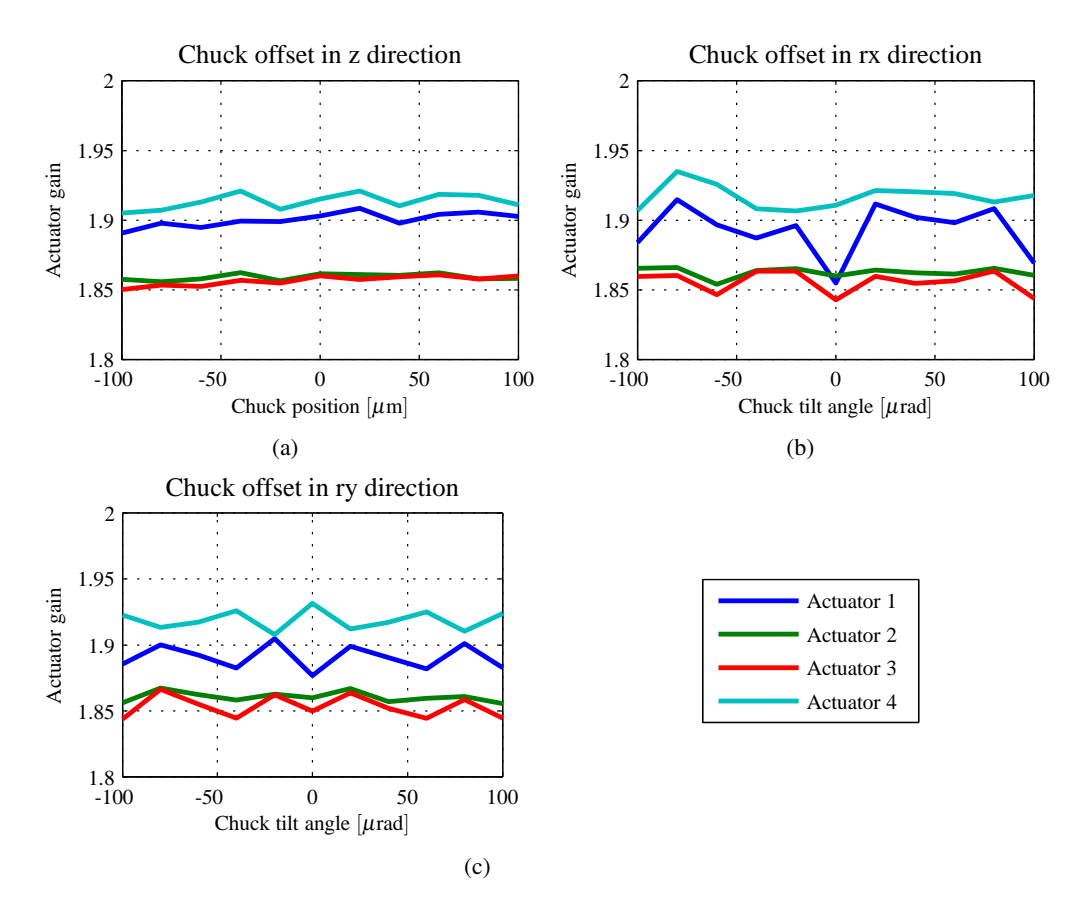


Figure A.3

Actuator gains with the chuck positioned and tilted in different directions.

force would have resulted in a different gain with a tilted chuck. This indicates that parasitic forces are negligible.

Appendix B

Additional measurements on control of the chuck

B.1 Transfer functions of the system

The 3 x 3 transfer function of the over-actuated and conventional actuated decoupled system is given in Fig. B.1. The decoupling of the plant is correct when the chuck behaves as a rigid body. In the flexible region the plant can be coupled. The non-diagonal terms should be considered when control is applied. The relative gain array is shown in Fig. B.2. The RGA also shows a good decoupling in the rigid body region.

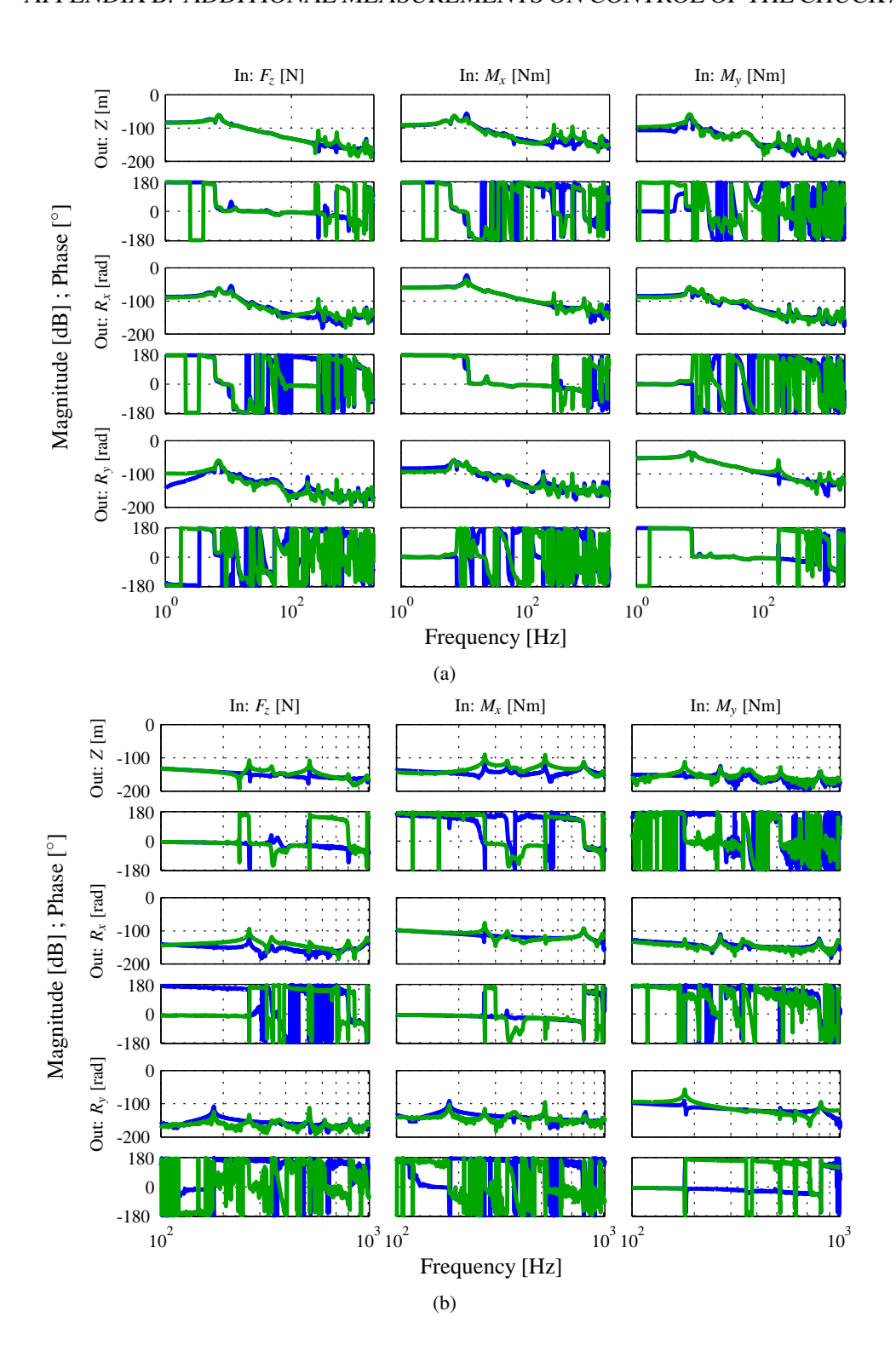


Figure B.1
Transfer function of the decoupled plant (glass chuck). The over-actuated system is given in blue (—), the conventional system is given in green (—) (a). Detailed view between 100 and 1000 Hz (b).

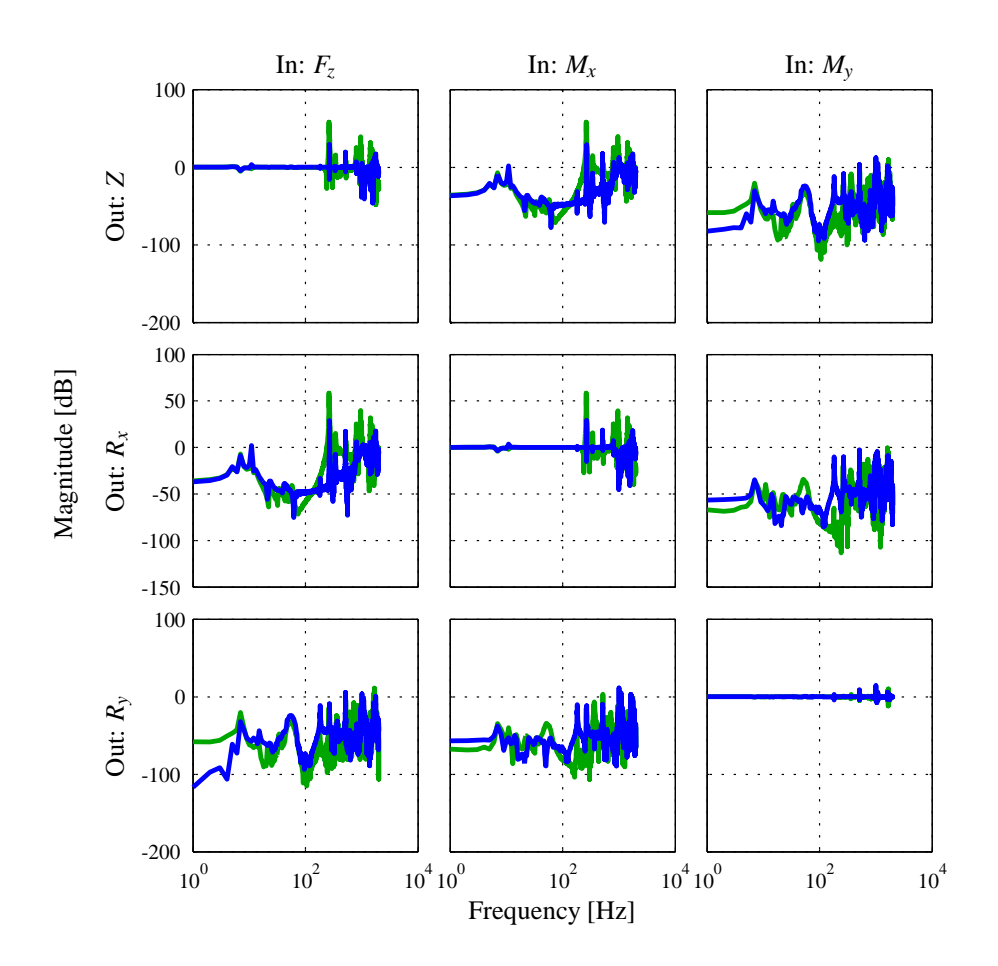


Figure B.2

Relative Gain Array of the decoupled conventional (—) and over-actuated (—) plant

B.2 Transfer function of the decoupled system including damping channel

In Section 4.5 an extra channel is added to the control system. TThis extra channel distinguishes the deformation of the chuck, caused by the excitation of the first and second eigenmode. The total decoupled plant is shown in Fig. B.3. In order to show that the fourth channel indeed actuates the first eigenmode, the RGA is shown in Fig. B.4.

B.3 Analytical addition of damping of the second eigenmode

The fifth actuator present in the system is able to excite the second eigenmode. A fifth sensor can be added to the system in order to distinguish the excitation of the second eigenmode. The fifth sensor is positioned in the middle of the bottom rim. The sensor decoupling transformation matrix can be extended with a channel for the deformation of the second mode. The choice is made not to fully decouple the output channel. With a fully decoupled output channel, the result will be that the other four

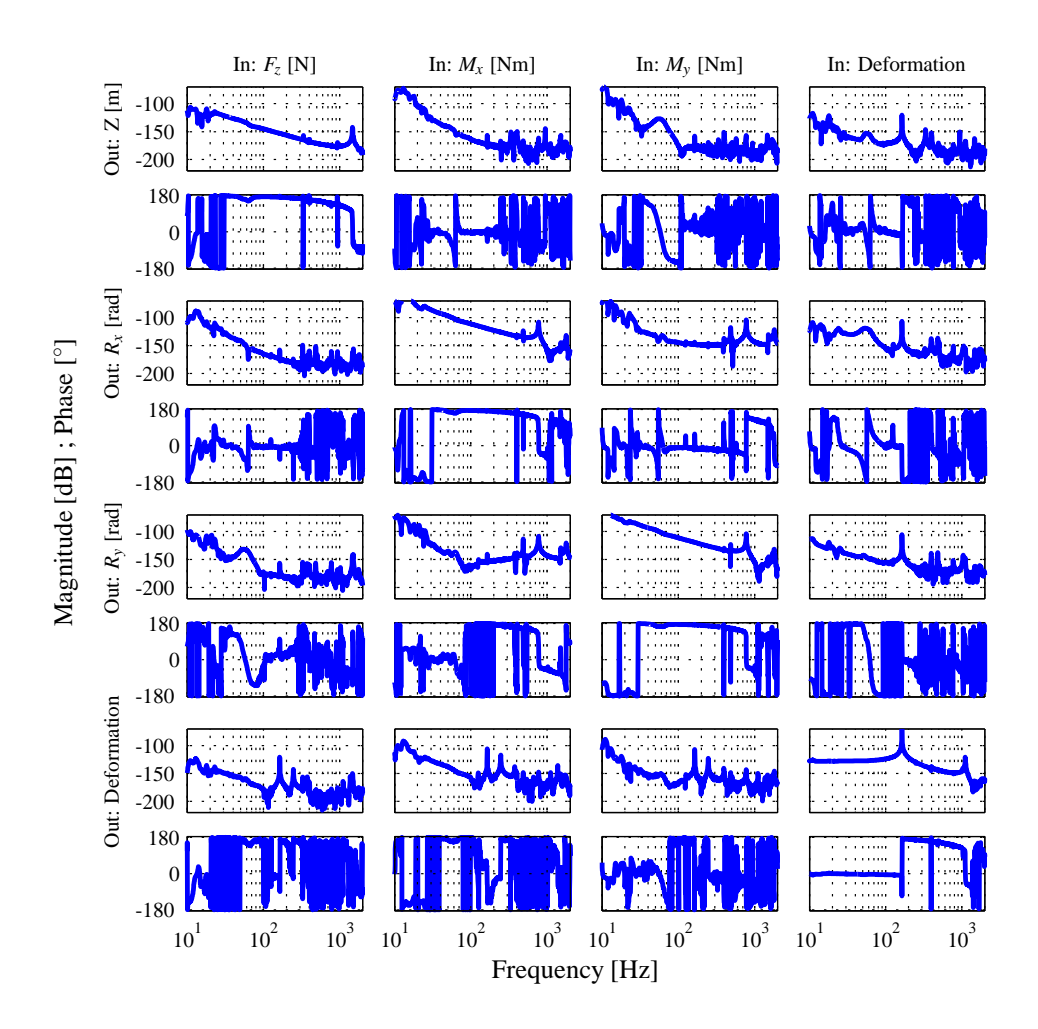


Figure B.3

Transfer function of the decoupled over-actuated plant including deformation channel.

actuators are used to compensate the rigid body movement caused by the fifth actuator. The resulting transfer function is shown in Fig. B.5(a). It can be seen that the second eigenmode can be distinguished, but that low frequent noise will be amplified. The control system in Z, R_x and R_y direction have to suppress this extra noise. The 5x5 decoupled plant is shown in Fig. B.6.

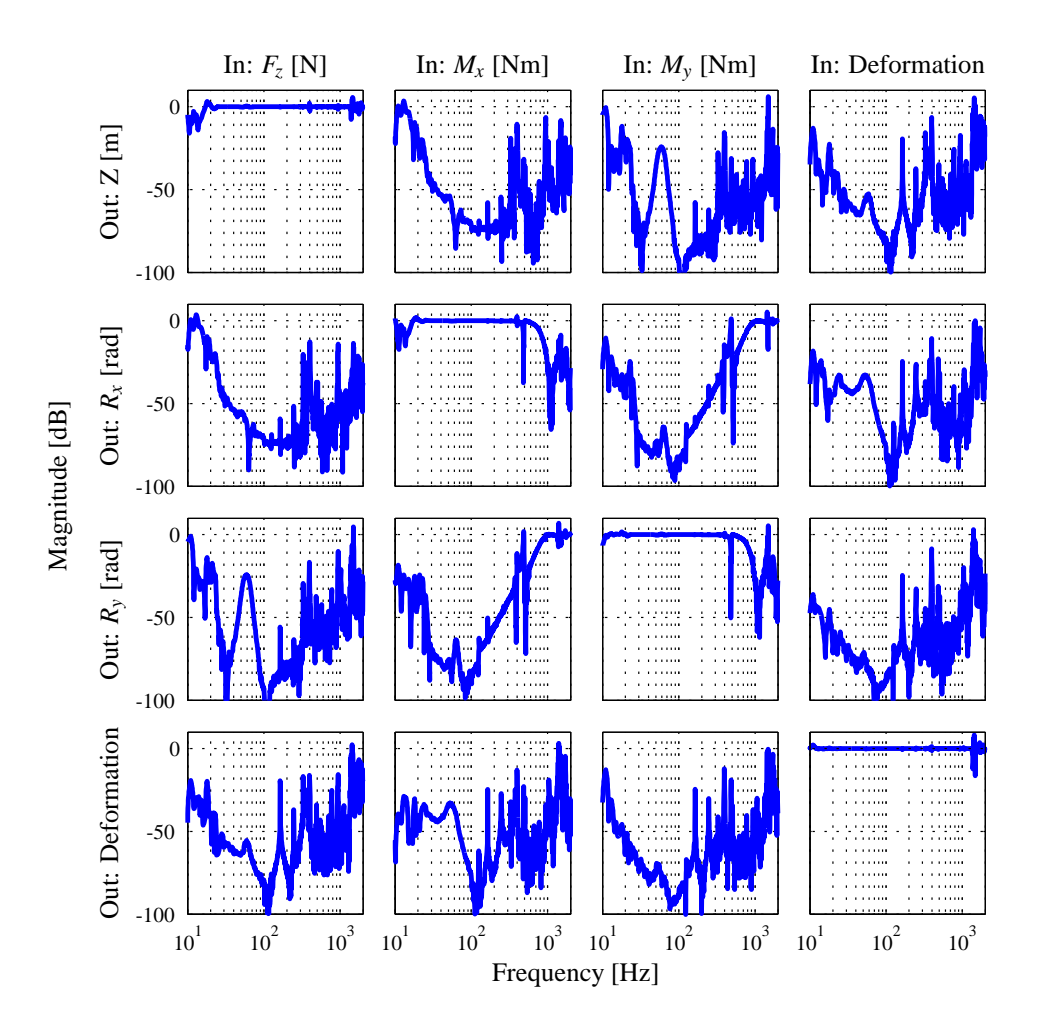


Figure B.4 Relative Gain Array of the decoupled over-actuated plant including deformation channel.

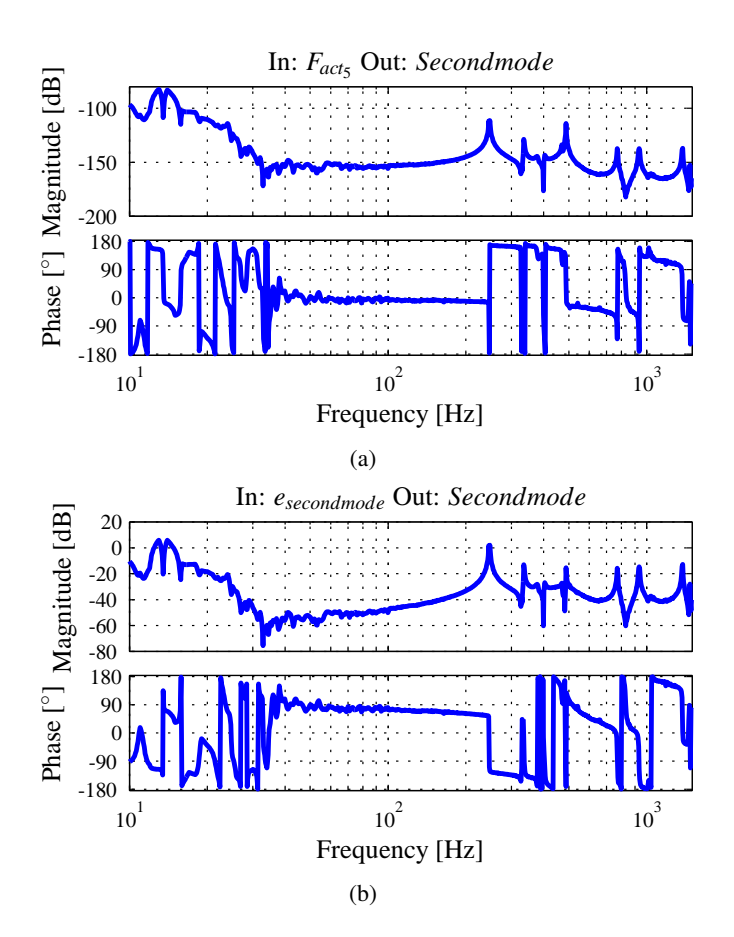


Figure B.5

Transfer function of the measurement of the second eigenmode to the fifth sensor (a). Open loop transfer function with a damping controller (b). A notch filter is applied at 480 Hz.

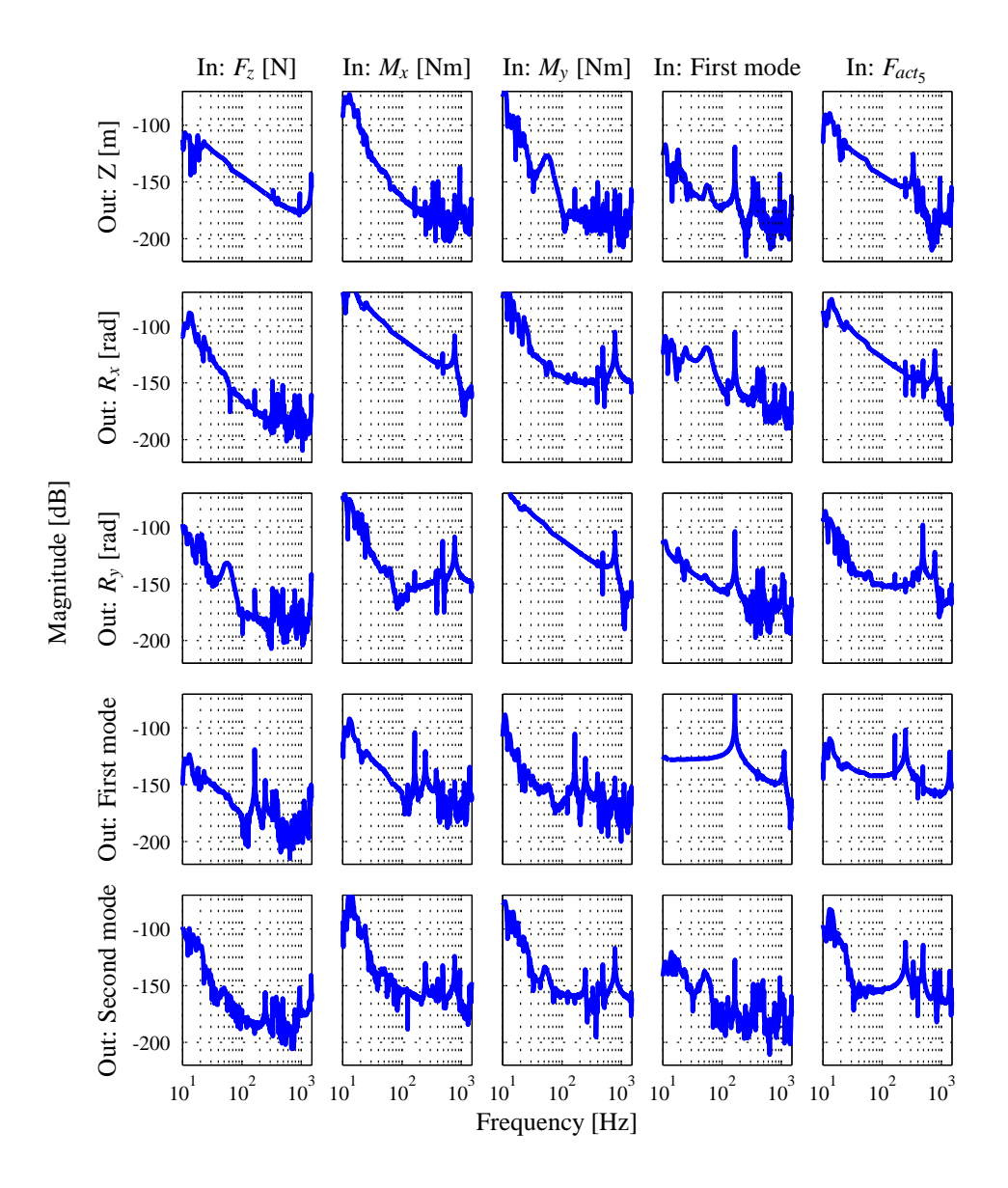


Figure B.6 Bode Magnitude plot of the 5×5 decoupled system with deformation channels for the first and second eigenmode.

Appendix C

Experiment Description

All the experiments are performed using the following equipment. The equipment has been provided by MI-Partners and the Delft, University of Technology.

Equipment used:

- XPC target computer with:
 - National Instruments PCI6052 AD converter
 - National Instruments PCI6713 DA converter
 - National Instruments PCI6602 Digital Counter card
- Quanser[©] LCAM Linear Current Amplifiers
- Renishaw Tonic T1000 linear encoder with TI20KD interpolator.
- Brüel & Kjær type 4506 accelerometers
- Brüel & Kjær type 2692 four channel charge conditioning amplifier

The used software is mainly available software for students. Software not available for students has been provided by MI-Partners.

Software used:

- Matlab[©] 2009b x64
- Matlab[©] 2009a x86 with XPC target connection
- Ansys[©] 11.0 professional

C.1 Starting the control system

Starting the control system is straightforward. The start of the system is described here:

- Start Matlab and the XPC target software.
- Make sure all the equipment is connected and powered on, as described in [2].
- Open the m-file overact.m in the .. $\XPC\$ newplate folder (three sensors) or the overact.m file in the .. $\XPC\$ sensoepos2 folder (four sensors).
- Choose option 1-4 in the overact file for conventional, or over-actuated system and press *F* 5.
- The application will be loaded and the control system will start.

The following Matlab functions are useful to perform measurements:

- *tracedata.m*Performs a trace of the data and gives the PSD and CPS of the traced signals.
- run_multisinedouble.m¹
 Adds a multi-sine to the different actuators in order to measure the system transfer function.

¹Thanks to Jasper Wesselingh for the initial file and Dick Laro for the initial XPC version of this file.

Bibliography

- [1] Daniel Abramovitch, Terril Hurst, and Dick Henze. The pes pareto method, uncovering the strata of position error signals in disk drives. *Proceedings of the 1997 American control conference in Albuquerque*, 1997.
- [2] R. Boshuisen. Design of an over actuated system. Internship report ME 09.029, Delft University of Technology, 2009.
- [3] W.K. Gawronski. Advanced Structural Dynamics and Active Control of Structures. Springer-Verlag New York, 2004.
- [4] W. Heylen, S. Lammens, and P Sas. *Modal Analysis Theory and Testing*. Katholieke Universiteit Leuven, 1997.
- [5] L. Jabben. *Mechatronic Design of a Magnetically Suspended Rotating Platform*. PhD thesis, Delft University of Technology, 2007.
- [6] M.P. Koster. *Constructieprincipes voor het nauwkeurig bewegen en positioneren*. Twente University Press, 2000.
- [7] B. de Kraker. A Numerical Experimental Approach in Structural Dynamics. Shaker Publishing BV, 2004.
- [8] M. Langelaar. Exploratory investigation into topology optimization of overactuated systems. Technical report, Delft University of Technology, 2009.
- [9] D.A.H. Laro. *Mechatronic Design of an Electromagnetically Levitated Linear Positioning System using Novel Multi-DoF Actuators*. PhD thesis, Delft University of Technology, 2009.
- [10] W. Monckhorst. Dynamic error budgetting, a design approach. Master's thesis, Delft University of Technology, 2004.
- [11] A.M. Rankers. *Machine Dynamics in Mechatronic Systems*. PhD thesis, Twente University of Technology, 1997.
- [12] S.S. Rao. *Mechanical Vibrations*, volume SI Edition. Pearson, Prentice Hall, 2005.
- [13] E.I. Rivin. Passive Vibration Isolation. ASME, 2003.

BIBLIOGRAPHY 88

[14] M.G.E. Schneiders, M.J.G. van de Molengraft, and M. Steinbuch. Introduction to an integrated design for motion systems using over-actuation. *Proceedings of the 2003 European Control Conference*, september 2003.

- [15] M.G.E. Schneiders, M.J.G. van de Molengraft, and M. Steinbuch. Benefits of over-actuation in motion systems. *Proceedings of the 2004 American Control Conference*, 2004.
- [16] Sigurd Skogestad and Ian Postlethwaite. *Multivatiable feedback control, Analysis and Design, Second Edition*. John Wiley & Sons, Ltd, 2005.